NO. DOT-TSC-194-1

ANALYSIS OF POTENTIAL NOISE SOURCES OF TRACKED AIR CUSHION VEHICLES (TACV)

E.K. BENDER
R.E. HAYDEN
H.H. HELLER
BOLT BERANEK AND NEWMAN INC.
50 MOULTON STREET
CAMBRIDGE , MA. 02138

JULY 1971
FINAL   REPORT

U.S. Transportation, Dept. of. Transportation
Systems Center,

1. Report No. DOT-TSC-194-1	2. Government Accession No.	3. Recipient's Catalog No.
4. Title and Subtitle Analysis of Potential Noise Sources of Tracked Air Cushion Vehicles (TACV)		5. Report Date July 1971
		6. Performing Organization Code 2178
7. Author(s) E.K. Bender, R.E. Hayden and H.H. Heller		8. Performing Organization Report No. UM-01
9. Performing Organization Name and Address Bolt Beranek and Newman Inc. 50 Moulton Street Cambridge, Mass. 02138		10. Work Unit No. DOT-TSC-194
		11. Contract or Grant No.
12. Sponsoring Agency Name and Address Urban Mass Transportation Administration 400 Seventh Street Washington, DC 20580		13. Type of Report and Period Covered Contractor Report
		14. Sponsoring Agency Code

15. Supplementary Notes

16. Abstract

This report presents an evaluation of the principal sources of noise from tracked air cushion vehicles (TACVs). The study is based on analyses of and laboratory experiments on existing TACVs and rapid transit systems.

Measurements of two French TACV systems were conducted, one a 44-passenger prototype suburban vehicle propelled by a linear induction motor (LIM), and the second an 80-passenger intercity vehicle powered by a gas turbine and shrouded pusher propeller.

Noise levels from a slider current-collection system were also obtained through measurements of the noise and vibration of a third-rail contact shoe on a rail rapid transit car.

17. Key Words Noise levels, Tracked Air Cushion Vehicles, Compressor Noise, Aerodynamic Noise, Linear Induction Motor Noise, Current-Collection noise.	18. Distribution Statement Unlimited	
19. Security Classif. (of this report) UNCLASSIFIED	20. Security Classif. (of this page) UNCLASSIFIED	21. No. of Pages 104 / 22. Price

PREFACE

This report presents an evaluation of the principal sources of noise from tracked air cushion vehicles (TACVs). The study is based on analysis of and laboratory experiments and measurements on existing TACVs and rapid transit systems.

Measurements of two French TACV systems were conducted under subcontract by Dr. Manfred Heckl of Müller-BBN GmbH, Munich, Germany. One of the systems, a 44-passenger prototype suburban vehicle located at Gometz, is propelled by a linear induction motor. The other system, an 80-passenger intercity vehicle located at Orleans, is powered by a gas turbine and a shrouded pusher propeller. Both systems are owned and operated by Sté Bertin & Cie, whose cooperation in obtaining noise data we gratefully acknowledge.

To estimate noise levels from slider type current-collection systems, we measured the noise and vibration of a third-rail contact shoe on a rail rapid transit car operated by the Massachusetts Bay Transit Authority. We appreciate the cooperation shown by the MBTA in conducting this experiment and especially by Messrs. R. Walsh, J. Baker, and A. McNulty.

TABLE OF CONTENTS

TABLE OF CONTENTS *(Continued)*

LIST OF FIGURES AND TABLES

LIST OF FIGURES AND TABLES *(Continued)*

LIST OF FIGURES AND TABLES *(Continued)*

LIST OF FIGURES AND TABLES *(Continued)*

x   <u>page</u>

1. INTRODUCTION

Tracked air cushion vehicles represent a promising means of increasing the mobility of our urban population. Because of their projected high speed (150-300 mph), these vehicles have the potential for reducing commuting time, improving access to outlying airports, and facilitating travel between city centers.

When these systems are built, they will of course have an impact on their environment. Since projected TACVs will incorporate electric propulsion, they will not emit air pollutants along their routes. Noise is then likely to be one of the most significant sources of concern to residents neighboring TACV lines. If TACVs do in fact generate substantial noise levels, communities may oppose or even block the construction of TACV lines through or near residential areas (as they have with new subway construction), severely limiting the routing of such lines. On the other hand, if TACVs are quiet, one would expect them to meet little community resistance. In addition, noise levels influence usage by passengers and will therefore be a vital factor in determining the success of TACVs.

Recognizing the importance of noise to the future development of TACV systems, the Department of Transportation has set exterior and interior noise standards for a TACV procurement. At a distance of 50 ft from the track, a TACV traveling at 150 mph will be allowed to generate no more than 73 dB(A), corrected for pure tone contributions.* This level is somewhat higher than the noise from an average automobile at 65 mph and is considerably quieter than

---

* Because pure tones are more disturbing to people than equivalent levels of broadband noise, an incremental level is computed and added to the dB(A) level according to a procedure specified in Federal Aviation Regulation, Part 36, Noise Standards.

a diesel truck under similar conditions. Specified maximum noise levels within the vehicle and in stations are 63 dB(A).

To ensure that the requisite technology will be available to meet these levels, DOT contracted with Bolt Beranek and Newman Inc. on 12 April 1971 to estimate the noise levels generated by TACVs and to develop certain aspects of the technology needed to predict and control TACV noise levels. Because of the undeveloped state of the technology associated with TACV noise and because system parameters have not yet been well-defined, the study focused on an identification of sources, a preliminary assessment of the noise generated by each source, and control requirements, as well as on technology development.

The study was, for two reasons, devoted exclusively to community noise. First, the community noise problem is felt to be far more difficult to control than is interior noise. Accordingly, noise control technology requires a longer development time. For example, the reaction rail, which extends the length of the system, radiates significant noise levels.* Controlling this sound contribution without extensive treatment of the entire rail (which may not even be feasible from other considerations) represents a difficult problem. The second reason for deferring a study of interior noise is that interior noise levels depend very much on the structure separating the source from the passenger occupancy space. This structure has not yet been defined, even in a rudimentary way. Once the basic structure is identified, appropriate treatment for effective interior sound control may be determined.

---

* A pure tone of 81 dB(A) at 21 ft was measured for the French LIM system at Gometz. [This extrapolates to 77 dB(A) at 50 ft, already 4 dB(A) above the level specified by DOT for all sources combined.]

Furthermore, the techniques for achieving reasonable levels of interior noise control have been largely developed for the treatment of aircraft and ground vehicles. Their application to TACV noise is not expected to represent as significant a task as the generation of new techniques for control of noise affecting the community.

The fundamental TACV configuration studied consists of a linear induction motor (LIM) straddling a vertical reaction rail for propulsion and low-pressure air cushions supplied by electrically driven axial flow compressors for suspension. The large electrical power levels needed for this system are drawn from the wayside by means of a mechanical current collector sliding along a "third rail". These systems, as well as aerodynamic flow over the vehicle structure, constitute the principal sources of noise. Other noise sources, which are felt to be of secondary importance, include cooling pumps for the LIM, signal-conditioning circuits for LIM current control, and ventilation systems.

2. TACV COMPRESSOR NOISE

Two axial flow compressors will supply the air cushions used for suspension. These compressors must deliver an airflow of 100-lb mass/sec and achieve a pressure rise of 1.5 psi above ambient in the plenum chamber. The estimated power requirement for each compressor is 500 hp. Thus, compressors may be a dominant source of TACV noise, and they will require special attention so that radiated sound levels will be within the bounds of currently envisioned noise specifications: 73 dB(A) for cruising and 63 dB(A) for station stopover, measured at a 50-ft sideline. For such relatively high-powered compressors, this is a stringent requirement which will undoubtedly call for special noise control measures.

The complexity of predicting compressor noise is illustrated in Appendix A, where we discuss representative source mechanisms involved in rotating aerodynamic machinery noise. Predicting noise levels of the TACV compressor presents a special problem, since we have very little information about its design and operational parameters. However, gross predictions of overall levels can be made on the basis of such parameters as rated horsepower, volume flow, and pressure rise. To do so, we first establish these parameters for the most likely system configuration and use three methods to predict the sound power level spectrum. We then convert the predicted sound power level spectrum into a sound pressure level spectrum at a 50-ft sideline to establish the noise reduction required for compliance with DOT specifications.

2.1 Compressor Noise Prediction

We assume the following specifications for each compressor
and then use prediction methods developed by Allen [1], ASHRAE [2],
and Wintermeyer and McKaig [3].*

One-stage	
Rated Horsepower	500 hp
Pressure Rise	40 in. H_2O
Mass Flow	50 lb/sec
Volume Flow	660 ft^3/sec = 40,000 ft^3/min
24 Rotor Blades	
4500 rpm = 75 rps	
Tip Diameter	2.5 ft
Tip Speed	585 ft/sec
Blade Passage Frequency	1800 Hz

After Allen

Using rated horsepower and pressure rise, we find the sound
power level (PWL) in dB re 10^{-12} watt radiated from intake:

$$PWL = 90 + 10 \log hp + 10 \log \Delta p = 133 \text{ dB} .$$

Using volume flow and pressure rise, we find

$$PWL = 55 + 10 \log q + 20 \log \Delta p = 133 \text{ dB} .$$

Using rated horsepower and volume flow, we find

$$PWL = 125 + 20 \log hp - 10 \log q = 133 \text{ dB} .$$

The spectral shape of radiated sound energy is plotted in Fig. 1.

---

* These and other predictions schemes are discussed in Appendix B.
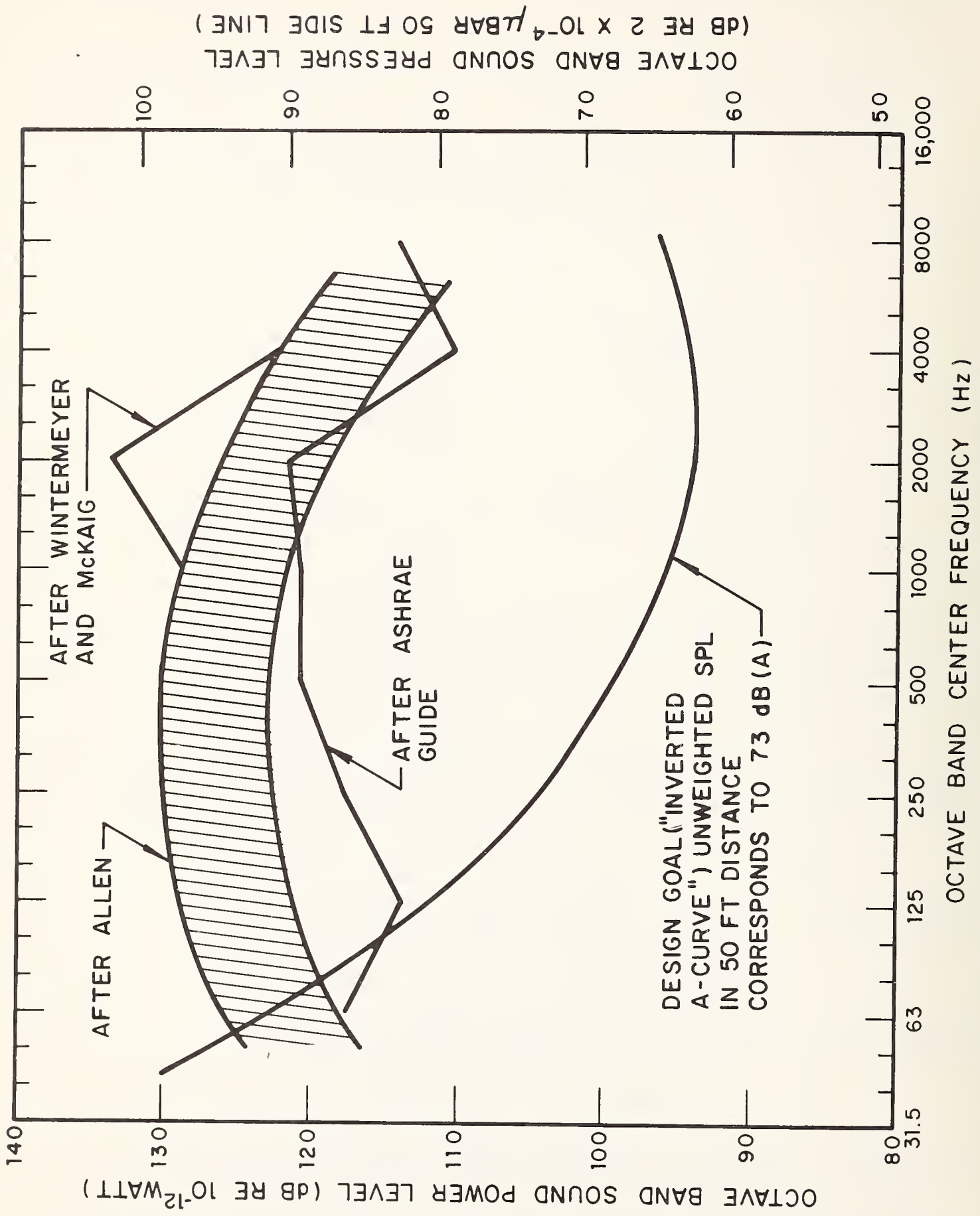
FIG. 1   PREDICTED PWL AND SPL SPECTRA FROM SINGLE TACV COMPRESSOR
           WITHOUT NOISE CONTROL TREATMENT

After ASHRAE Guide

The ASHRAE Guide procedure yields sound power levels below those predicted by the Allen method (see Fig. 1).

After Wintermeyer and McKaig

The octave-band sound power level in the blade passage frequency band (1800 Hz) is approximately 133.5 dB.

The righthand ordinate of Fig. 1 shows the sound *pressure* levels (SPL) that would be obtained at a 50-ft sideline, assuming hemispherical spreading of sound energy over hard-reflecting ground.

2.2 Required Noise Suppression

One technique for obtaining an SPL spectrum that yields a specified dB(A) value is to attenuate a given (unweighted) SPL spectrum so that the spectrum shape follows an inverted A-curve. A-weighting then results in a flat spectrum with equal energy per relative constant bandwidth. For the predicted spectra shown in Fig. 1, most of the attenuation is required in the frequency range of 125 to 4000 Hz, where it is comparatively easy to obtain.

Figure 2 shows the attenuation required for two of the predicted spectra to obtain an overall sound level of 73 dB(A) at a 50-ft sideline. Approximately equal portions of the total sound energy will be radiated from the compressor intake and exhaust. However, since exhaust sound will enter the plenum chamber where there is likely to be some acoustic treatment, we concentrate here on the transmission path from the compressor intake through the intake duct and establish specifications for an intake
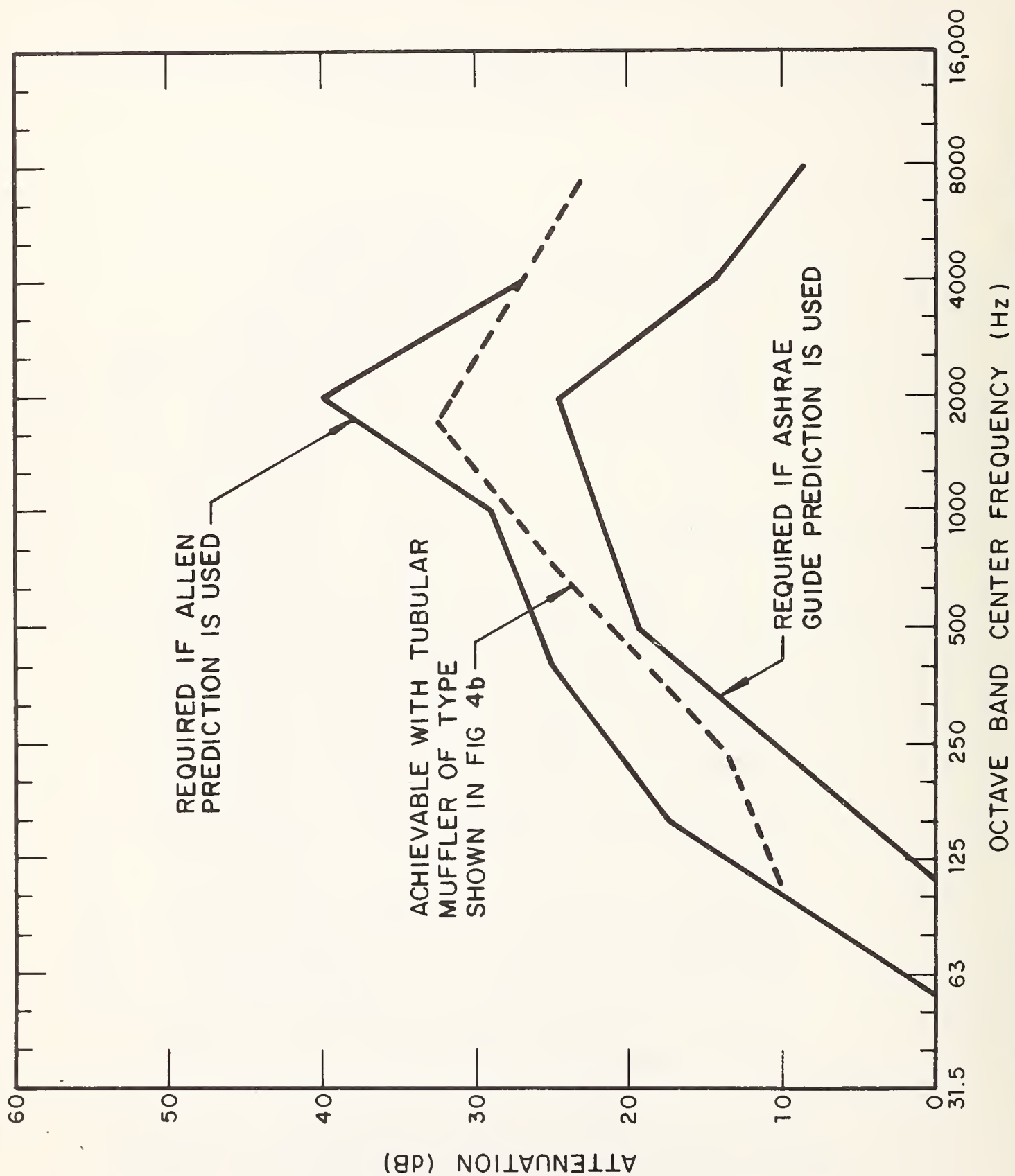
FIG. 2 REQUIRED ATTENUATION OF TACV COMPRESSOR NOISE AND ATTENUATION ACHIEVABLE BY VARIOUS TYPES OF MUFFLERS.

muffler that will provide the required attenuation. (In Appendix C, we discuss some means to control noise at the source by design modifications of the compressor.)

To attenuate compressor noise along the air intake duct, one may use narrowband resonant absorption to suppress discrete-frequency sound, broadband absorption to suppress broadband acoustic energy, and/or inlet flow choking to prevent sound energy from passing through an intake opening. Inlet choking might offer some advantage for reducing the noise radiated by TACVs entering and leaving a station, but since choking reduces the operational efficiency of a compressor engine, there are serious disadvantages for normal cruising conditions.

Narrowband Absorption

The compressors should operate continuously at or near a design condition (due to the requirement of an air cushion independent of the cruise speed, including station stopovers). Narrowband resonant absorption could be an effective means for controlling the predominant sound radiation at the blade passage frequency. Figure 3a illustrates the basic concept of a narrowband resonant duct lining — i.e., a honeycomb structure with a porous facing sheet. In an intake duct, lining material is exposed to high-speed flow and, because of the high acoustic pressure, to large particle velocities. For such conditions, the acoustic resistance of the perforation increases nonlinearly above the theoretical value of no-flow and low-particle velocity. Thus, considerable effort is required to assess the behavior of a selected porous material under operational conditions and to optimize the design.
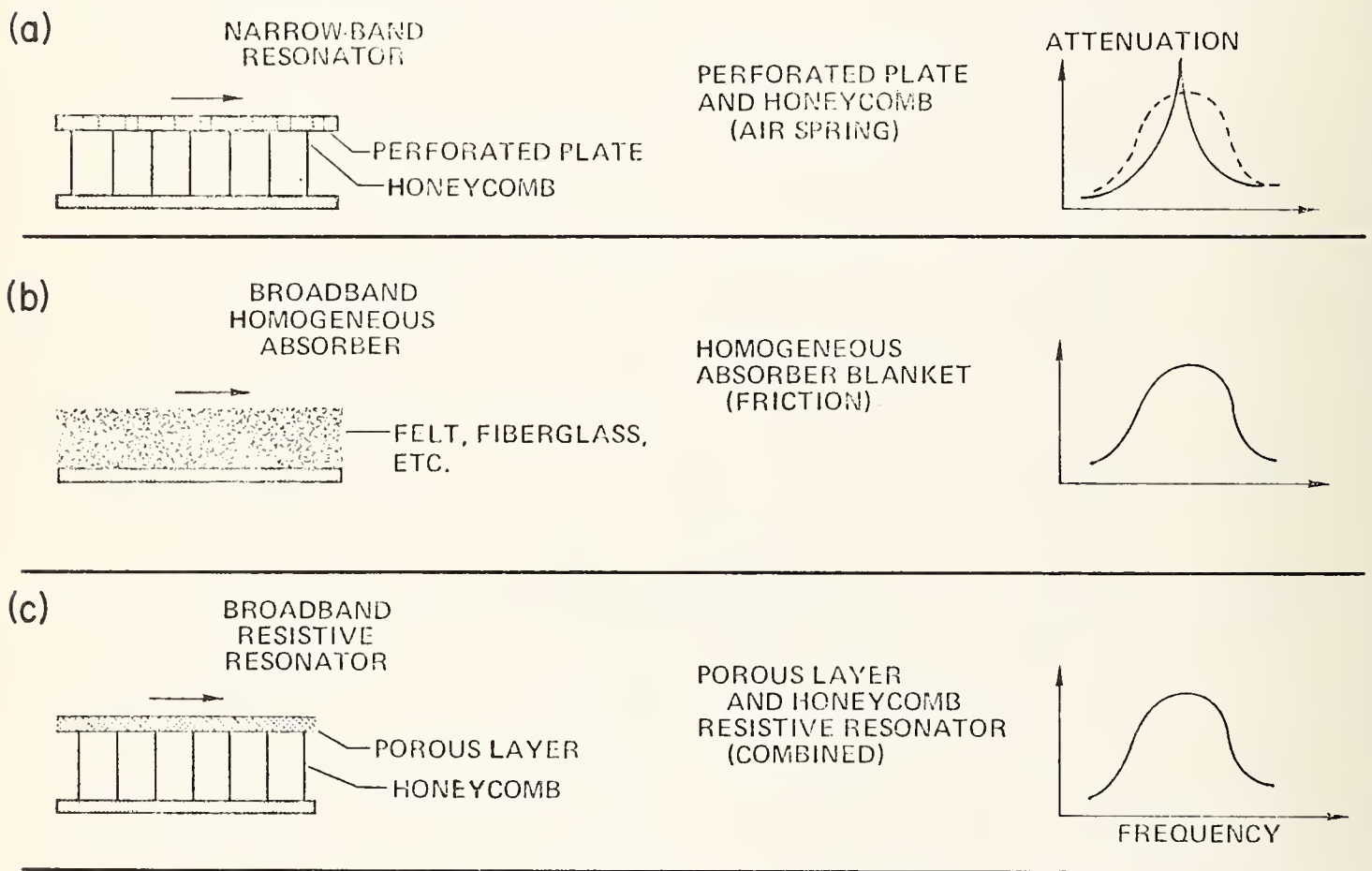
FIG. 3. ACOUSTIC LINING CONCEPTS AND TYPICAL ABSORBTION
         CHARACTERISTICS FOR ATTENUATION OF SOUND IN DUCTS.

In addition to narrowband absorbers for suppressing discrete-frequency sound energy in selected bands, the TACV compressors will require muffling for the broadband acoustic energy.

Broadband Absorption

Broadband sound absorption can be achieved by lining an intake duct with an homogeneous layer of such absorptive material as is illustrated in Fig. 3b or with a combination of a porous layer on a honeycomb structure, resulting in a "broadband resistive" absorption such as is illustrated in Fig. 3c. Several materials, recently developed for aircraft engine nacelle treatment and appropriate for use on a TACV intake muffler, include (a) solid-sheet perforated material; (b) sintered fiber-metal sheets available in copper, silver, or stainless steel; (c) sintered woven-screen sheet composed of two or more fine woven metallic wire screens; and (d) sintered continuous-filament sheet made of unwoven metallic fibers sintered into a uniform mat.

A hard-walled, unlined intake duct of approximately 3-ft diameter provides attenuation of about 0.02 dB/ft in the frequency range above 250 Hz. A 2-in. thick, homogeneous, absorptive lining provides approximately 1 dB/ft attenuation in the middle of the audible frequency range.

A tubular muffler, however, can provide significantly greater attenuation. For the case of an intake muffler, we can expect from a 10-ft long, 36-in. diameter tube with an absorbtive centerbody and hard reflecting walls (Fig. 4a) the following typical attenuation:

f(Hz)	100	200	400	800	1600	3200	6400
dB	10	12	17	18	15	12	11

Typical total pressure drop would be on the order of 1 in. H_2O.

HARD OUTER CASING

ABSORBTIVE OUTER CASING

a

b
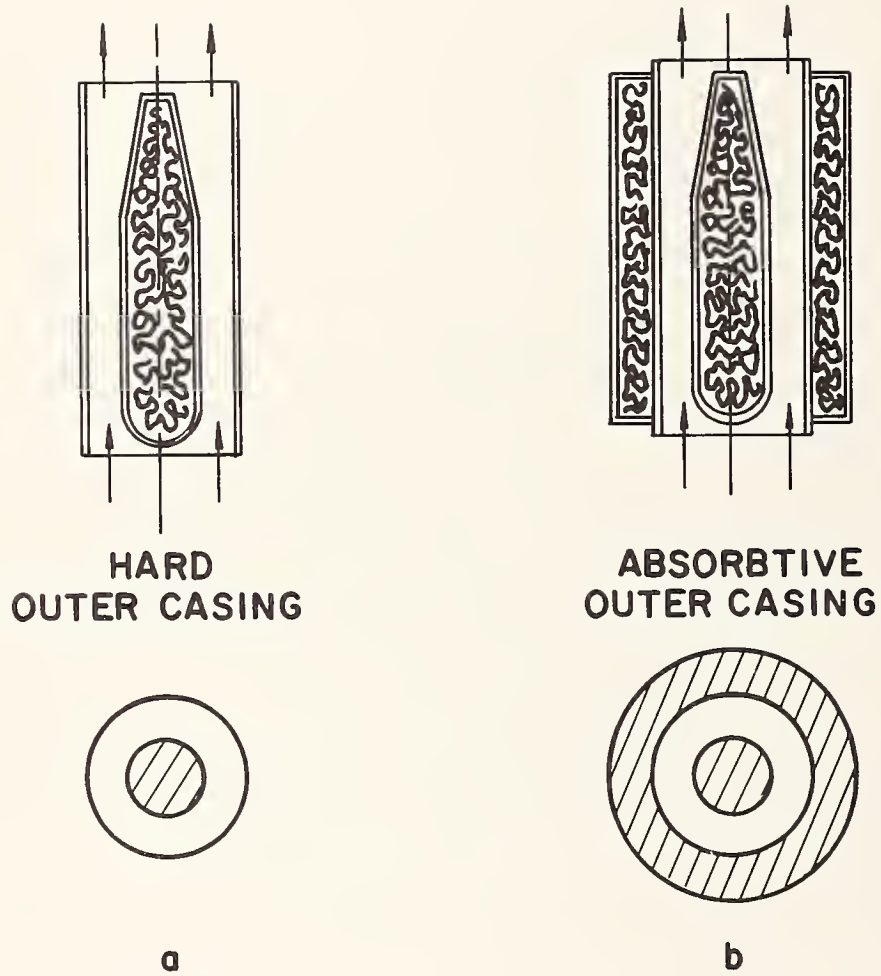
FIG. 4.   TUBULAR MUFFLER CONCEPTS FOR
          SUPPRESSING COMPRESSOR NOISE

A 5-ft long, 30-in. diameter, tubular muffler with absorbtive centerbody and absorbtive walls (Fig. 4b) would provide typical attenuation of:

f(Hz)	100	200	400	800	1600	3200	6400
dB	10	14	19	26	32	27	23

Pressure drop would again be on the order of 1 in. H_2O.

The attenuation offered by this second type of tubular muffler is plotted in Fig. 2 for comparison of required and achievable attenuation. Figure 2 shows that the tubular muffler of Fig. 4b would provide sufficient attenuation, if the "ASHRAE-guide" derived predictions are valid, to reduce noise levels to below 73 dB(A) at a 50-ft sideline.

Directivity Effects

Directivity effects may minimize the sound pressure levels observed at a 50-ft sideline. If the intake ducts were oriented parallel to the vehicle axis, most of the acoustic energy would be radiated forward, and levels at a 90° azimuthal angle could be 10 to 20 dB below the peak levels observed closer to the duct axis. A prior evaluation of this effect, however, is not possible until further details of compressor acoustics, vehicle geometry, and intake duct arrangements are available.

3. TACV AERODYNAMIC NOISE

The sources of aerodynamic noise are shown schematically in Fig. 5, along with the geometry of a typical vehicle. In addition to those sources associated with fans and compressors, aerodynamic noise may be radiated from

• the turbulent boundary layer developed upon the skin of the TACV,

• the interaction of this turbulent boundary layer with surface discontinuities,

• the interaction of the turbulent boundary layer developed under the vehicle with the lip of the air cushion skirts (lip noise),

• the flow noise of the peripheral jet and fluctuations in aerodynamic force at the surface of the track caused by flow impingement upon surface roughness, and

• the turbulent flow over the edges of the track (edge noise).

Below, we develop analytical models for the basic source mechanisms in a form which allows estimates for full-scale situations. We describe our laboratory experiments and, using both the model and the experimental results, we predict aerodynamic noise levels of the TACV.

3.1 Source Mechanisms

Lower Bound: Direct Radiation from the Turbulent Boundary Layer

Our analytic model for sound radiated from the turbulent flow surrounding the smooth surface of a high-speed vehicle is based on
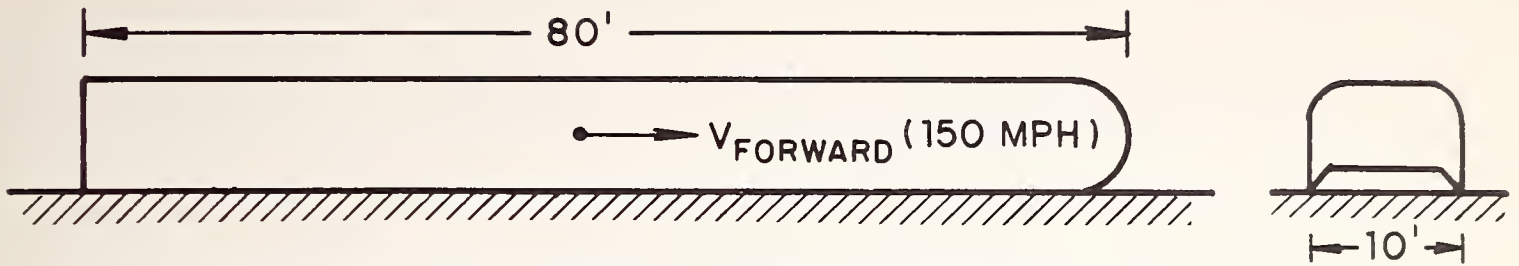
(a) DIMENSIONS OF VEHICLE USED IN EXAMPLE
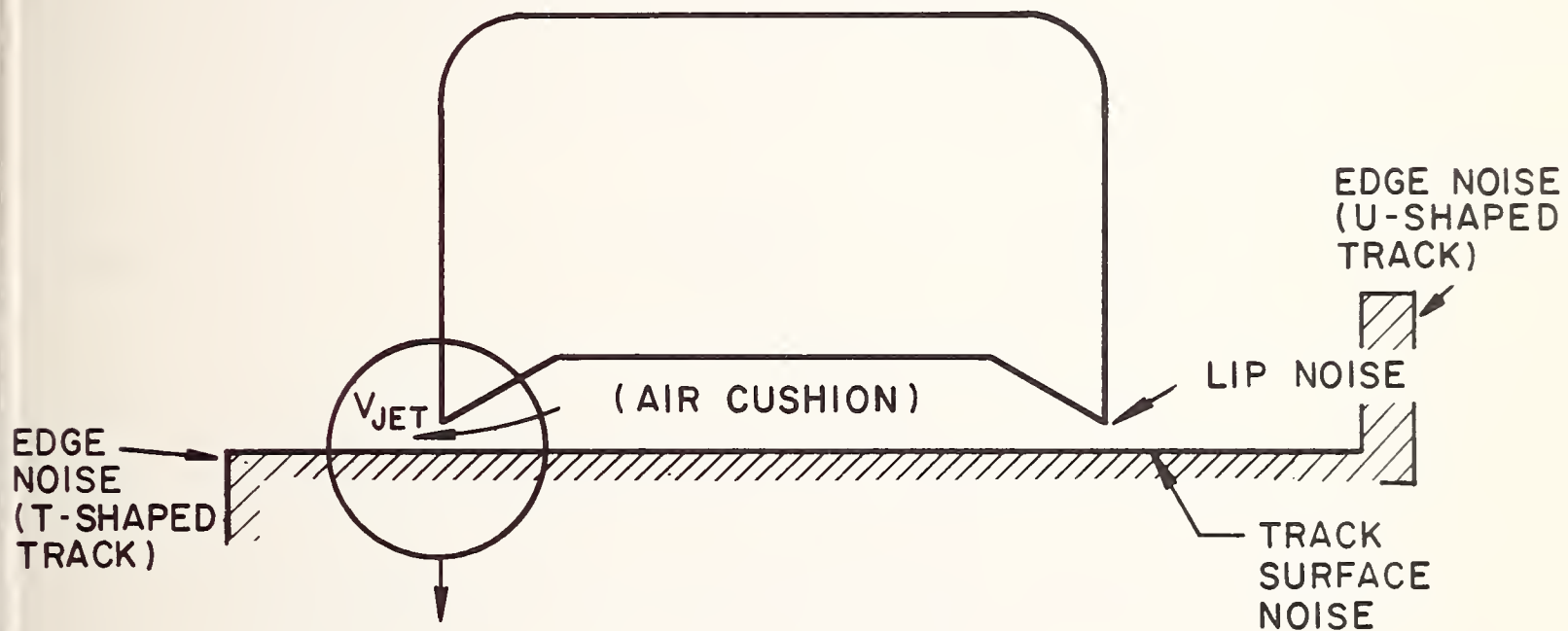
(b) SCHEMATIC OF NOISE SOURCES AND TERMINOLOGY FOR
     TRACK AND SKIRT NOISE

FIG. 5 AERODYNAMIC NOISE SOURCES IN TRACKED AIR CUSHION
        VEHICLES

wall-pressure fluctuation measurements made on glider wings, ship
hulls, and wind-tunnel walls; this model assumes an infinite
surface that is free from discontinuities. These fluctuations
are measured with large-area transducers, which average out the
pressures due to convecting eddies but give accurate measurements
of the sound pressure.

Results of several such wall-pressure measurements have been
summarized by Chandiramani [4], who describes the normalized wall-
pressure spectral density at low wavenumbers as a function of
Strouhal frequency:

$$\frac{\Phi(\omega)U}{q^2\delta*^3} = d \cdot 10^{-8} \left[\frac{\omega\delta*}{U}\right]^{-4} , \qquad (1)$$

where $\Phi(\omega)$ is the low-wavenumber spectral density at frequency ω,
q is the dynamic pressure, U is the free-stream speed, and $\delta*$
is the boundary layer displacement thickness. The constant d has
a value of unity for smooth walls and a larger value for rough
walls such as vehicle surfaces. Scatter in the wall-pressure data
indicates that d is of the order of 10 for rough walls.

The wall-pressure spectral density $\Phi(\omega)$ is used to compute
the intensity of sound at the wall. This computation involves an
assumption. Chandiramani has collected values of $\Phi(\omega)$ that apply
to the low-wavenumber region where wavenumber magnitudes are two
to three times greater than the acoustic wavenumber. In this
region the value of $\Phi(\omega)$ is nearly constant (with change in wave-
number). It is assumed here that this constant value extends into
the wavenumber region having a wavenumber magnitude less than the

16

acoustic wavenumber. With this assumption, the mean-square pres-
sure of sound waves measured in a frequency band $\Delta\omega$ at the wall is

$$p_W^2 = 2\pi k_0^2 \Phi(\omega)\Delta\omega , \qquad (2)$$

where k_0 is the acoustic wavenumber and is equal to ω/c_0, c_0 being
the sound speed.

The sound power W is

$$W = Sp_W^2/\rho c , \qquad (3)$$

where S is the lateral surface area of the vehicle. Combining
Eqs. 1, 2, and 3, we have

$$W = d\pi^2\rho c^2 S \ 10^{-8} \ M^7\Delta f/k_0^2\delta^* , \qquad (4)$$

where $M = U/c$ is the Mach number.

The estimated values (in cgs units) of the parameters for a
typical TACV are $\rho c = 42$ gm/cm^2/sec, $c = 3 \times 10^4$ cm/sec, and $d = 10$.

The classical flat plate relation for δ^* is

$$\delta^* = .05 \left(\frac{\nu}{U}\right)^{1/5} x^{4/5} , \qquad (5)$$

where ν is the kinematic viscosity and x is the distance from the
leading edge. Combining Eqs. 4 and 5, taking the logarithms of
both sides, and accounting for dimensional units, we find the
equation for the power level (in dB re 10^{-12} watts) to be

$$PWL = 70 \log U[mph] + 10 \log S[ft^2] - 8 \log \ell[ft]$$

$$- 10 \log f[Hz] - 35 , \qquad (6)$$

where the appropriate units of each parameter are indicated by square brackets.

The frequency at which the boundary layer radiation contribution is expected to be maximum corresponds to a Strouhal frequency of about unity,

$$\delta^* \omega_{peak} / u = 1 \ . \tag{7}$$

In terms of convenient parameters,

$$f_{peak}[Hz] = 86 \ \frac{U[mph]}{(\ell[ft])^{4/5}} \ . \tag{8}$$

An analysis similar to the above has been made for predicting radiated noise from glider aircraft [5]. When compared with measured data, the levels predicted by considering only turbulent boundary layer radiation were 20 to 24 dB too low and the Strouhal peak had shifted from $\omega\delta^*/U = 1.0$ predicted for turbulent boundary layer radiation to $\omega\delta^*/U \approx 0.4$. It is clear from this observation that the finiteness of the surface supporting the turbulent boundary layer is important in computing the sound radiation. Some recent research directed toward identifying and studying edge noise can be applied to explain the substantial increase in actual sound over that predicted from a turbulent boundary layer on a relatively smooth infinite surface. This subject is discussed in the next section.

Noise From Turbulent Boundary Layer Flow Over an Edge

When a "frozen field" eddy pattern traveling along a rigid surface reaches the edge of that surface, the eddies may exert a fluctuating force on the surrounding fluid medium. A fluctuating

force on a fluid medium characterizes an acoustic dipole. The
spectrum of sound due to fluctuating forces exerted by a turbulent
boundary layer when it encounters a trailing edge has been studied
[6-8] and modeled in terms of mean flow parameters. The essential
results of these studies may be applied to the prediction of (1)
sound from the interaction of a turbulent boundary layer with the
lip of the air-cushion skirt on a TACV and (2) to the sound
produced when the air escaping from beneath the cushion encounters
the edges of the track.

The overall power level radiated [6] is, at sea level condi-
tions,*

$$PWL(dB\ re\ 10^{-12}\,w) = -32 + 10\ \log\ \delta[ft] + 10\ \log\ P[ft]$$

$$+ 60\ \log\ V_j[ft/sec]\ , \tag{9}$$

where δ is the boundary layer thickness at the lip, P is the peri-
meter of the lip or span of the edge, and V_j is the free-stream
value of the jet emanating from the nozzle.

The spectrum relative to the overall level is shown in
Fig. 6. The key parameter to be estimated is δ, which may vary
greatly depending upon the condition of the flow and the wall up-
stream of the lip. One should note that both the level given by
Eq. 9 and the spectrum given by Fig. 6 apply to a thin edge (or
lip). Hayden [6] found that increasing the thickness of the edge
decreases the level of the radiated sound, especially in the
vicinity of the spectral peak. This result has been confirmed in
the current study and is likely to be of practical significance in
considering proposed track designs for the TACV.

----

* We note that the constant in this expression may be applied rig-
  orously only when the flow field under consideration is identical
  to that of Ref. 6. In cases where the flow field is different,
  the levels predicted by Eq. 9 may be somewhat in error.
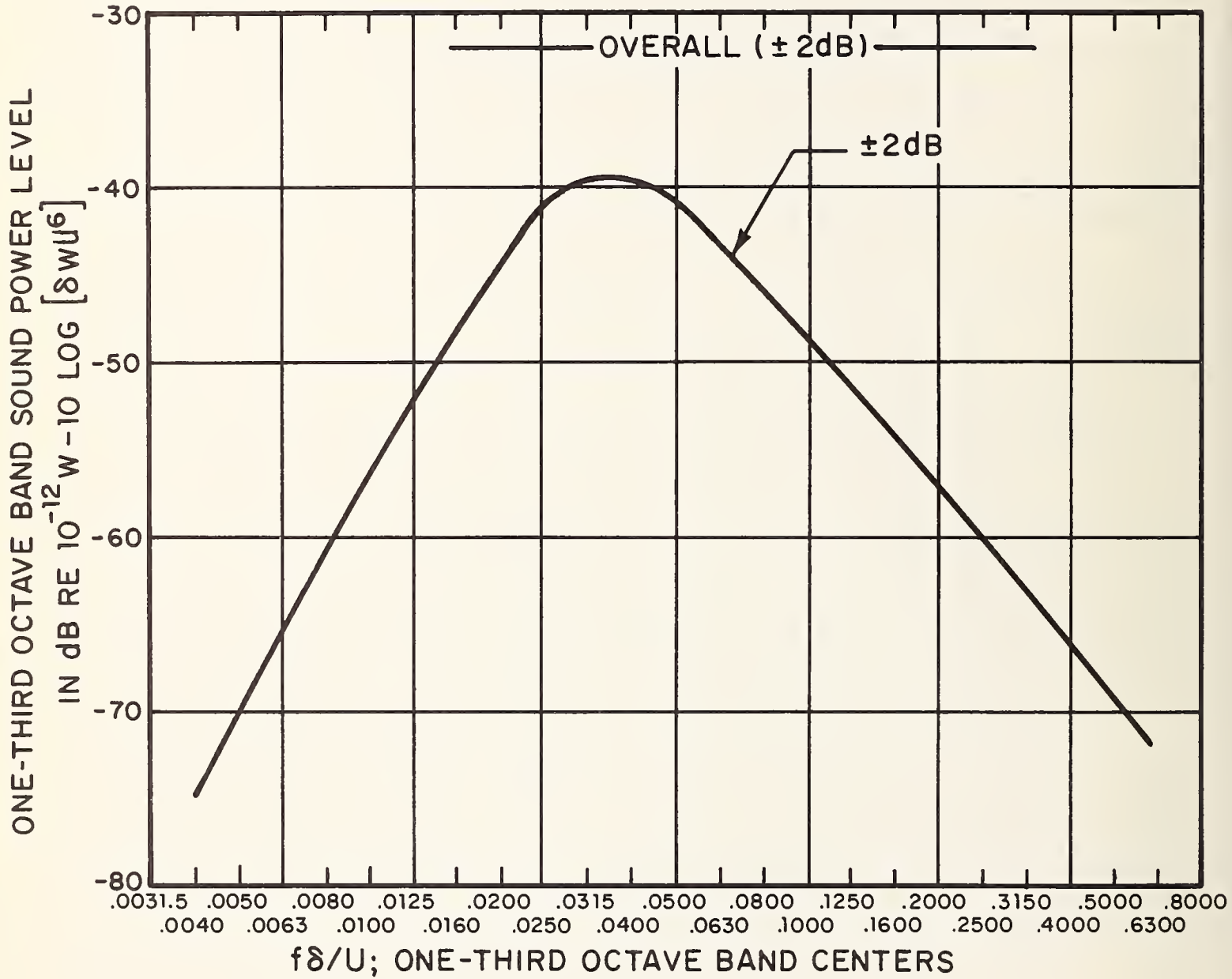
FIG. 6   TRAILING EDGE NOISE FOR FULLY DEVELOPED TURBULENT
         BOUNDARY LAYER OVER A THIN EDGE AT 1 ATM., 70°F.

Impingement of Airflow on Rough Track Surface

The dipole sound arising from the interaction of a turbulent boundary layer with a single small-scale "bump" in the surface can be found as follows:

$$\text{Dipole Sound Power, } W_D = \frac{\pi(F')^2 f^2}{3\rho c^3} , \tag{10}$$

where F' is the fluctuating force exerted on the medium by the fluid-solid interaction. F' may be estimated by first considering the geometry of the process (Fig. 7).

If U is the velocity at the roughness element, and u' and v' are turbulence components, then the total (steady and unsteady) force on the roughness granule is, neglecting higher order terms,

$$F + F' = (C_D h \cdot w) \frac{1}{2} \rho(U^2 + 2Uu' + 2Uv') . \tag{11}$$

If $u' \approx v'$, then, after disregarding the steady-state force, we find

$$F' = C_D \cdot h \cdot w \cdot \rho(Uu') .$$

The drag coefficient C_D for bluff bodies is approximately equal to unity and the product Uu' may be rewritten in terms of the turbulence intensity u'/U as $U\, u'/U$; if $u'/U \approx 0.2$, then assuming the usual turbulent boundary layer velocity distribution (1/7 power law), we find

$$F' = .4\rho U^2 h \cdot w = .4\, V_\delta^2 \left(\frac{h}{\delta}\right)^{2/7} h \cdot w , \tag{12}$$

$$\left(\frac{V_{(y)}}{V_j}\right) = \left(\frac{y}{\delta}\right)^{1/7}$$

$V_\delta = 0.99 V_j$

VELOCITY PROFILE FOR FULLY
DEVELOPED TURBULENT
BOUNDARY LAYER
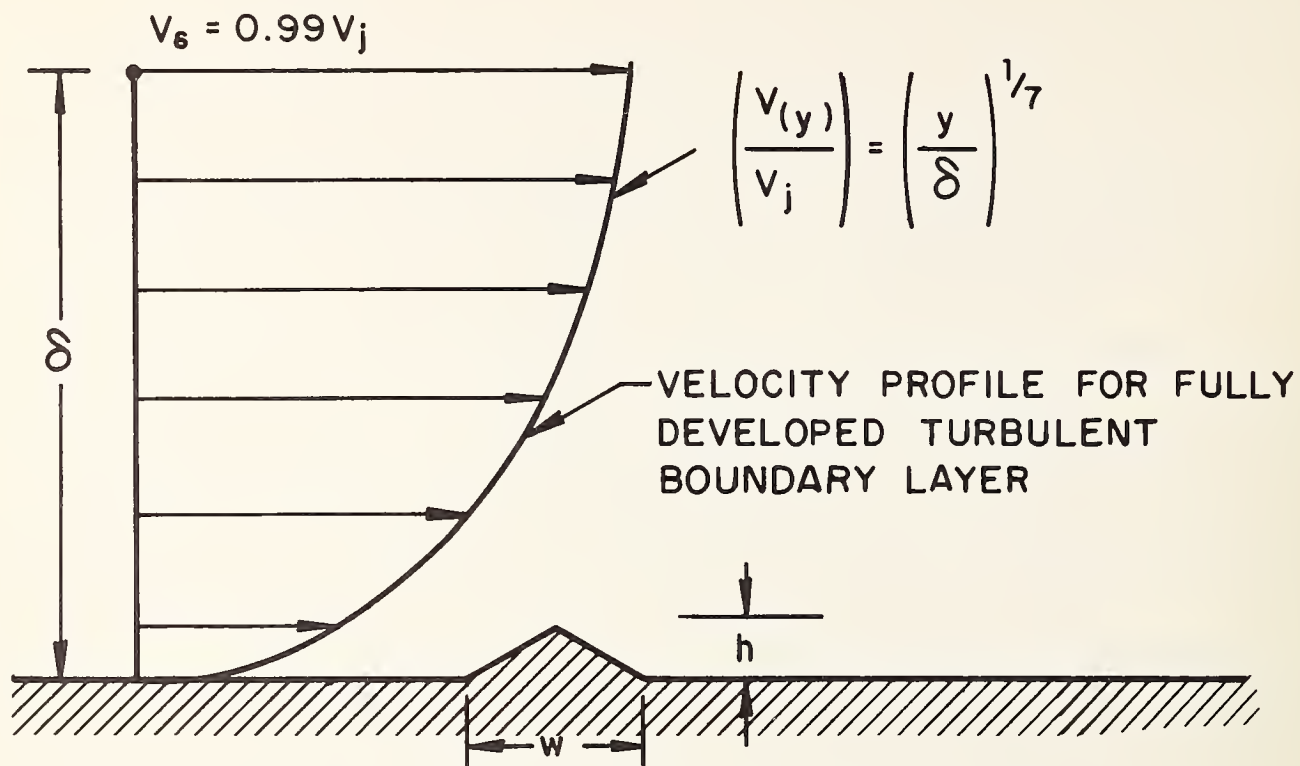
(a) AIRSTREAM AND ROUGHNESS TERMINOLOGY

SKIRT

TACV
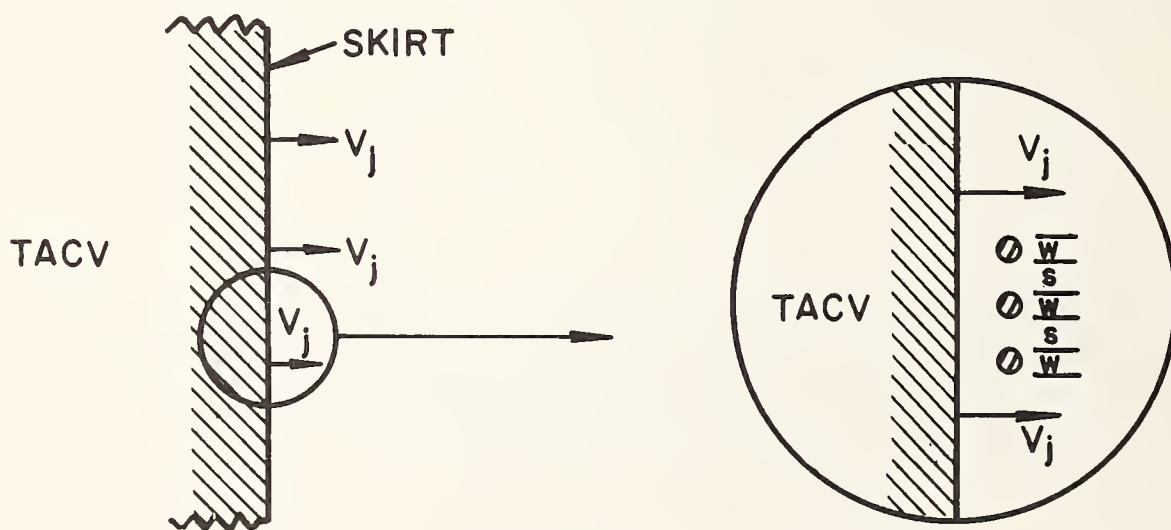
(b) PLAN VIEW OF ROUGHNESS DISTRIBUTION AROUND
VEHICLE PERIPHERY

FIG. 7   SCHEMATIC OF NOISE GENERATION BY AIRFLOW OVER
SMALL-SCALE TRACK ROUGHNESS

and the sound power from one roughness element becomes

$$W = \frac{.4\rho V_\delta^2 \ h \cdot w \left(\frac{h}{\delta}\right)^{2/7} f^2}{3\rho c^3} .$$ (13)

The characteristic frequency of the turbulence and thus of the sound may be derived from the peak in the Strouhal number spectrum where $S \approx fw/U = 0.2$. (Alternatively, h could be used to define the characteristic frequency.)

$$f \approx .2\frac{U}{w} \approx \frac{.2V_j \left(\frac{h}{\delta}\right)^{1/7}}{w} .$$ (14)

Then

$$W = \frac{\pi(.08)^2 \rho \ V_j^6 \left(\frac{h}{\delta}\right)^{6/7} h^2}{3c^3} ,$$

which, after the constants have been evaluated, becomes

$$W \approx 7 \times 10^{-3} \ \frac{\rho V_j^6}{c^3} \ \left(\frac{h}{\delta}\right)^{6/7} h^2 .$$ (15)

For a jet issuing from a TACV skirt, δ varies with distance from the center of the cushion. The cushion flow field for the actual vehicle will be quite disturbed by the compressor turbulence, and thus accurate prediction of δ is difficult at this point. However, for an order of magnitude estimate, the flat plate relation of Eq. 5 may be modified as follows:

$$\delta \approx 0.4 \left(\frac{U}{V}\right)^{1/5} \cdot x^{4/5} ,$$ (16)

where $x = 0$ will be taken as the TACV centerline.

To be completely accurate, one should perform a surface integral of Eq. 15 to include all the roughness elements which participate in the sound-generation process. However, for the present, let the integral be approximated by mW where m is the number of elements (or bumps) that are exposed to the air jet at one instant. Since the sound power is dependent upon U, it can be assumed that only those bumps nearest the source of the air jet will contribute significantly to the radiated sound. Thus, the total roughness noise can be estimated to the first order by a line of dipole sources, each component having a source strength as defined by Eq. 15.

For turbulence intensities other than the value assumed (0.2), the sound power will increase or decrease in the same manner as the turbulence intensity. Meecham [9] gave, without derivation, an expression for the sound intensity from a single bump of height a on a rigid surface; when integrated over a semi-infinite half space, Meecham's expression becomes

$$W \approx \frac{(2\pi)\cdot(10^{-2})\ \rho U^6 \left(\frac{a}{\delta}\right)^{6/7} a^2}{c^3}. \tag{17}$$

This relation approximates Eq. 15 but predicts about 10 dB more sound power for equivalent roughness elements. For the present, let us continue to rely upon Eq. 15. An engineering expression can be derived for the total sound power from a line of roughness elements of length L, height h, base width W, and spacing S and exposed to a jet velocity V_j.

$$PWL(dB\ re\ 10^{-12}\ w) = -18.1 + 60\ \log V_j + 20\ \log h$$

$$+ 8.6\ \log\left(\frac{h}{\delta}\right) + 10\ \log\left(\frac{L}{S}\right). \tag{18}$$

The exact spectrum shape will of course depend upon the spectrum of the turbulence and the ratio of roughness granule size to acoustic and hydrodynamic wavelength. One could use a spoiler noise spectrum based upon the hypothesis that a fluctuating drag (or drag-like) force acting on a roughness element radiates as the fluctuating drag force on rigid flow spoilers removed from a surface. The presence of the track surface, acting as an acoustical barrier and diffractor, will undoubtedly affect the sound output, but we are at this time not prepared to speculate as to what or how much this effect will be. Thus, for the present, let us approximate the spectrum of noise from flow impingement upon track roughness by band-limited white noise one decade wide and centered about the frequency defined in Eq. 14.

3.2 Laboratory Experiments

Since some of the analytical or empirical models developed in the foregoing sections were previously either experimentally unconfirmed or restricted to specialized geometric and aerodynamic conditions, exploratory wind-tunnel tests were conducted to assist in achieving reliable predictions of noise from the various aerodynamic sources. The tests were conducted in the BBN free-jet acoustic wind tunnel, which is shown schematically in Fig. 8.

A section of the TACV skirt was modeled by a smooth inclined aluminum plate having a sharp edge near the "track". Gaps of 1 and 2 in. were left for the air to escape, and parallel restraints prevented air from discharging out the side of the simulated skirt section. To isolate the lip noise source, we attached a long (10-ft) smooth plate to the bottom of the skirt, thereby simulating an infinite smooth track. During tests of noise from track roughness, the long plate was retained and roughness elements were
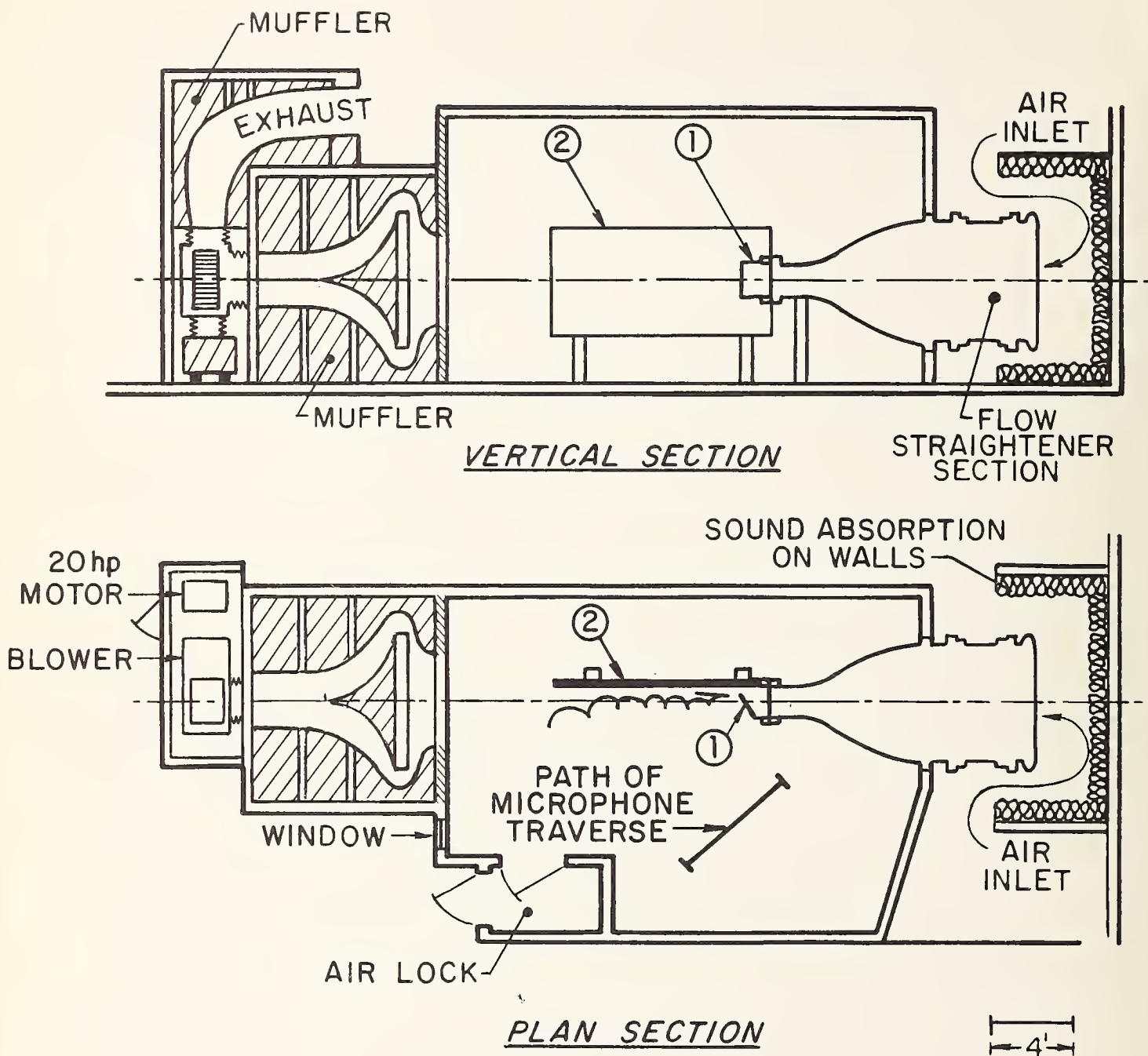
1. SIMULATED SECTION OF TACV SKIRT
2. RIGID, FLAT SURFACE SIMULATING TRACK

FIG. 8 EXPERIMENTAL SETUP IN BBN FREE-JET ACOUSTIC WIND TUNNEL
FOR STUDYING TACV AERODYNAMIC NOISE SOURCES

attached to various sections of the plate. To test the effect of track configuration on sound generation, we replaced the long plate with shorter straight sections or with U-shaped sections of various dimensions.

Acoustic measurements were made with a B&K model 4131 1-in. condenser microphone with random incidence corrector. Spectrum analysis was performed on a GR Model 1521 1/3-octave band real-time analyzer; the analyzer has a weighting network which allows direct recording of the sound power spectrum through a known con-version from sound pressure level to sound power level for the semireverberant space surrounding the free jet. Steady flow mea-surements were made with a Pitot-static tube attached to a pace Model P71 differential pressure sensor. Turbulence spectra were measured, when applicable, with a BBN hot-wire probe and a DISA Model 55015 anemometer and DISA linearizer.

3.3   Experimental Results

Lip Noise

The laboratory simulations of lip noise proved difficult for several reasons: (1) the boundary layer on the inclined plate was inherently laminar and the favorable pressure gradient combined with the smooth inflow tended to preserve that condition; (2) arti-ficial tripping of the boundary layer resulted in a nonrealizeable flow field; (3) noise from leaks in the room appeared at the same frequencies in the spectrum as the lip noise. The lip noise pre-diction scheme outlined in Sec. 3.1 was specialized to fully de-veloped turbulent boundary layers and turbulent wall jets. Since the flow field for the TACV lip noise studies was not like a naturally developed turbulent boundary layer, exact conformance of the experimental results with the previously described prediction

scheme was not expected. Figure 9 presents a summary of the lip-
noise data measured in the wind-tunnel simulations and can be
compared with Fig. 6 for both naturally developed and artificially
tripped boundary layers. The agreement is reasonably good, al-
though the prediction scheme overestimates the radiated sound.
(We note here that the parametric dependence of lip noise predicted
by Eq. 9 was verified experimentally.)

Since the predictions are in reasonable agreement with mea-
sured data, we have taken the liberty to extrapolate the labora-
tory measurements to full-scale jet speeds using the boundary
layer thicknesses obtained in the wind-tunnel tests. (Boundary
layer thicknesses on the real TACV will be substantially greater
unless boundary layer control measures are employed.) The immedi-
ately obvious result is that the 1/2 psi cushion pressure gives
lower lip noise than the 1 psi pressure — i.e., 248 fps vs 350 fps
exit velocity. This result is consistent with the basic parametric
dependence of lip and edge noise and suggests a means of control-
ling this noise at the source. Further studies of lip noise should
include the effect of upstream turbulence and fully developed tur-
bulent boundary layers.

The boundary layer thickness on the lip of the full-scale
TACV may be estimated by Eq. 16, with 1/2 the vehicle width (i.e.,
5 ft here) as the pertinent length dimension and the exit velocity
as the pertinent velocity term. The results in predicted lip
boundary layer thicknesses are 0.077 ft for the 1 psi cushion
pressure and 0.08 ft for the 1/2 psi cushion pressure. Applying
Eq. 9 and Fig. 6 to each of these cases results in the two curves
shown in the upper left-hand portion of Fig. 9. These are the
predicted lip-noise spectra for the full-scale TACV, if no boundary
layer control measures are taken. By way of comparison, the extra-
polated laboratory data probably represents the lower bound of lip
noise, if boundary layer control is applied.
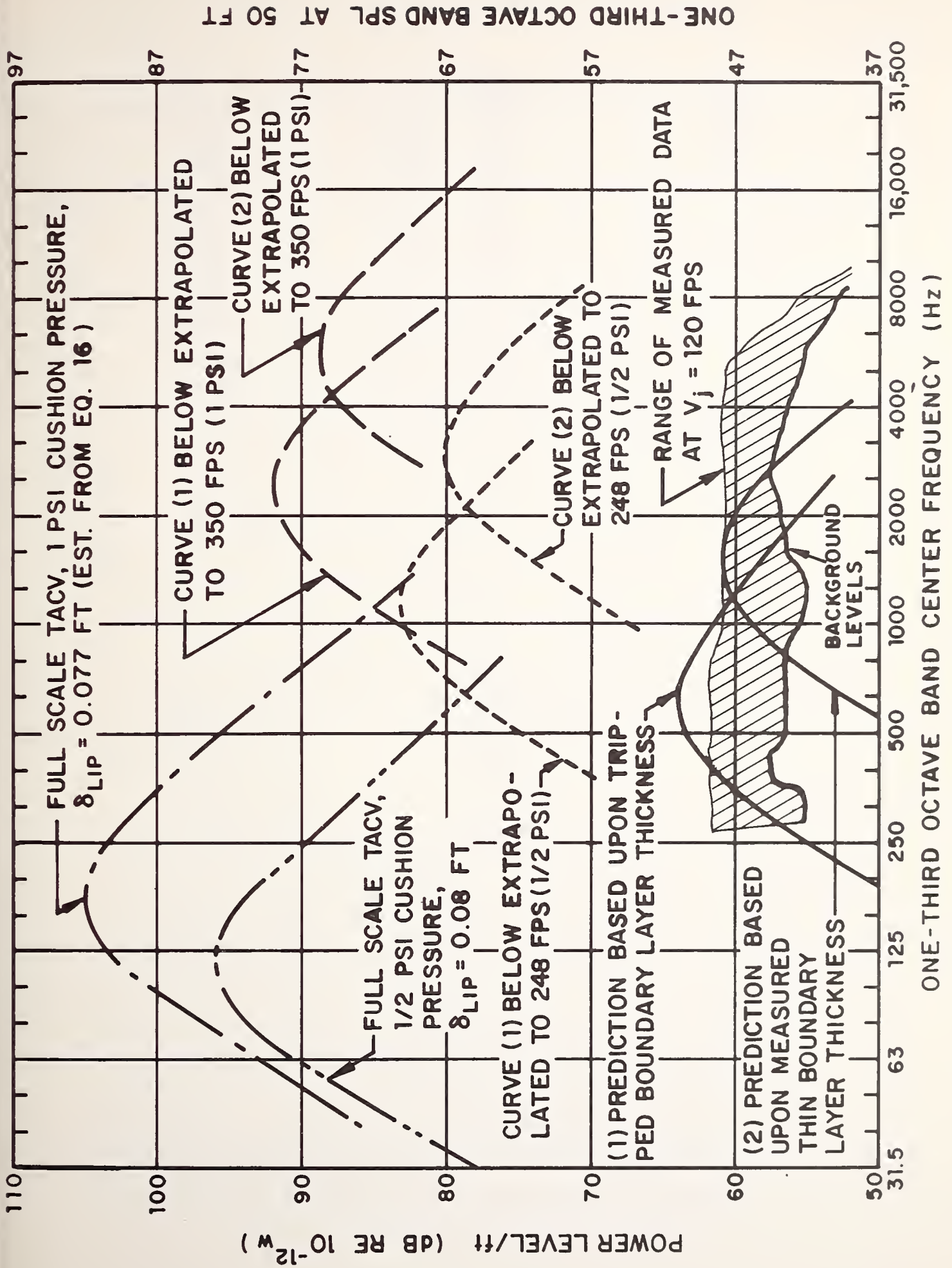
FIG. 9   TACV LIP NOISE FROM A 1-FT SKIRT SECTION; LABORATORY DATA AND PROJECTION TO FULL-SCALE OPERATING CONDITIONS

Edge Noise

The two proposed track configurations, a U and an inverted T, have been subjected to a preliminary study of the edge noise resulting from the interaction of the escaping air with the edges of the track. Results show that edge noise may be one of the predominant sources associated with TACV operation. The noise, as expected, was reasonably modeled by Eq. 9, although this equation and the associated nondimensional spectrum (Fig. 6) consistently underestimated the edge sound measured. We assume that the reason for this discrepancy is that the local turbulence intensity and wall shear stress were not explicitly included in the formulation of Eq. 9 and that this turbulence shear stress interaction is responsible for fluctuating wall pressures and, thus, edge sound. This hypothesis is supported by experimental results which show that edge noise increased as turbulence intensity increased, while the mean velocity profile (i.e., shear stress distribution) remained constant. In any event, the parametric dependence of the measured edge noise was in agreement with Eq. 9, and Fig. 6 closely predicted the frequency of the spectral peak in all cases.

T-shaped (Flat) Track

A section of T-shaped track was modeled by a 6-in. flat plate (3/4-in. thick) extending from the "ground plane" of the air cushion. Sound measurements were made at air speeds up to 120 fps. Figure 10 shows a comparison of the typical measured spectrum at 120 fps exit velocity with the predicted spectrum based on the mean flow parameters. (At this point, no explanation beyond that given above is offered for the higher measured sound levels.) The lab data and predicted spectrum are extrapolated to full-scale for the case of 1 psi and 1/2 psi cushion pressure — i.e., V_j of 350 and 248 fps, respectively. It appears that this noise source would be most

ONE-THIRD OCTAVE BAND SPL AT 50 FT

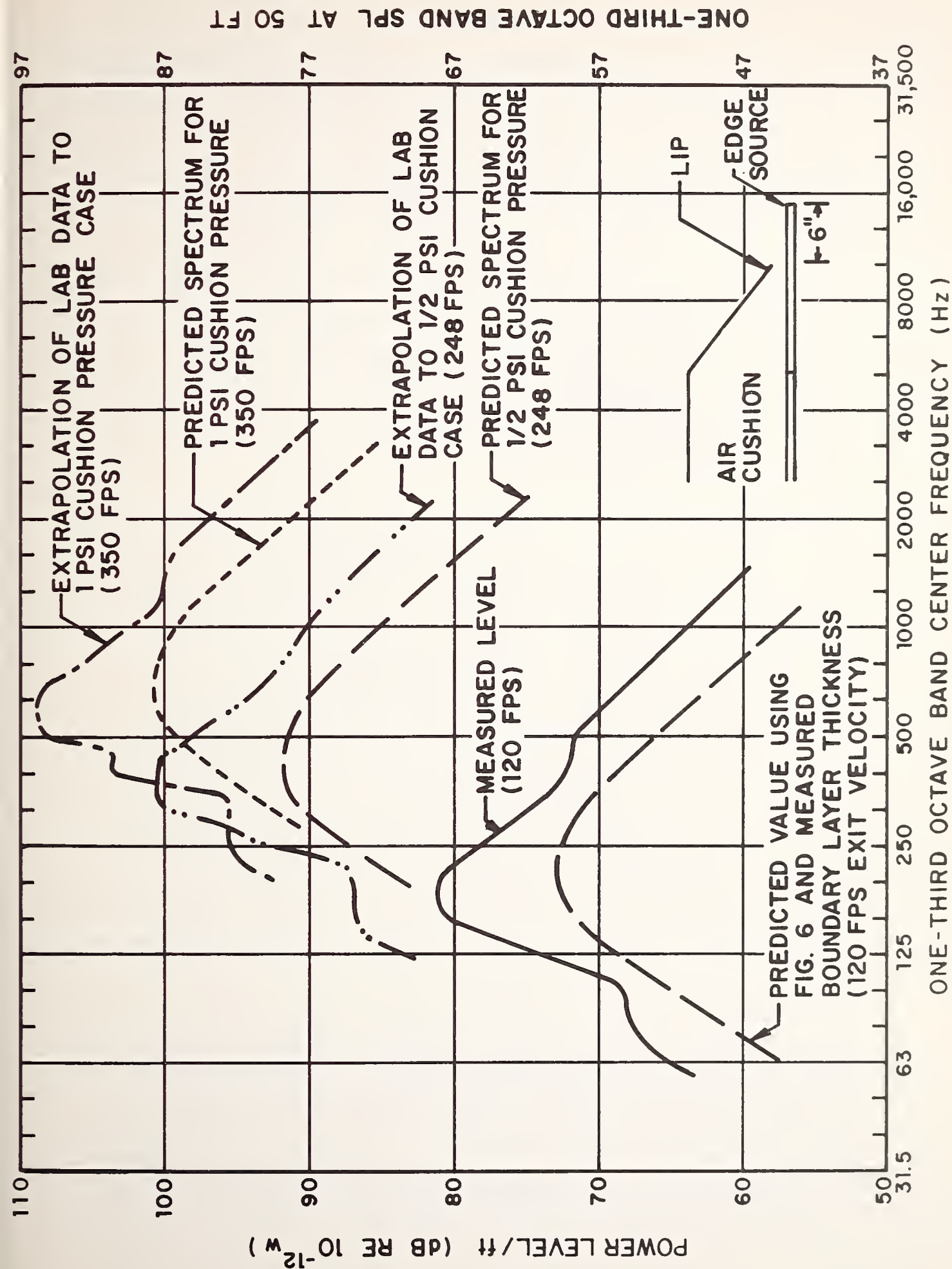FIG. 10   NOISE DUE TO FLOW FROM A 1-FT SECTION OF TACV SKIRT OVER THE EDGE OF A
3/4-IN.-THICK FLAT PLATE, 6 IN. FROM SKIRT LIP

ONE-THIRD OCTAVE BAND CENTER FREQUENCY (Hz)

POWER LEVEL/ft (dB RE 10⁻¹² w)

troublesome in view of the sideline criteria. However, some further considerations are in order. The directivity pattern of the sound has a null in the plane of the plate [6-8] and the peak of the sound spectrum is reduced by a thicker edge. In addition, the smaller gap expected for TACV cushions will probably lead to lower noise levels. All these effects would be advantageous toward achieving low sideline noise levels. The reduction achievable as a function of edge thickness is illustrated in Fig. 11. The beneficial effects of edge thickness appear to be wavelength-dependent, but such a parametric description has not yet been achieved. The important scaling parameters associated with the "thick edge" effect should be studied further.

U-Shaped Tracks

U-shaped track sections of various heights were simulated by attaching plates at 90° angles to the end of the 6-in. plate (see Fig. 12). Again, the general parametric behavior of the sound was predicted by Eq. 9 and Fig. 6. However, in some instances, secondary peaks appeared in the spectrum, apparently resulting from high-speed flow in the right-angle bend. An example is shown in Fig. 12 for the case of the 17-in.-high leg of the U. Equation 9 and Fig. 6 predicted quite accurately the primary spectral peak but the lower frequency peak is presently unexplained. As before, the laboratory data and predicted spectrum (at 120 fps) are extrapolated to full-scale for 1/2 psi and 1 psi cushion pressures and, again, rather high levels are found.

The following points should be considered with regard to the U-shaped track: (1) the sideline directivity pattern has no null since the source orientation has been turned 90° from the case of the T-shaped track; (2) edge thickness should have the effects shown previously; and (3) a higher side wall (deeper U) would result in lower velocities in the vicinity of the edge, and thus,
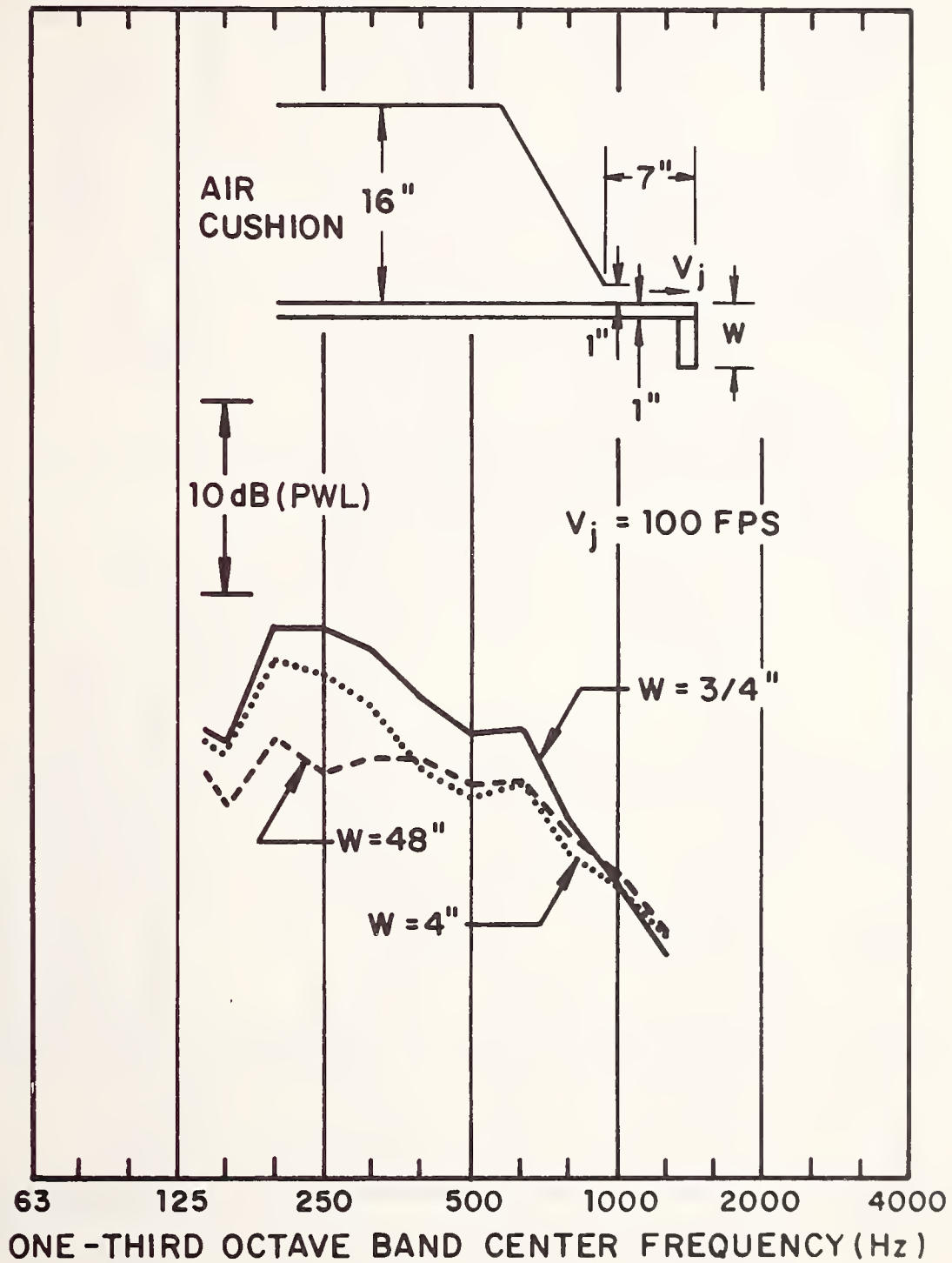
FIG. 11   RELATIVE REDUCTION OF EDGE NOISE DUE TO EDGE THICKNESS
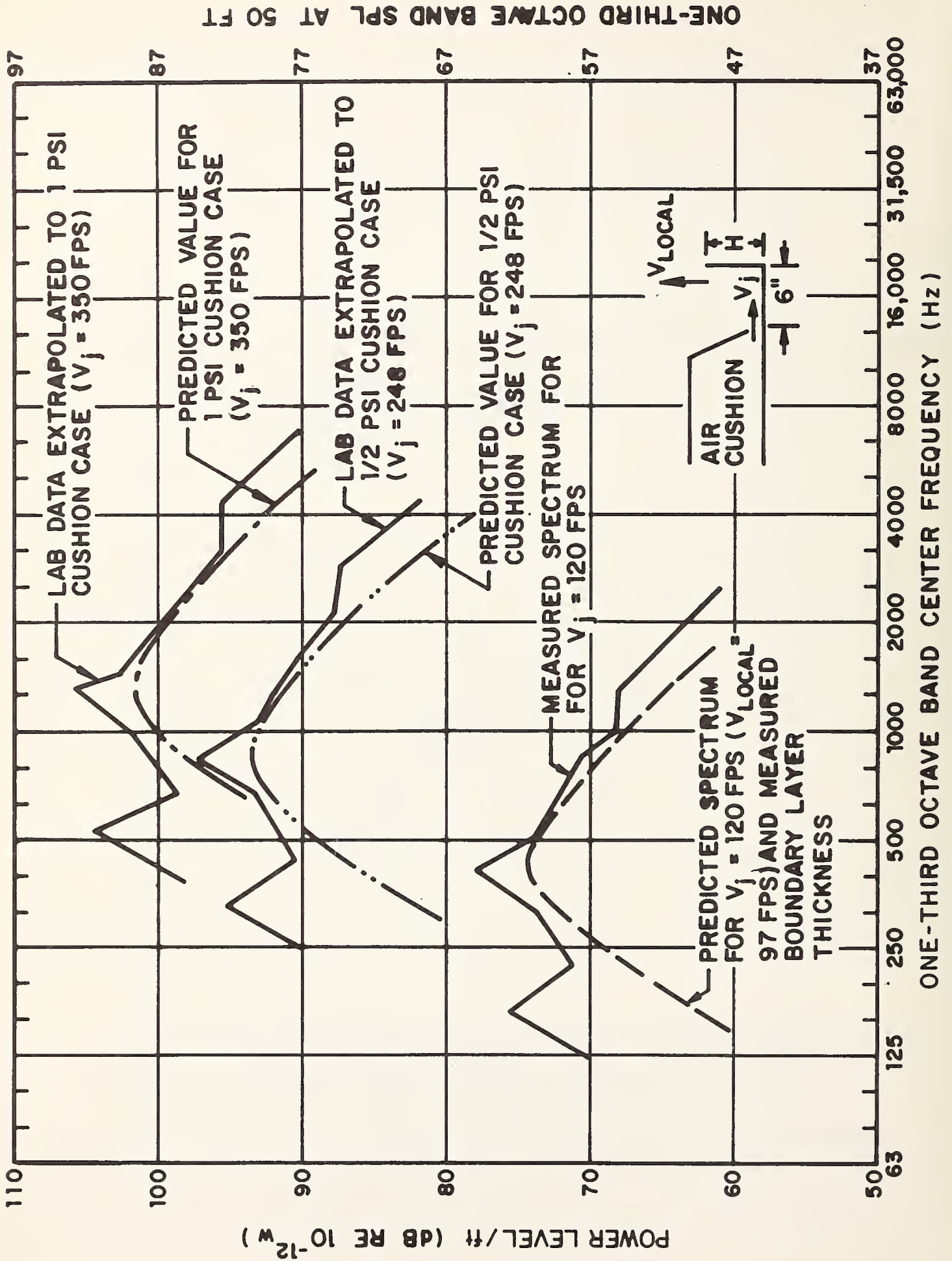
FIG. 12   NOISE DUE TO FLOW OVER A 1-FT SECTION OF U-SHAPED TRACK (H=17 in.);
LAB DATA AND PREDICTION FOR FULL SCALE

in lower sound levels as predicted by Eq. 9. Similarly, short
sidewalls will result in higher sound levels; for example, in wind-
tunnel tests, a 5-in.-high track produced about 9 dB more sound
than the 17-in.-high U-shaped track.

Noise From Flow Over Small-Scale Track Roughness

The relationship of Eq. 18 was tested experimentally and
found to agree reasonably well with measured data. The prediction
scheme overestimated, by about 5 dB, the sound measured from flow
interaction with coarse sandpaper granules attached to the large
(10-ft) smooth surface. Figure 13 shows the comparison of experi-
ment with predictions and the contribution of "roughness noise" to
full-scale track noise for the case of 1 psi cushion pressure. It
is apparent that, if the spectral peaks of lip and edge noise are
successfully reduced, roughness noise will become very important.

Direct Radiation From T.B.L.

Equations 6 and 8 were applied to the predictions of boundary
layer noise from a smooth-skinned TACV having the following geo-
metric and aerodynamic parameters:

Geometric

Length	$\ell \approx 80$ ft
Width	10 ft
Surface Area	$S \approx 3 \cdot 10 \cdot 80 = 2400$ ft^2

Aerodynamic

Forward Speed	$V_F = 150$ mph
Displacement Thickness at Rear of TACV	$\delta^* \approx 0.108$ ft
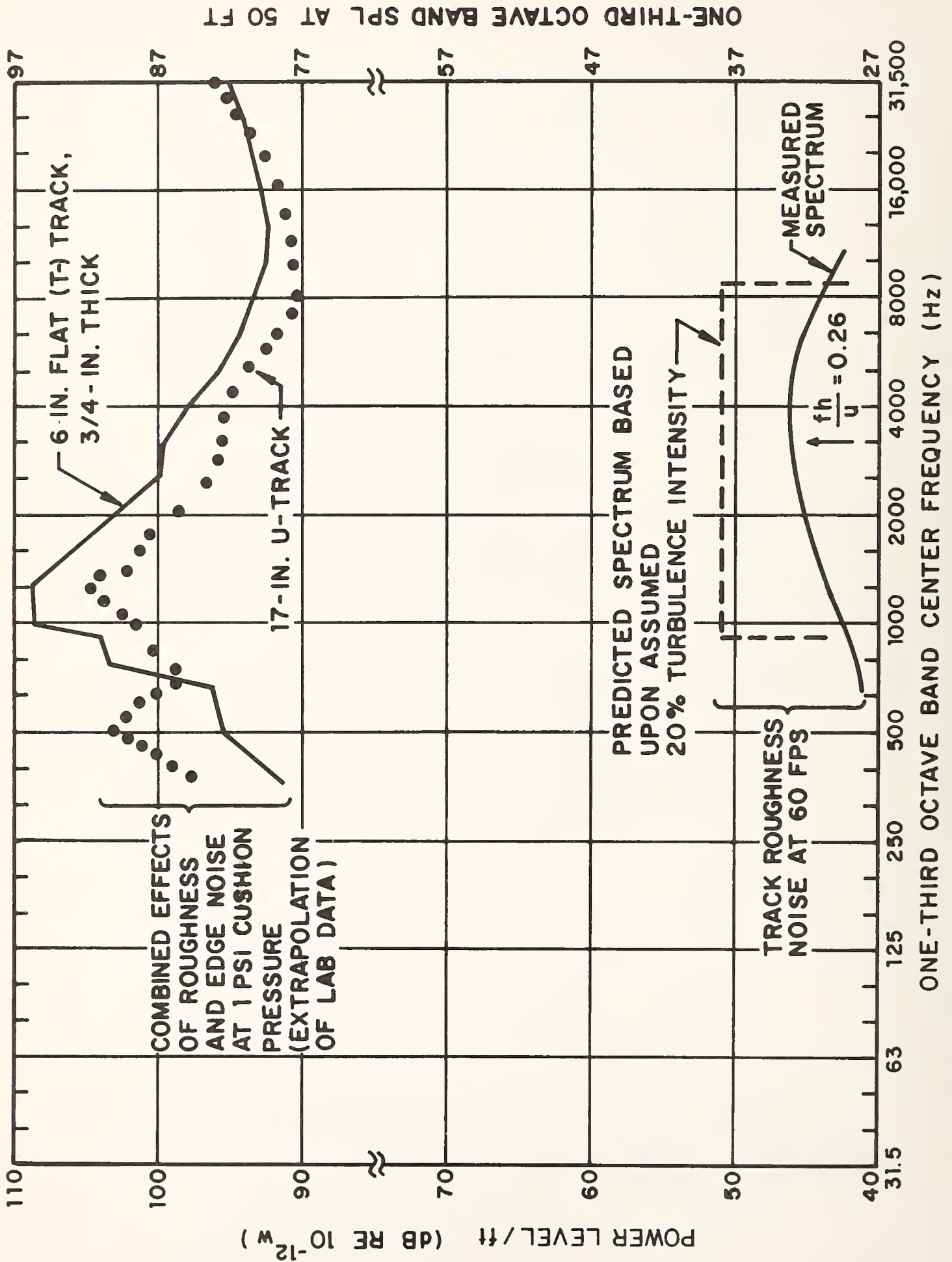
FIG. 13   EFFECT OF SURFACE ROUGHNESS ON TRACK NOISE

Equation 6 thus predicts an overall sound power level of 110 dB, and Eq. 8 predicts a spectral peak at 330 Hz. If one considers qualitatively the observation in Ref. 5 for flow over gliders with surface discontinuities, then a higher level is expected with a spectral peak at a lower frequency. Both these effects are shown in Fig. 14; the actual spectrum to be expected probably lies some- where between the two curves shown here.

ONE-THIRD OCTAVE BAND SPL AT 50 FT

TBL INTERACTION WITH
SURFACE DISCONTINUITIES
USING GLIDER OBSERVATION

TBL RADIATION FROM
VEHICLE FREE FROM
DISCONTINUITIES

ONE-THIRD OCTAVE BAND CENTER FREQUENCY (Hz)

POWER LEVEL (dB RE 10^{-12} W)
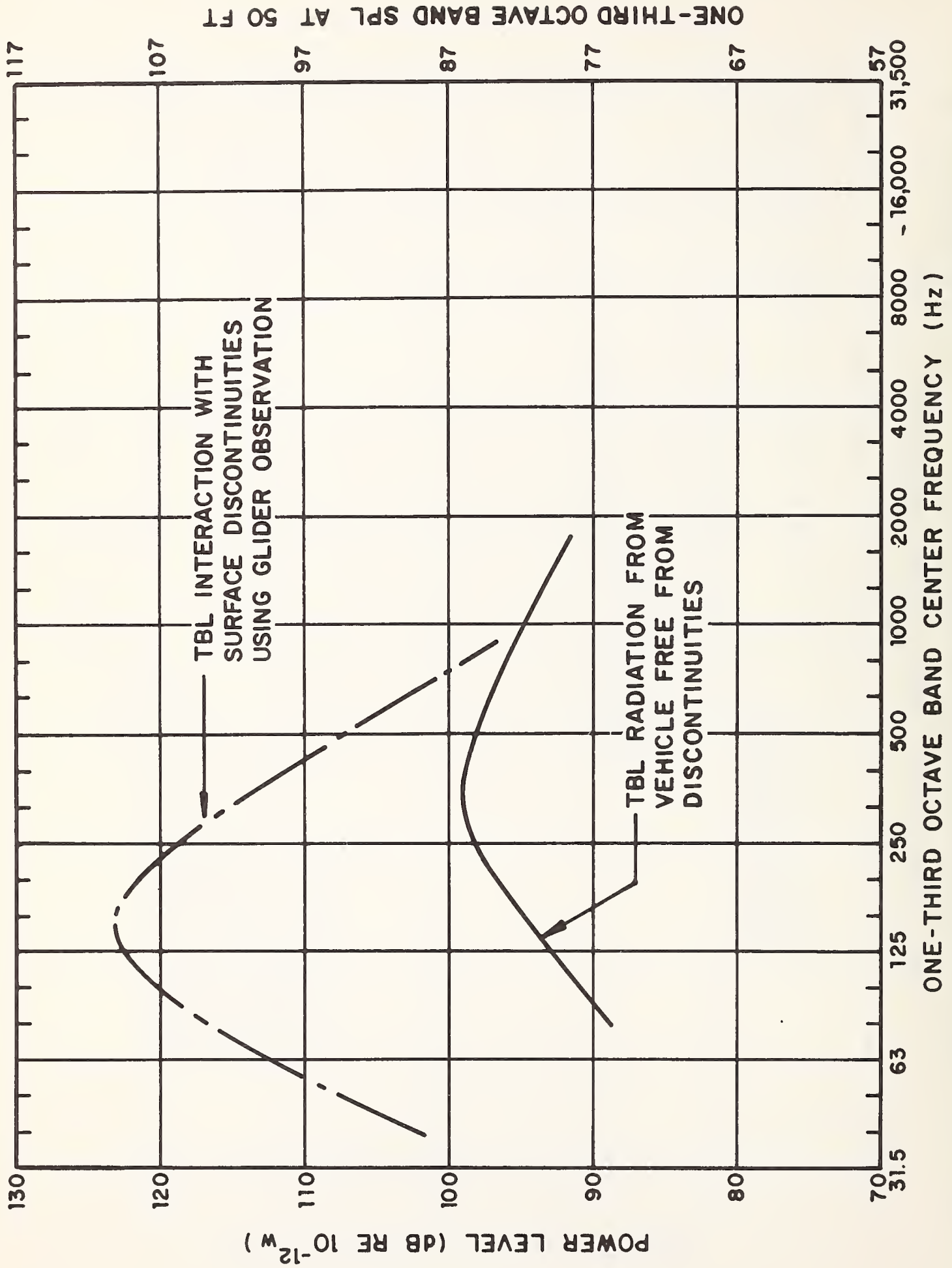
FIG. 14   ESTIMATE OF SOUND RADIATED FROM BOUNDARY LAYER FROM 80-FT TACV TRAVELING
AT 150 MPH

4. LIM NOISE

The principal source of data on linear induction motor (LIM) noise was obtained from the French LIM vehicle at Gometz (see Appendix E). At 21 ft from the reaction rail, we measured a pure tone component of 82 dB at approximately 800 Hz. The A-weighted level is 81, which projects* to 76 dB(A) at 50 ft, 4 dB(A) above the 73 dB(A) DOT criterion. Observers report that this noise is radiated from the reaction rail, which is said to ring during a vehicle passby.

The implications of reaction-rail ring with regard to U.S. TACV operation are unclear at this time, largely because of the present uncertainty associated with the mechanism of reaction-rail excitation and radiation. Considering only differences in power and size, one would expect the larger U.S. TACV system, traveling at higher speed, to generate higher noise levels. If, however, the French and U.S. propulsion systems differ significantly in the way they excite a reaction rail, wayside noise could possibly be less. Clearly, the mechanisms of rail excitation and radiation must be diagnosed to ensure — before the U.S. system is built — that it will be quiet.

----

* Since the reaction rail is a "line source", we extrapolate noise on the basis of 3 dB per distance doubled.

5. CURRENT-COLLECTOR NOISE

As the current collector slides along the third rail, sound
is generated by a variety of mechanisms, which may be identified
as

- vibration due to macroroughness,

- vibration due to microroughness,

- vibration due to intermittent contact, and

- electrical arcing.

The first mechanism involves fluctuating forces at the interface
of the rail and contact shoe as the shoe passes over bumps and
depressions in the third rail. These irregularities have char-
acteristic wavelengths that are long compared to the dimensions
of the shoe. Vibratory motion of both the rail and the shoe
radiates sound to the environment. Although this mechanism is
easily characterized, it may not be the most important source
of current-collector noise, because of its low frequency.

The second mechanism involves irregularities that have wave-
lengths that are small compared to the dimensions of the contact
shoe. This relationship seems to account for the broadband "hiss"
that normally emanates from two bodies (e.g., a book on a table)
sliding over each other. The manner in which surface roughness
contributes to vibration and sound is not at all clear at this
time.

Vibration due to intermittent contact (bouncing of the con-
tact shoe) is a significant phenomenon in rapid transit systems.

When the shoe reaches a joint in the third rail*, contact is lost and the resulting series of impacts can be a significant noise source.

Associated with loss of shoe/rail contact is electrical arcing. When contact is lost, electric current does not cease to flow. Rather the air between the shoe and rail is ionized and carries large current levels. This ionized air is extraordinarily hot and expands very rapidly, causing a cracking sound that may sometimes be heard near rapid transit vehicles.

We expect that TACV current collection systems will be designed to avoid loss of contact and concomitant bounce and arcing. We therefore concentrate on sound generated by rail roughness.

5.1 Vibration Due to Macroroughness

We present an analytical model of the vibration and radiation associated with large-scale rail roughness to (1) provide some guidance for tolerances that can be applied to rail alignment and roughness, (2) indicate the effects on noise of various rail and shoe parameters, and (3) allow for estimating the contribution from macroroughness to the total noise level. The schematic diagram in Fig. 15 shows a rail, with greatly exaggerated roughness, and a contact shoe moving along it with vehicle velocity V. If $y(x)$ is the undeformed elevation profile of the rail, then the position of the shoe w may be defined by

$$w = y - \delta , \tag{19}$$

_____

* Third-rail joints are frequent on many conventional rapid transit systems which often use 39-ft sections of worn-out running rail.
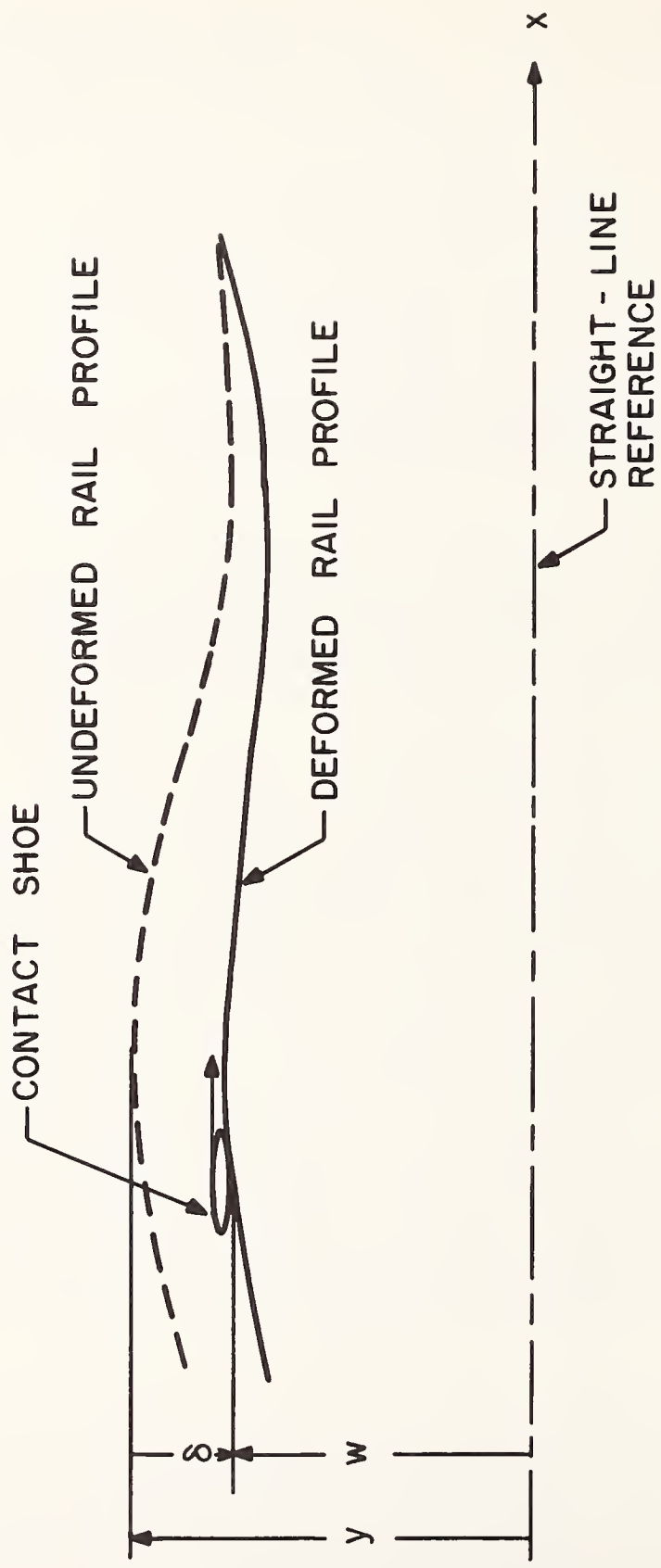
FIG. 15. RAIL/CONTACT SHOE GEOMETRY

where δ is the vertical deformation of the rail beneath the shoe.
Differentiating both sides of Eq. 19 gives

$$\dot{w} = y'V - \dot{\delta} , \tag{20}$$

where the dot denotes differentiation with respect to time and
the prime with respect to distance x. Noting that the fluctuating
force F acting at the interface is related to the shoe and rail
impedances (Z_s and Z_r) by

$$F = Z_s \dot{w} = Z_r \dot{\delta} , \tag{21}$$

we find that the motion of the shoe and rail may be given by

$$\dot{w} = \frac{Z_r}{Z_r + Z_s} \, y'V ; \tag{22}$$

$$\dot{\delta} = \frac{Z_s}{Z_r + Z_s} \, y'V . \tag{23}$$

Equations 22 and 23 illustrate several significant phenomena.
First, the vibration level is linearly proportional to the vehicle
speed. Hence, sound radiation from this mechanism would depend on
20 log V*. Second, if the rail impedance is significantly higher
than that of the shoe, which is likely, then

$$\left. \begin{array}{l} \dot{w}_1 \approx y'V \\[2em] \dot{\delta} \approx \dfrac{Z_s}{Z_r} \, y'V \end{array} \right\} \quad \text{for } Z_r >> Z_s \quad . \tag{24}$$

---

* Assuming that all of the excitation of any significance lies
  in the acoustic frequency region for speed ranges of interest.

These relations show, as one might expect, that the shoe almost
exactly follows the rail contour. However, the rail motion is
proportional to Z_s/Z_r. Hence, it is desirable to make the shoe
mass m as small as possible so as to minimize Z_s, which approxi-
mately equals $j\omega m$ at frequencies below the first shoe bending mode.

5.2 Radiation from the Current-Collector Shoe

Although we were unable to obtain data on noise generated by
a rapid transit current-collection system (see Appendix F), we
were successful in measuring shoe vibration levels. A sample
spectrum is shown in Fig. 16. From these data, we may estimate
the sound radiated by the shoe.

At low frequencies, where the wavelength of sound is larger
than the shoe dimension, the shoe behaves like an acoustic dipole.
As the shoe vibrates, air flows from one face to another. Slight
forces accelerate the air as it "sloshes" back and forth and
compress and expand it, causing sound waves. The resulting
radiated power W may be related to the rms acceleration a by

$$W = \frac{\delta\omega^2 A^3 a^2}{48\pi^2 c^3} \quad \text{for } \lambda \gg r \; , \tag{25}$$

where ρ is the density of air, c is the speed of sound, A is the
shoe planform area, λ is the wavelength of sound, and r is the
effective show radius as shown in Fig. 17a.

Equation 25 is based on a dipole model of shoe vibration
with each element of the dipole separated by twice the radius r,
as illustrated in Fig. 17b. The volume velocity associated with
each element is taken to be the shoe planform area multiplied by
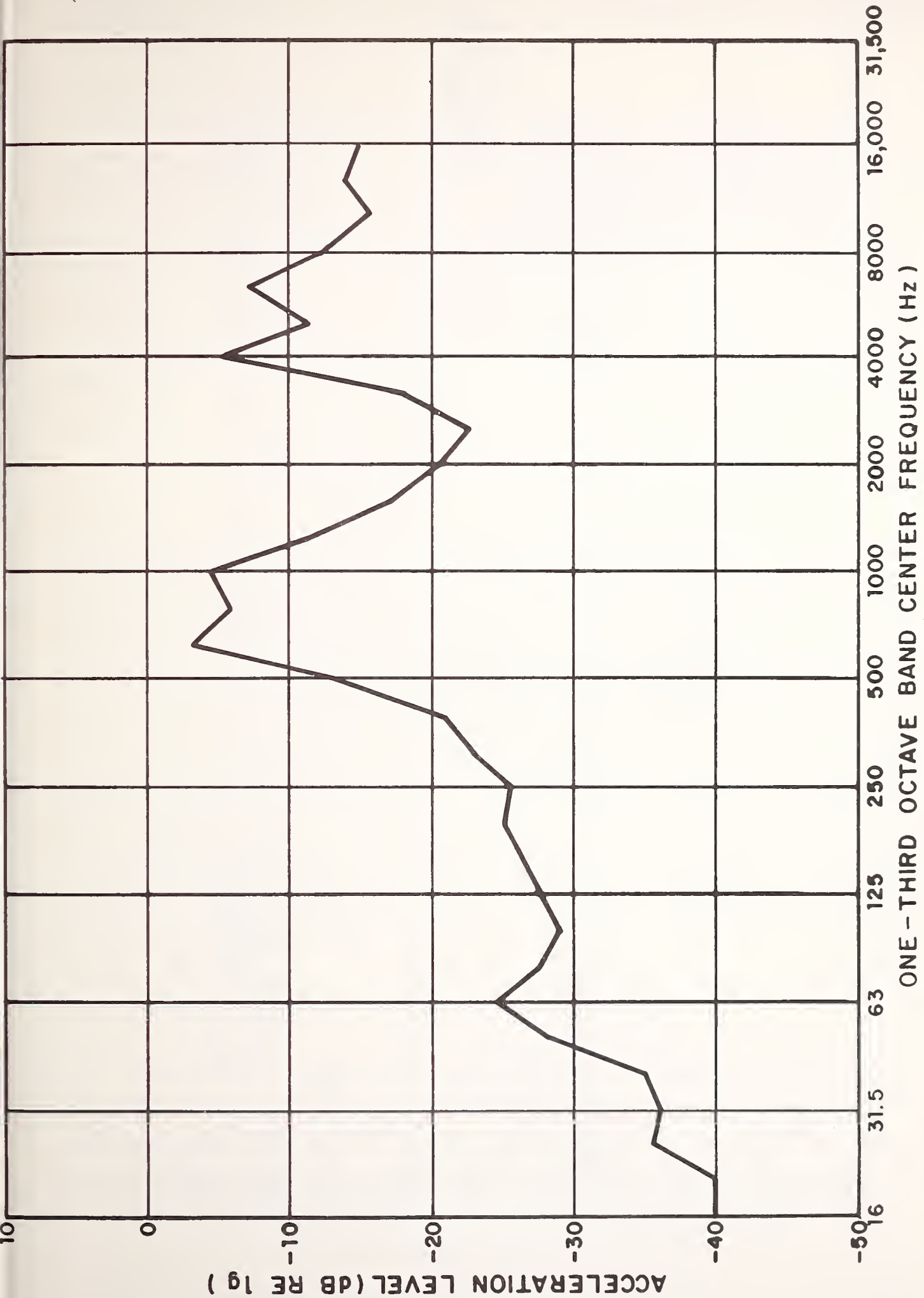the vertical velocity.

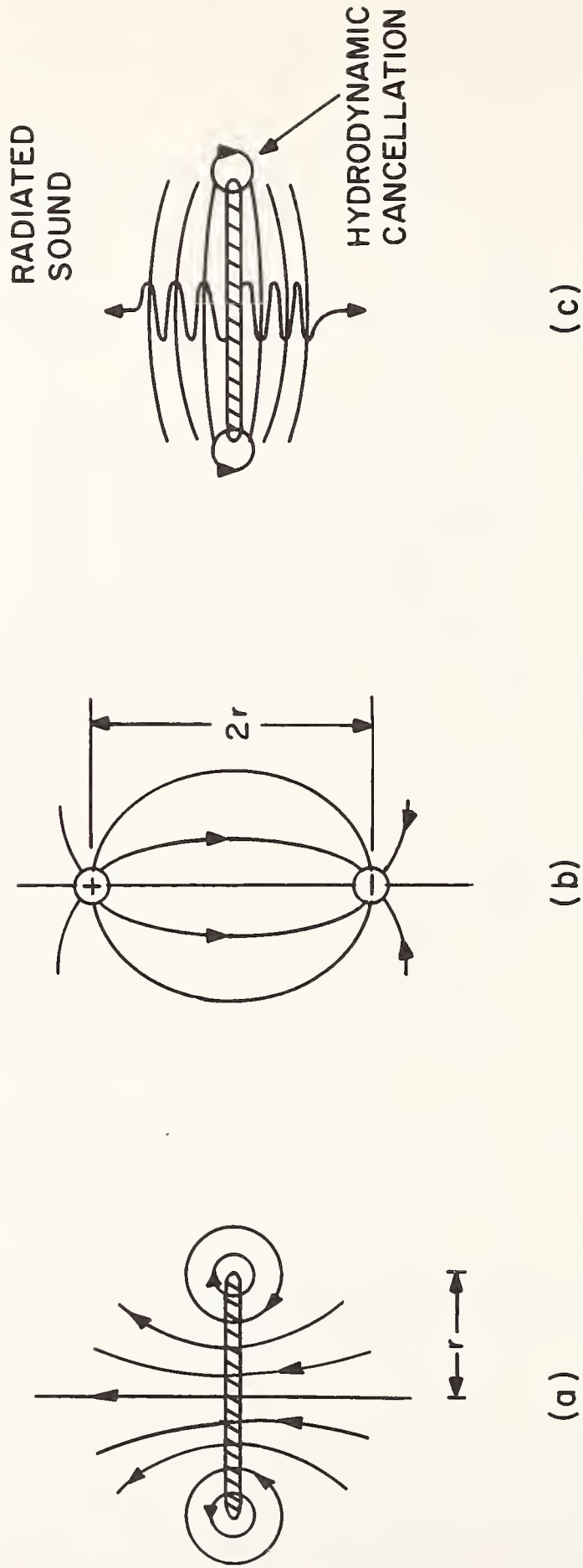FIG. 16 RAPID TRANSIT CAR CONTACT SHOE VIBRATION AT 17 mph

FIG. 17.   HYDRODYNAMIC FLOW AND SOUND RADIATION PATTERNS FOR (a) A CONTACT SHOE
AT LOW FREQUENCIES (b) AN EQUIVALENT DIPOLE MODEL, AND (c) A SHOE AT
HIGH FREQUENCIES

At high frequencies, where the wavelength of sound is a
great deal smaller than the shoe width, the air cannot flow from
one face to another, except in the vicinity of approximately one-
half wavelength from the edge (see Fig. 17c). The air at the
remaining surface portions cannot "push" other air particles
around the edge. Instead, it is compressed and expanded. Ac-
cordingly, sound radiation is very efficient and the acoustic
power flow may be expressed

$$W = \frac{\rho c A a^2}{4\pi^2 f^2} \quad \text{for } \lambda << r .\tag{26}$$

Equations 25 and 26 are used to determine the sound power level
PWL (dB re 10^{-12} w) and the acceleration level AL (dB re 1 g); the
results are plotted in Fig. 18, using the measured shoe area of
1/3 ft^2. The actual PWL/AL relation is likely to follow the
smoothed curve shown by the dashed line. From this smoothed curve
and the data in Fig. 16, we estimate the radiated PWL and SPL at
50 ft (see Fig. 19); the dB(A) level is only 40. If the noise
follows the 20 log (speed) law suggested by Eq. 24, the wayside
level at 50 ft will be approximately 60 dB(A). Even if the level
increases according to 30 log (speed), as it does from the inter-
action of steel wheels on steel rails, the wayside noise level
would be about 70 dB(A).

5.3 Role of Current Collector Noise

The total contribution of current collector noise is uncertain
at this time. It appears that radiation from a current-collector
shoe will not be significant (This conclusion is tentative owing
to the small amount of data and rather large extrapolations on
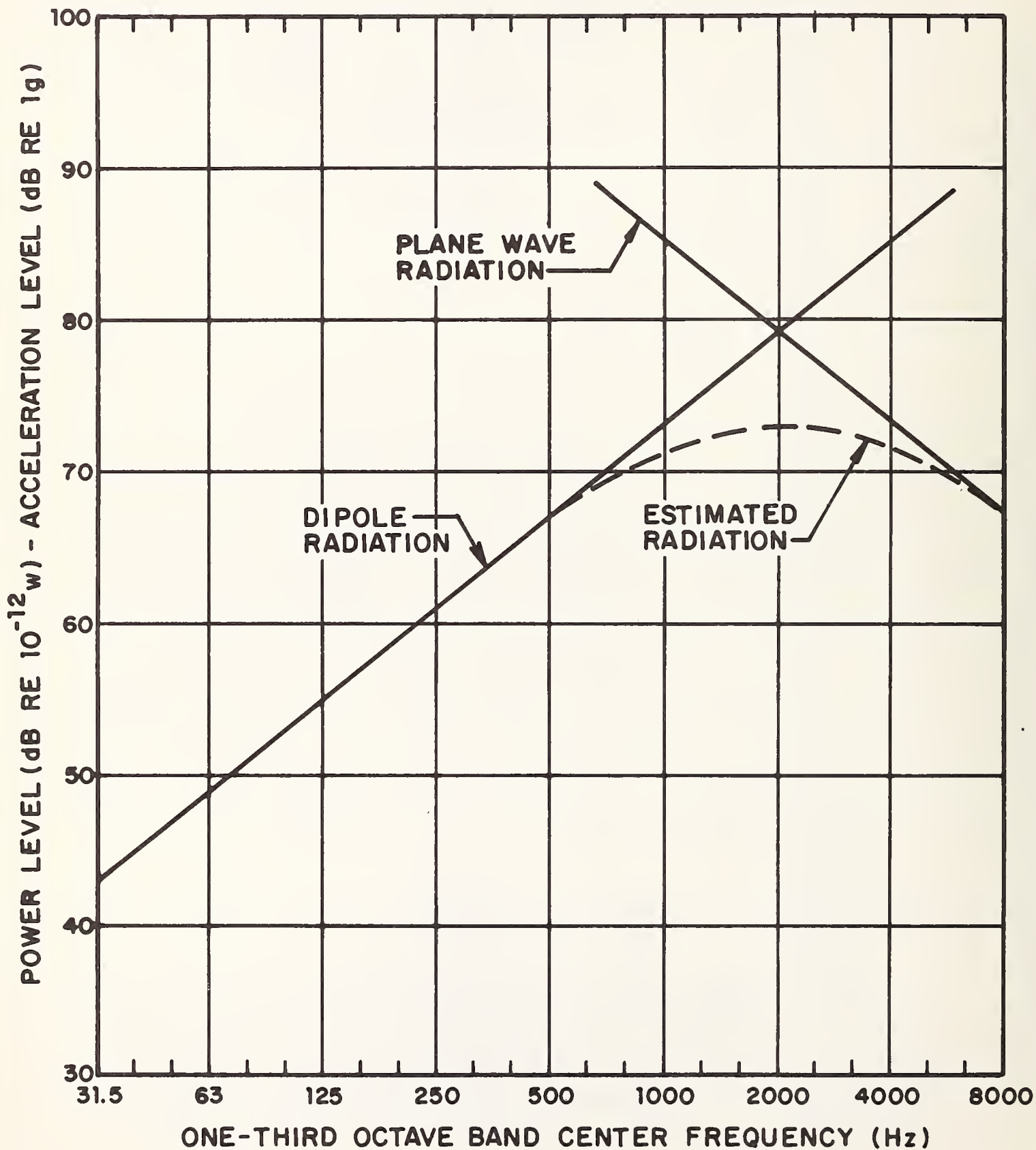
FIG. 18   ESTIMATED RELATION BETWEEN PWL AND AL FOR CONTACT SHOE
          RADIATION
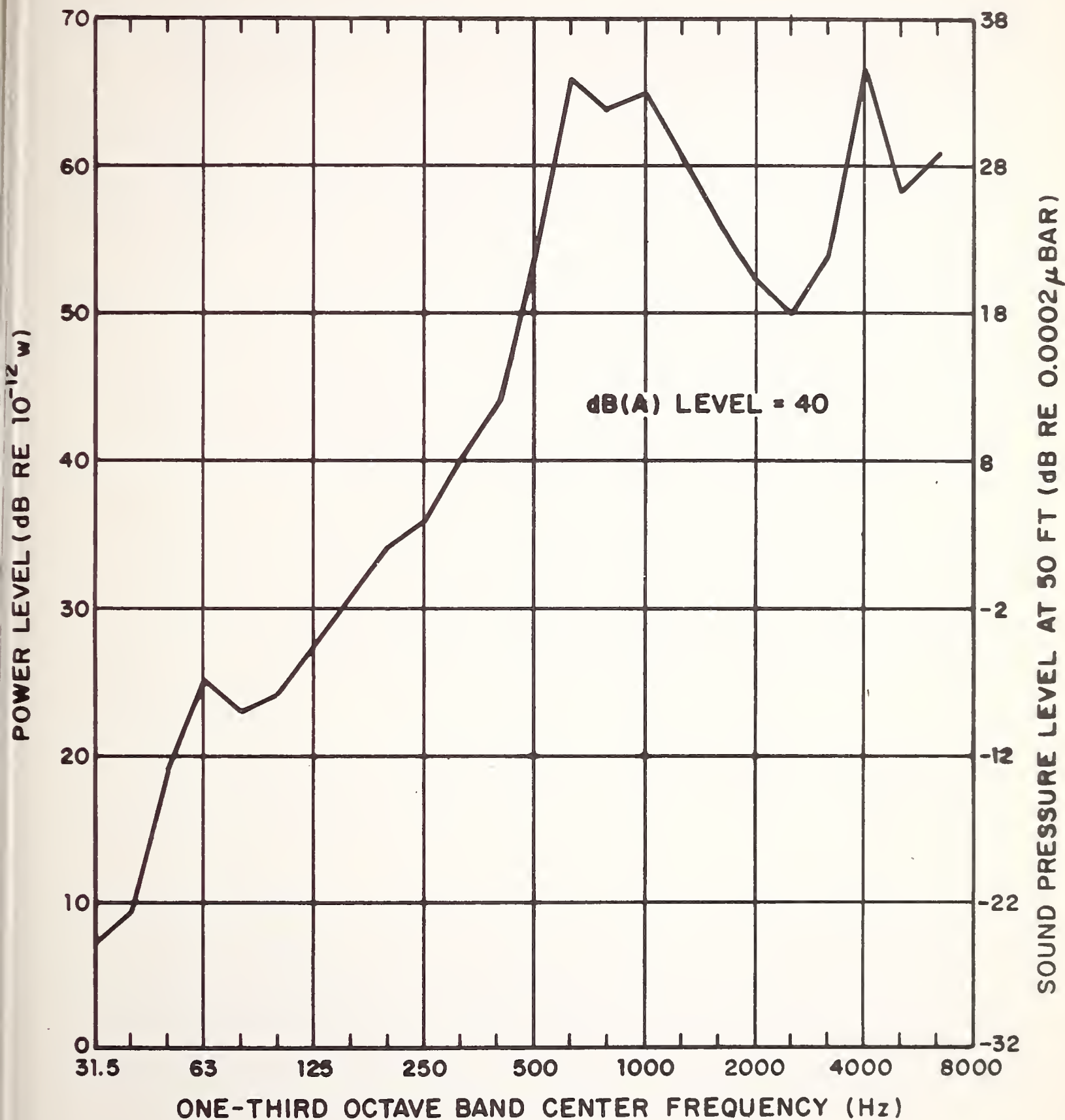
FIG. 19   ESTIMATED NOISE LEVEL FROM A THIRD RAIL CONTACT SHOE
AT 17 mph

which it is based). However, radiation from a vibrating rail,
which has a much larger area, could be 10 to 20 dB higher, a
level that probably would be significant at high speed.

If current-collection systems are designed with a view to-
ward noise control, collector noise will probably not be a sub-
stantial problem. Such design would require lightweight, small
current-collector shoes and third rails of minimum cross-sectional
dimensions. The desirability of using thin third rails is obvious
when Eq. 25 is applied to the vibration of a rail modeled as a line
of dipoles. The radiated power is proportional to the area (one
decimeter for a line) cubed. Thus, minimizing the width and
height of the rail will also minimize the sound radiation.

6. SUMMARY AND CONCLUSIONS

Six categories of potential noise sources associated with TACVs have been identified in the present study: (1) the air compressors, (2) the air cushion, (3) lip and edge noise, (4) the boundary layer on the vehicle surface, (5) the linear induction motors, and (6) the current-collector devices.

There is practically no available information on the noise emission characteristics of the first four sources and relatively little on the last two. Therefore, a major portion of the effort within this study was directed toward identifying source mechanisms and developing appropriate models and prediction techniques. In the light of these limitations, we attempted to predict the noise generated by and radiated from each of these sources and to assess their relative importance in overall sound emission, so that noise control measures can be directed towards the more predominant sources. The results of the study show clearly the need for substantial control measures to meet specified 50-ft sideline levels of 73 dB(A) for cruising and of 63 dB(A) for station stopover.

The evaluation of the various source categories led to the following conclusions:

Compressor Noise

Noise emission from the axial flow compressors was estimated on the basis of some available empirical prediction schemes. These estimates indicate that compressor noise — with the exception of air cushion noise — is highest of all sources considered.

Since only very preliminary specifications on the compressors were available, several important geometric and aerodynamic parameters had to be assumed and used as a basis for prediction.

Air enters the compressor intake through an intake duct, and/or through an intake plenum, sound can be attenuated along these transmission paths.

Air Cushion and Flow over Track

Associated with the ejection of the cushion air from the skirt are several individual sources: (a) fluctuations in forces on the track surface due to flow impingement; (b) interaction of turbulent boundary layer developed under the skirt with the lip of the skirt (c) interaction of the turbulent wall jet with the edges of the track; and (d) free turbulent mixing along the periphery of the line-jet emanating along the lip of the skirt. Estimates on the sound generation of these various mechanisms indicate the predominance of lip-noise and edge noise.

Surface-Flow Turbulence

Radiation from the turbulent boundary layer on the vehicle surface is likely to be of minor importance compared to the other sources. Protuberances or cavities in the surface structure of the vehicle could give rise to discrete frequency noise radiation, but such sources can easily be eliminated. However, vibrations of the vehicle skin can be excited by the boundary layer; thus, until specific TACV designs are decided upon, the importance of skin vibration cannot be accurately estimated.

Linear Induction Motor

Noise measurements on the French TACV at Gometz indicate that linear induction motors cause a high intensity ringing of the reaction rail at a discrete frequency. There is also an indication that rail bending vibration might cause a relatively low-frequency discrete sound emission. Since the French system is smaller than the system anticipated for the United States, one would project rather high levels for a comparable U.S. system.

Current Collector

Some measurements on a current-collector system were conducted on a rapid transit rail car. The data has not yet been fully reduced, so no reliable evaluation of the role of current-collector noise in the overall sound emission of a TACV can be presented.

7.   RECOMMENDATIONS FOR FURTHER STUDY

The results of the present study indicate several areas in which available information and understanding of noise generating mechanisms is still rather sparse. Therefore, to obtain a better definition of several poorly understood source mechanisms associated with TACV operation and to evaluate the environmental impact of an operational TACV along anticipated routes, technology should be developed in the following areas:

Air Cushion

Better understanding of the effects of skirt-associated turbulence and nozzle geometry on noise emission is necessary. We recommend experiments with well-simulated cushion geometry and upstream turbulence, as well as detailed studies of specific track geometries for edge-noise phenomena. Roughness traces from actual track surfaces should be used to study associated noise phenomena.

Linear Induction Motor

Further investigation of linear induction motor and reaction rail dynamics is required to determine the mechanisms of noise generation and the means for control.

Current Collection

If reduction of currently available current-collector data indicates that this source is important, additional transit car tests and data analysis should be performed.

Compressor Noise

As specific aerodynamic and geometric parameters of the air
compressors become available and details of their installation
are defined, it will be possible to assess their noise output
and the required attenuation much more accurately than at present.
However, there is still much to be accomplished, particularly in
understanding the relationship of the detailed compressor geo-
metry and aerodynamics to discrete-frequency sound emission.
Other areas requiring research are the relationship of the char-
acteristics of the turbulent-wake, impinging on blade rows shed
from upstream blade rows, to sound generation; the transmission
of sound through compressor stages; and the coupling of rotating-
source patterns into adjacent duct work.

Environmental Impact of TACV Noise

Once the noise sources have been defined and the sound power
emitted by each has been determined, the next important step is
to assess peak-dB(A) contours around both the stationary and the
moving vehicle. Selected measurements of background noise in
several candidate communities should be compared with projected
noise levels to arrive at a qualitative assessment of environ-
mental impact.

REFERENCES

1. C.H. Allen, "Noise Control in Ventilation Systems," Chap. 21 in *Noise Reduction*, L.L. Beranek (ed.), McGraw-Hill Book Co., 1960.

2. ASHRAE Guide 1967/68. American Society of Heating, Refrigerating and Air Conditioning Engineers, Inc., New York, New York.

3. Fig. 20 from "Theoretical Studies of Compressor Noise," Wyle Reports WR-68-15, 1968.

4. K.L. Chandiramani and R.W. Pyle, "Vibration and Radiation Properties of a GRP Model Dome (U)," BBN Report No. 1942, November 1970 (Confidential).

5. E.E. Ungar *et al*, "A Guide for Predicting the Aural Detectability of Aircraft," BBN Report No. 2014, January 1971.

6. R.E. Hayden, "Sound Generation by Turbulent Flow over a Trailing Edge," M.S. Thesis, Purdue University, 1969.

7. R.E. Hayden and R.C. Chanaud, "Sound Generation by a Turbulent Wall Jet Flow over a Trailing Edge," Paper FF-10 Presented at the Meeting of the Acoustical Society of America, Spring 1970.

8. R.C. Chanaud and R.E. Hayden, "Edge Sound Caused by Two Turbulent Wall Jets," Paper FF-11 Presented at the Meeting of the Acoustical Society, Spring 1970.

9. W.C. Meecham, "Surface and Volume Sound from Boundary Layers," *J. Acoust. Soc. Amer.*, **37** (3), 1965.

APPENDIX A

COMPRESSOR SOURCE MECHANISMS

A rotating blade is subjected to both steady and fluctuating loads. Steady loads, which are related to the torque, the thrust, and the blade thickness, cause sound radiation because at a fixed point in front of the rotor disk the rotating field appears as an oscillating pressure. The acoustic radiation frequency (the frequency of oscillation) is thus the frequency with which the blade passes the (fixed) point.

Fluctuating loads can be either random or periodic. Inflow turbulence, turbulent blade-surface boundary layers, flow-separation on the blade, and vortex shedding cause *random loads* and generate broadband sound. Peridoic loads, which arise from blade passage through a periodic wake field, from potential field interactions, and sometimes from rotor imbalance and blade vibrations, generate discrete tones.

The frequency and amplitude of the *discrete sound* due to periodically varying loads is basically a function of the geometry of the compressor; radiation frequency is determined by the ratio of the number of rotor to the number of stator blades, the amplitude of the radiated sound being determined by the magnitude of the loads acting on blades. Hence, the most direct way to predict discrete frequency sound is to determine the amplitude from the load characteristic on the blades and to establish the radiation frequencies from the interaction mechanism of subsequent blade rows.

To predict *broadband sound* power, one should determine the magnitude of the random loads on the blades.

A.1 Discrete Frequency Sound Generation

One can expect a sound pulse to be emitted from a blade each
time it experiences a lift or drag force change due to an imping-
ing wake shed from a passing upstream blade. For equally spaced
blades on a rotor or stator disk, this implies the emission of
periodic signals. In a gross sense a pulse is emitted each time
a rotor blade is in line with a stator blade. For an equal number
of rotor and stator blades, this implies the *simultaneous* emission
of pulses from all rotor/stator blades, while for unequal number
of rotor and stator blades (which is the more common case in real-
istic compressors), pulses are emitted at different times, so that
a source pattern rotates around the rotor/stator disk. The rota-
tional speed of this source pattern is not equal to the physical
rotational speed of the rotor. Figure A-1 illustrates the inter-
action of a three-bladed rotor with a two-bladed stator. In condi-
tion (a) a pulse is emitted due to interaction of rotor blade 1,
and stator blade I; the next pulse is emitted due to interaction
of rotor blade 2 and stator blade II, when the rotor has moved a
sixth of the circumference. Thus, in this particular example, the
speed with which the pulses travel around the disk is three times
the rotational speed of the rotor. The speed of the phased array
of source pulses, therefore, depends on the number of rotor and
stator blades that are involved and on the rotational speed of the
rotor. The phase speed is given by

$$U_{ph} = \frac{mB}{|mB - kV|} \, \Omega \; ; \qquad\qquad (A-1)$$

here, B is the number of rotor blades, V the number of stator
blades, and Ω is the shaft rotational speed; m and k are integers
whose importance will be discussed further on.
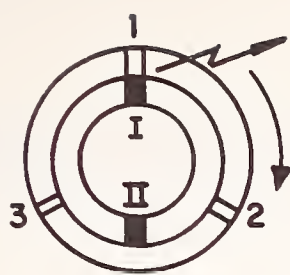
EMISSION OF SOUND PULSE

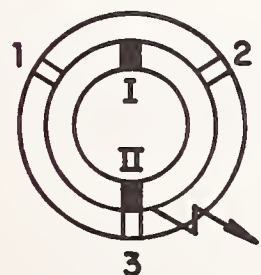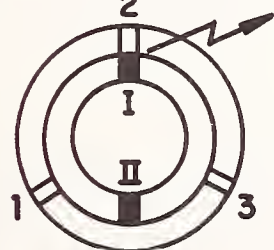1, 2, & 3 REFER TO ROTOR BLADES

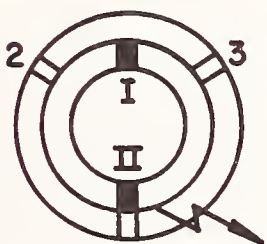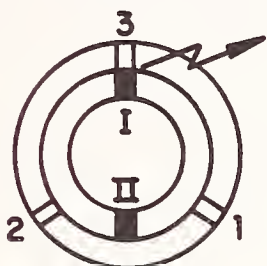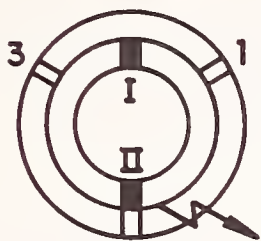I & II REFER TO STATOR BLADES

FIG. A-1.   INTERACTION OF A 3-BLADED ROTOR WITH A 2-BLADED STATOR

Phase speed is important, since sound radiation is far more efficient for supersonic phase speeds than for subsonic phase speeds — see the example of a moving line source in Fig. A-2 for three cases: phase speed U_{ph} larger than, equal to, and smaller than the speed of sound. Even though a rotor tip speed is subsonic, sound may radiate efficiently because of the high effective (supersonic) phase speed of the source pattern.

From Fig. A-1, it is also evident that any particular rotor blade downstream of a stator blade experiences kV loading pulses per revolution, whereas a sound pulse is emitted mB times per revolution. Thus, k determines the loading harmonic order, m the sound harmonic order.* The analytical relationship of the loading harmonic amplitude (force at the loading harmonic number kV) and the resultant sound power radiation at the particular sound harmonic number for the case of a rotor/stator configuration has recently been established by Widnall [1] for the case of a rotor/ stator configuration radiating (a) directly into a free-field environment and (b) radiating in an annular duct and from the duct into the free-field environment. These two cases are illustrated in Fig. A-3. Table A-1 presents the analytical results.

---

* Depending on the particular combination of m, k, B and V, certain sound harmonics will be radiated very efficiently (namely, those that correspond to a supersonic sound speed) while others, though they are generated, will "die out" in the nearfield of the rotor. Generally, for typical compressors where B and V are only slightly different, equality of m and k (say, both being 1, or 2, or 3, etc.) usually leads to supersonic phase speed, while unequal combinations of m and k (say, m=1, k=2) leads to subsonic phase speed and inefficient radiation.
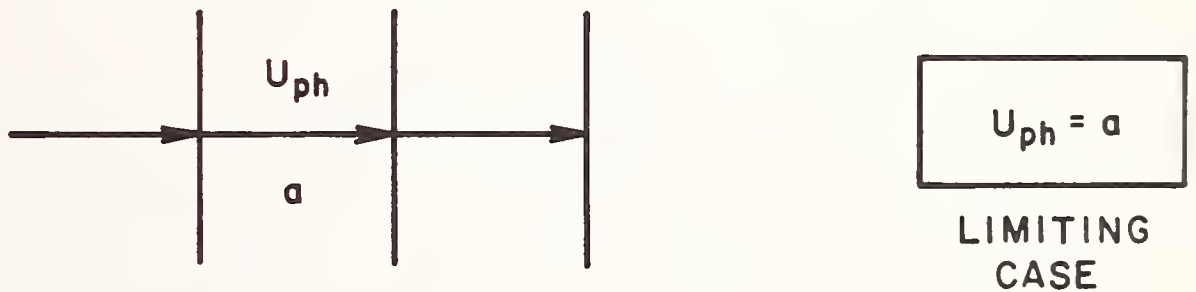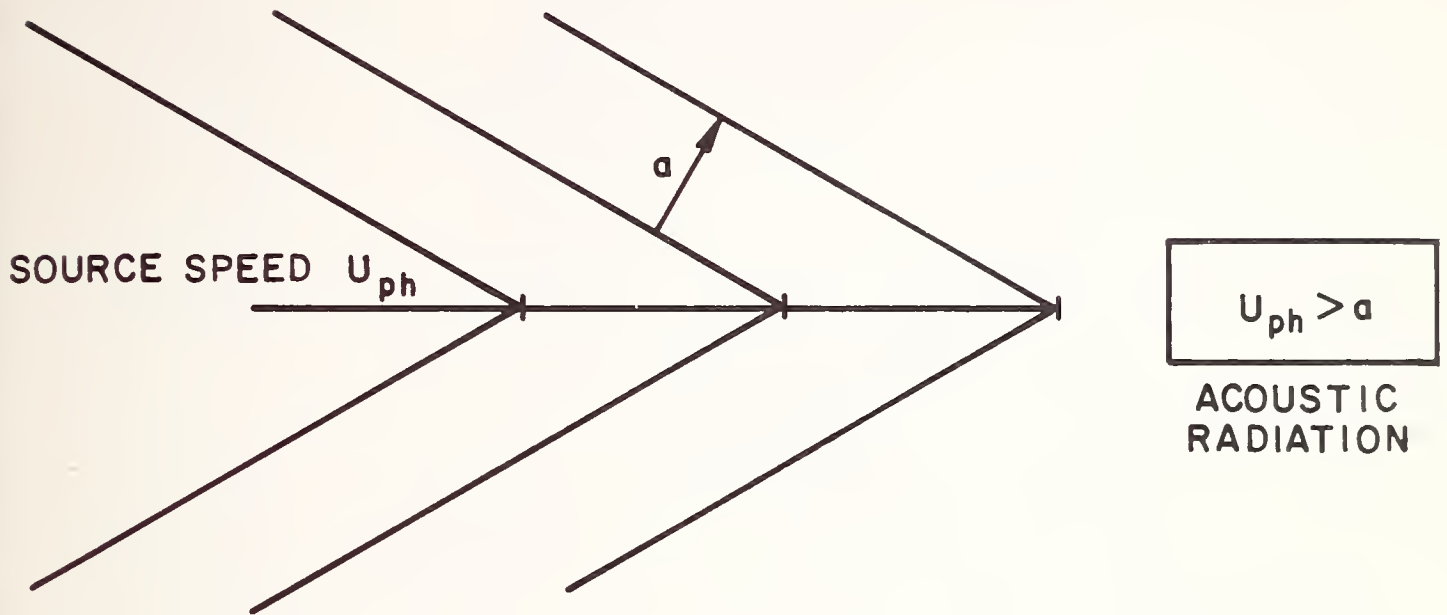
SPEED OF ACOUSTIC WAVE a

FIG. A-2.   EFFECT OF RATIO OF PHASE SPEED U_{ph} AND SOUND SPEED a
ON RADIATION
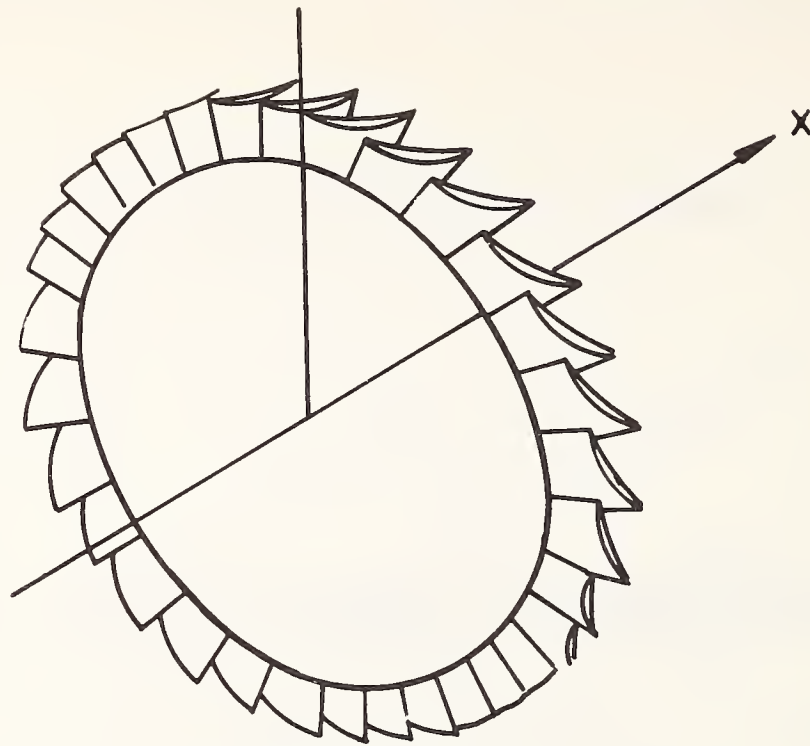
a) FREE ROTOR
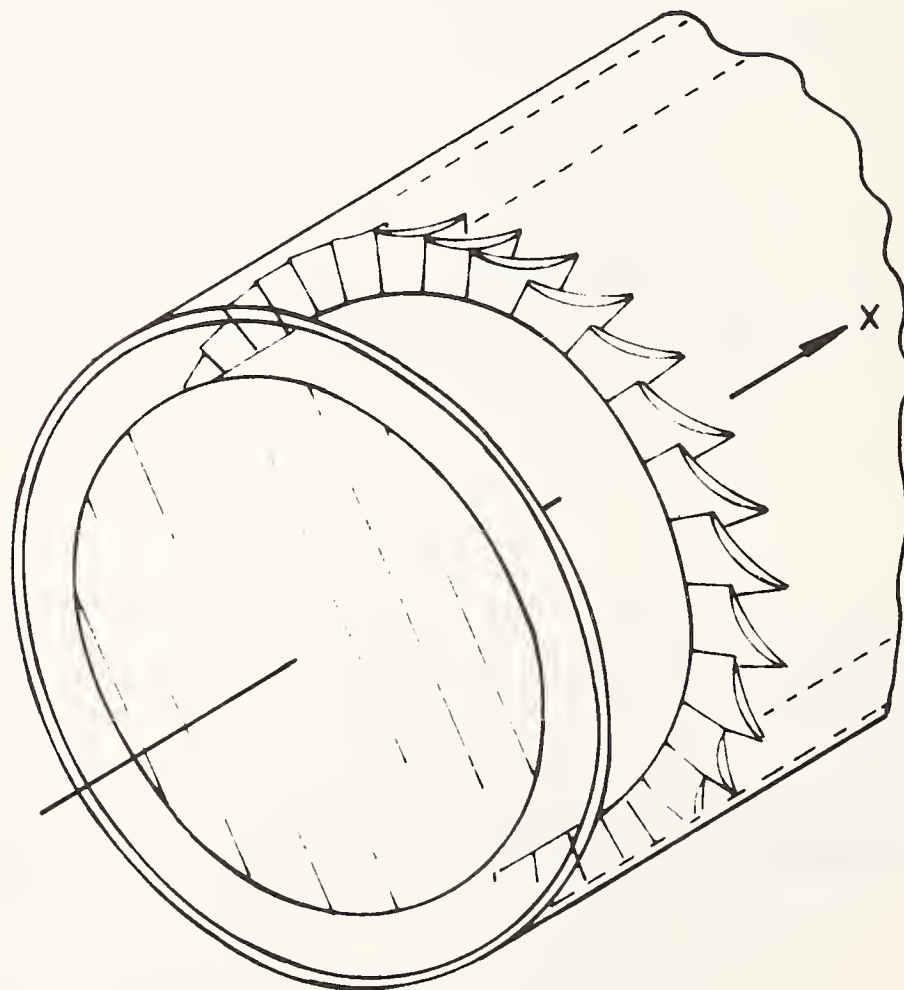
b) ROTOR IN ANNULAR DUCT

FIG. A-3.   ROTOR/STATOR CONFIGURATION IN (a) FREE-FIELD ENVIRON-
MENT AND IN (b) ANNULAR SEMI-INFINITE DUCT

TABLE A-1: Sound Power Radiation From Rotor/Stator Configuration for Two Cases

Radiation from Unconfined Rotor/Stator

$$\Pi_{n\lambda} = \left(\frac{B^2 T_\lambda^2}{8\pi R_0^2 \rho c}\right) \cdot T_1 \qquad T_1 = \frac{1}{nM}\left\{\frac{1}{4}\left[(nM)^2 - \mu^2\right] + \left(\frac{D}{T}\right)_\lambda^2 \cdot \frac{\mu^2}{2}\right\}$$

Radiation from Confined Rotor/Stator

$$\Pi_{n\lambda} = \left(\frac{B^2 T_\lambda^2}{8\pi R_0^2 \rho c}\right) \cdot T_3 \qquad T_3 = \frac{1}{2nM}\left[\sqrt{(nM)^2 - \mu^2} - (D/T)_\lambda \mu^2\right]^2$$

The equations presented in Table A-1 give the radiated power $\Pi_{n\lambda}$ (observed in the free-field environment) of a particular sound harmonic $n \equiv mB$ due to a loading harmonic $\lambda \equiv kV$ of strength T_λ ; T_λ is thus a "force" acting on the blade at a particular frequency, and one sees that sound power is proportional to the square of the force term T_λ — in agreement with the aerodynamic-dipole character of a fluctuating-force source.

The nondimensional "weighting functions" T_1 and T_3 contain contain the ratio of the drag and thrust force on the blade, D/T, whose value is basically determined by blade orientation and mean angle of flow incidence. T_1 and T_3 also contain information on (a) the geometry of the rotor/stator configuration in terms of number of rotor blades B and stator blades V (since n is mB and μ, the modal order, is $|mB-kV|$) and (b) rotational speed in terms of rotational Mach number M. The nondimensional weighting function T_1 is plotted in Figs. A-4a,4b vs the frequency parameter nM = mB·M for several values of the modal order μ. These figures illustrate the strong dependence of the radiated power on modal order and the particular thrust-to-drag ratio.

Thus, to predict harmonic sound radiation, one needs to know magnitude and direction of the particular loading harmonic on a blade.*

In estimating the force magnitude on a blade due to impingement from an upstream wake,[†] one needs information on the wake strength and its downstream decay. Thus, one must have some

---

* In a research program, reported in Ref. 1, an attempt was made to measure these forces directly on rotating blades.

† Potential field interactions can play a role in defining the forces on a blade; however, for typical rotor/stator disk separations — on the order of one chord length — potential field interaction is not important.
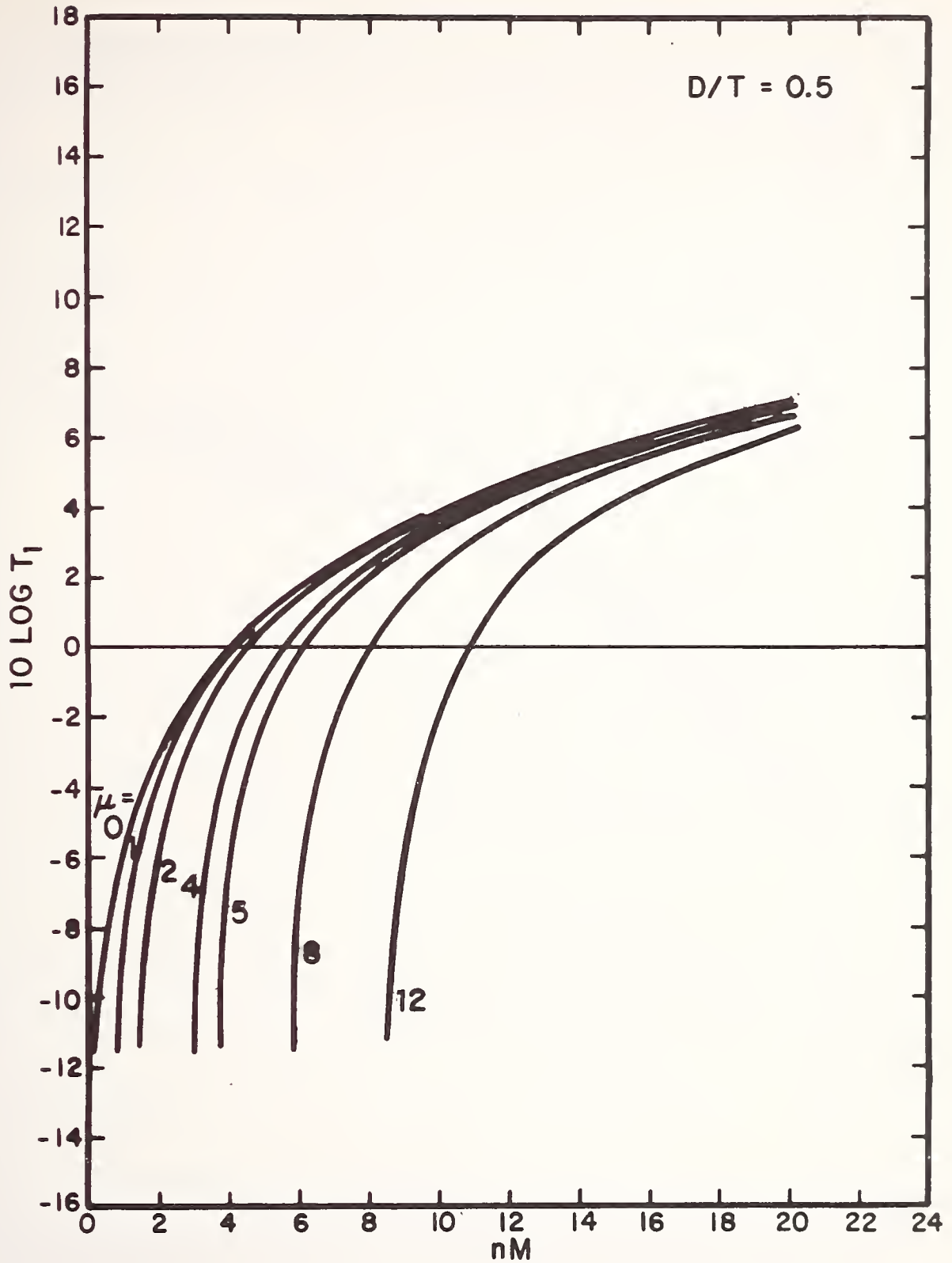
FIG. A-4a. T_1 (FROM TABLE A-1) AS A FUNCTION OF SOUND HARMONIC,
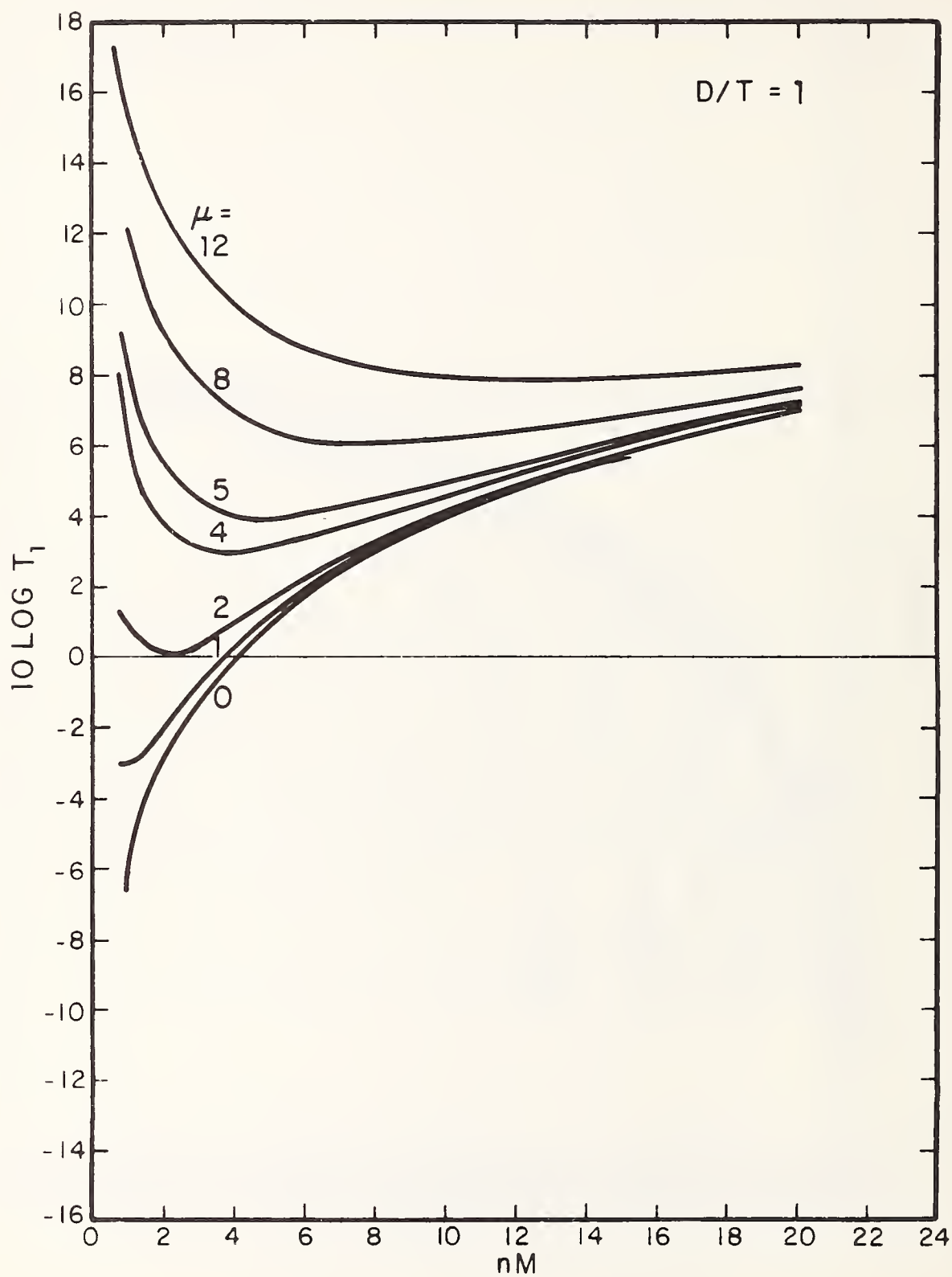MACH NUMBER, AND MODAL ORDER

FIG. A-4b. T_1 (FROM TABLE A-2) AS FUNCTION OF FREQUENCY PARA-
METER nM AND MODAL ORDER

knowledge of the velocity profile of the wake at the location of interference with the subsequent blade row.

A.2 Broadband Sound Generation

The theoretical prediction of broadband noise from a compressor could be based on Curle's [2] classical aerodynamic dipole analysis which relates radiated sound power $\Pi(\omega)$ to fluctuating forces $\tilde{F}(\omega)$ by

$$\Pi(\omega) = \frac{\omega^2 F^2(\omega)}{12\pi\rho c^3} \quad . \tag{A-2}$$

Knowing the fluctuating force magnitude in the band ω permits prediction of the radiated sound power Π in that band. This equation is valid for the aerodynamic dipole (i.e., the fluctuating-force source) radiating into free space. Radiation into an "obstructed" environment — as is the case for a compressor — can increase the power output by 3 dB [3], depending on the effective orientation of the dipole axis.

If the wavelength of the force field becomes smaller than typical blade dimensions, local cancellation takes place, reducing the amount of radiated acoustic energy at high frequencies.

A.3 Conclusions

Obviously, accurate definition of the various source terms is imperative for an accurate prediction of compressor noise. In the above discussion, only force sources were treated because steady and fluctuating forces constitute the most important source mechanism in the generation of compressor noise. However, fluctuating masses also generate compressor noise. The periodic wakes shed

from upstream rotors or stators and impinging on downstream rotors
or stators cause mass fluctuations, as well as force fluctuations,
on subsequent blade rows.

Consider a rotating periodic velocity profile caused by a
rotor acting on a stator row. The profile, being steady with
respect to the rotor, is periodically intersected by the stator,
as the rotor moves past the stator rows. Hence, fluctuating masses
are set up on the stator. The same basic mechanism applies to rotor
mass sources. Here, the velocity field of the stator interacts with
the downstream rotor. However, these "siren" sources are of minor
importance at tip speeds typical of practical compressors. Off-
design operation can lead to an increase in wake thickness (due to
local flow separation, for example), which would result in in-
creased "siren" source strengths.

The complex interaction and dependence of compressor noise
sources on geometric and aerodynamic parameters indicates the need
for a more detail study of the relevant source mechanisms.

A.4 Sound Propagation in a Duct

Sound in a duct can travel in plane waves or higher order
modes. In the case of a source pattern radiated from an axial flow
fan into a duct, only those source patterns that correspond — at a
given frequency — to possible duct modes will propagate along the
duct. Higher order modes whose pressure does not change sign once
in a radial direction in the duct cross-sectional area or repeatedly
in a circumferential direction are of greatest importance in com-
pressor noise propagation within a duct. Such phase patterns are
illustrated in Fig. A-5. In the case of a rotor/stator source
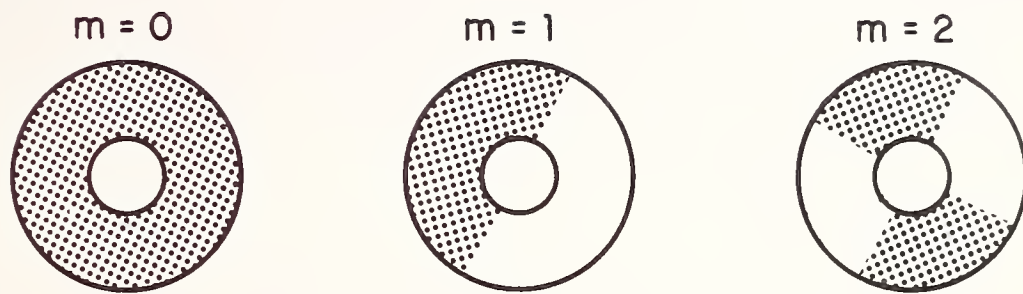pattern, the modes can be envisioned as traveling along the duct

69

FIG. A-5.   PHASE PATTERNS FOR DUCT MODES

in a spiraling manner — i.e., as spinning waves. Plane waves and their permissible modes travel along a duct almost unattenuated; others decay rapidly. Plane waves are strongly excited if the number of interacting stator and rotor blades is equal; otherwise, tones are propagated through the duct predominantly as spinning waves.

Spinning waves are subject to the cut-off phenomenon, which means that they cannot propagate when their frequency falls below a critical value. This frequency is given approximately by

$$f \approx \frac{c \cdot m}{2 \pi R} , \tag{A-3}$$

where m is the order of sound harmonic. If we take R, the mean radius of the compressor annulus as 1.12 ft, then

m	0	1	2	3
$f_{cut-off}$ (Hz)	0	160	320	480

Since the blade passage frequency of the TACV compressor is already as high as 1800 Hz, all conceivable important modes of rotor/stator interaction are likely to be above the cut-off frequency of a circular duct of rotor diameter.

The shapes and the attenuation of the modes in the duct are affected by the wall impedance, the airflow in the duct, and the airflow's cross-sectional development. Absorptive treatment of the duct will increase the axial attenuation of the modes.

Convection of sound with uniform airflow decreases frequency because of the Doppler effect which tends to decrease the attenuation for a given wall treatment. Sound can also be *refracted* towards or away from the wall, depending on whether it travels with or against the flow.

References

1.   H. Heller and S. Widnall: "The Role of Fluctuating Forces
     in the Generation of Compressor Noise," BBN Report No. 2160,
     July 1971.

2.   N. Curle, "The Influence of Solid Boundaries Upon Aerodynamic
     Sound," *Proc. Roy. Soc.* **231A**, 505, 1955.

3.   H. Heller and S. Widnall, "Correlation of Fluctuating Forces
     with Sound Radiation from Rigid Flow Spoilers," *J. Acoust.
     Soc. Amer.* **47**, May 1970.

APPENDIX B

EMPIRICAL PREDICTION SCHEMES

The following prediction schemes are based on easily available geometric and operational parameters.

Allen Method

Allen's method [1] for predicting centrifugal and axial compressor noise requires knowledge of (a) rated horsepower hp, (b) static pressure rise Δp (inches of water), and (c) fan discharge q (ft^3/min). This scheme was introduced in 1957 and claims an accuracy of ± 4 dB; overall sound power level PWL in dB re 10^{-12} watt can be computed from:

$$PWL = \ 93 + 10 \log hp + 10 \log p, \text{ or}$$

$$PWL = \ 58 + 10 \log \ q + 20 \log p, \text{ or}$$

$$PWL = 128 + 20 \log hp - 10 \log q \ .$$

Sound power radiated through the intake only is about 3 dB less.

Allen's equations were originally developed for single-stage compressors; therefore, it is recommended that for a multistage axial-flow compressor one compute the sound power generation per stage and then sum the individual power levels to determine the total power. One objection to such a procedure is that sound propagation from one stage through another stage is not yet understood, and simple adding of per-stage power levels may overpredict total power output.

Figure B-1 presents a dimensional spectrum for axial-flow compressors, referenced to the overall sound power level.
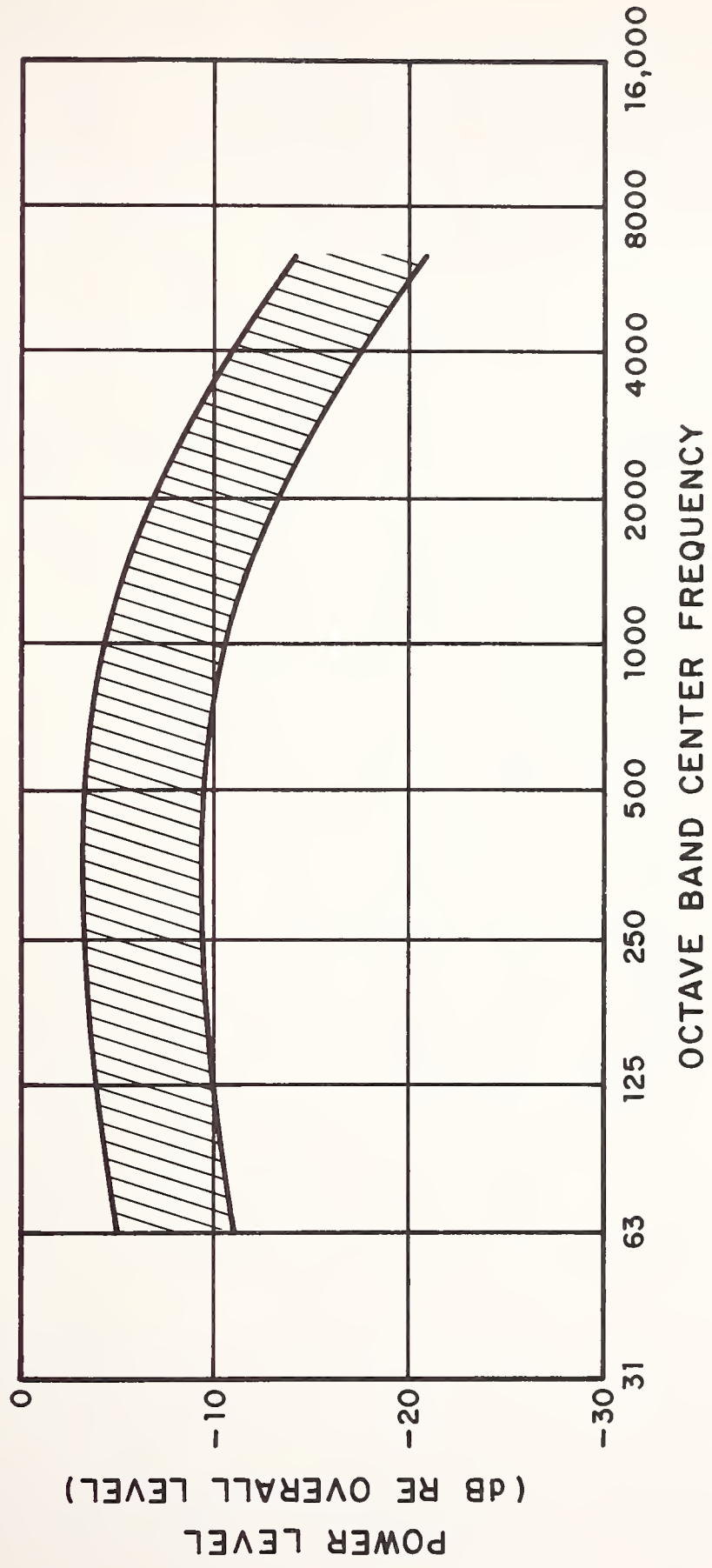
FIG. B-1.   OCTAVE BAND SOUND POWER LEVEL RE OVERALL SOUND POWER LEVEL FOR AXIAL
FLOW COMPRESSORS OPERATING NEAR PEAK EFFICIENCY (AFTER ALLEN).

ASHRAE Guide Method

Table B-1 presents octave-band base sound power levels for three different axial compressor types. The tabulated base PWLs are quoted for 36-in.-diameter fan wheels operating at a speed of 1000 rpm.

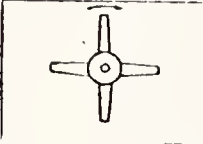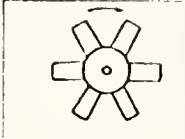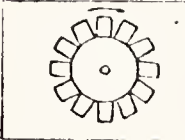### TABLE B-1. BASE SOUND POWER LEVELS dB re 10^{-12} WATT

Solidity	Configuration	63	125	250	500	1000	2000	4000	8000	Hz
low		92	93	92	91	91	88	84	80	dB
medium		96	93	97	96	94	90	86	85	dB
high		90	86	90	93	93	89	83	87	dB

Figure B-2 presents corrections for actual fan diameter (in inches) and rotational speed (in rpm). The procedure shifts the base spectrum, as a whole, to higher or lower levels. To account for the acoustic energy contained in the blade-passage frequency band, 5 dB are added to this band. This procedure is valid for the compressor working at peak efficiency (i.e., at the design condition), where acoustic levels are a minimum.

Morfey Method

The method developed by Morfey [2] involves a large number of parameters, some of which may not be easily available for prediction purposes. However, for completeness, his method shall be presented.
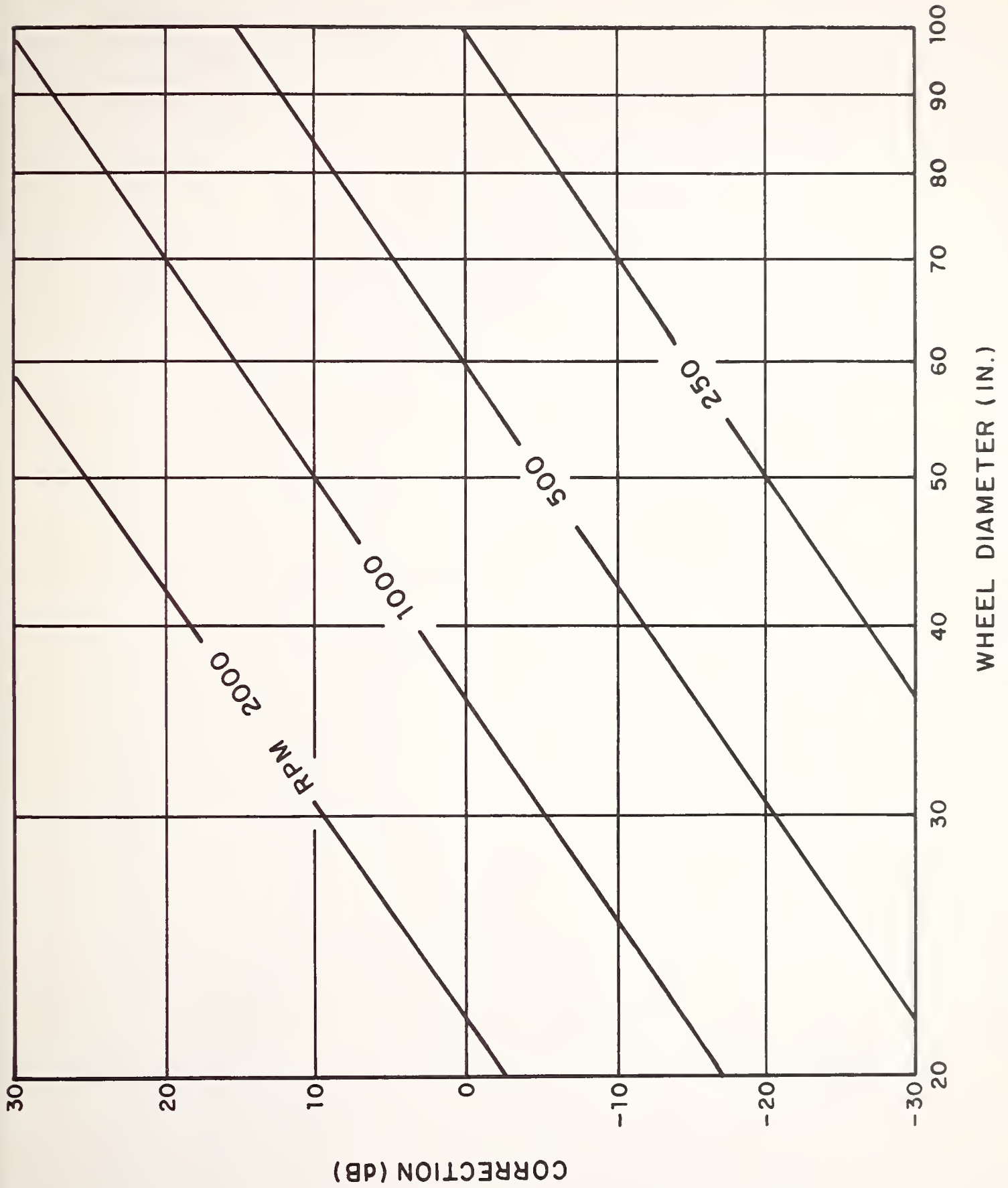
74

FIG. B-2. CORRECTION TO BE APPLIED TO BASE SOUND POWER LEVELS TO COMPENSATE FOR ACTUAL WHEEL DIAMETER AND RPM.

Morfey combines various parameters to define a broadband parameter:

$$\frac{dW}{df} \cdot \frac{Re_d}{f \cdot p \cdot c \cdot C^3 n \ B \ Ma^4} \cdot$$

This parameter is plotted in Fig. B-3 versus the ratio of mass flow W and design mass flow W_0; the frequency parameter F is defined as

$$F = \frac{fC}{U} \quad (Re_C)^{-\frac{1}{6}} \quad ,$$

where

$\frac{dW}{df}$ = broadband sound power spectral density,

$Re_d = \frac{C \cdot U}{\nu}$,

U   = flow speed relative to rotor blade tip,

C   = rotor blade chord,

f   = frequency,

h   = rotor blade height (span),

B   = number of blades,

M   = flow Mach number relative to rotor blade tip, and

ν = coefficient of kinematic viscosity.

A nondimensional discrete-frequency parameter is defined by

$$\frac{W \rho S}{w^2 \cdot \alpha} \cdot \frac{(Re_m)^{\frac{2}{3}}}{\partial_R^2 \cdot \partial_S^2}$$
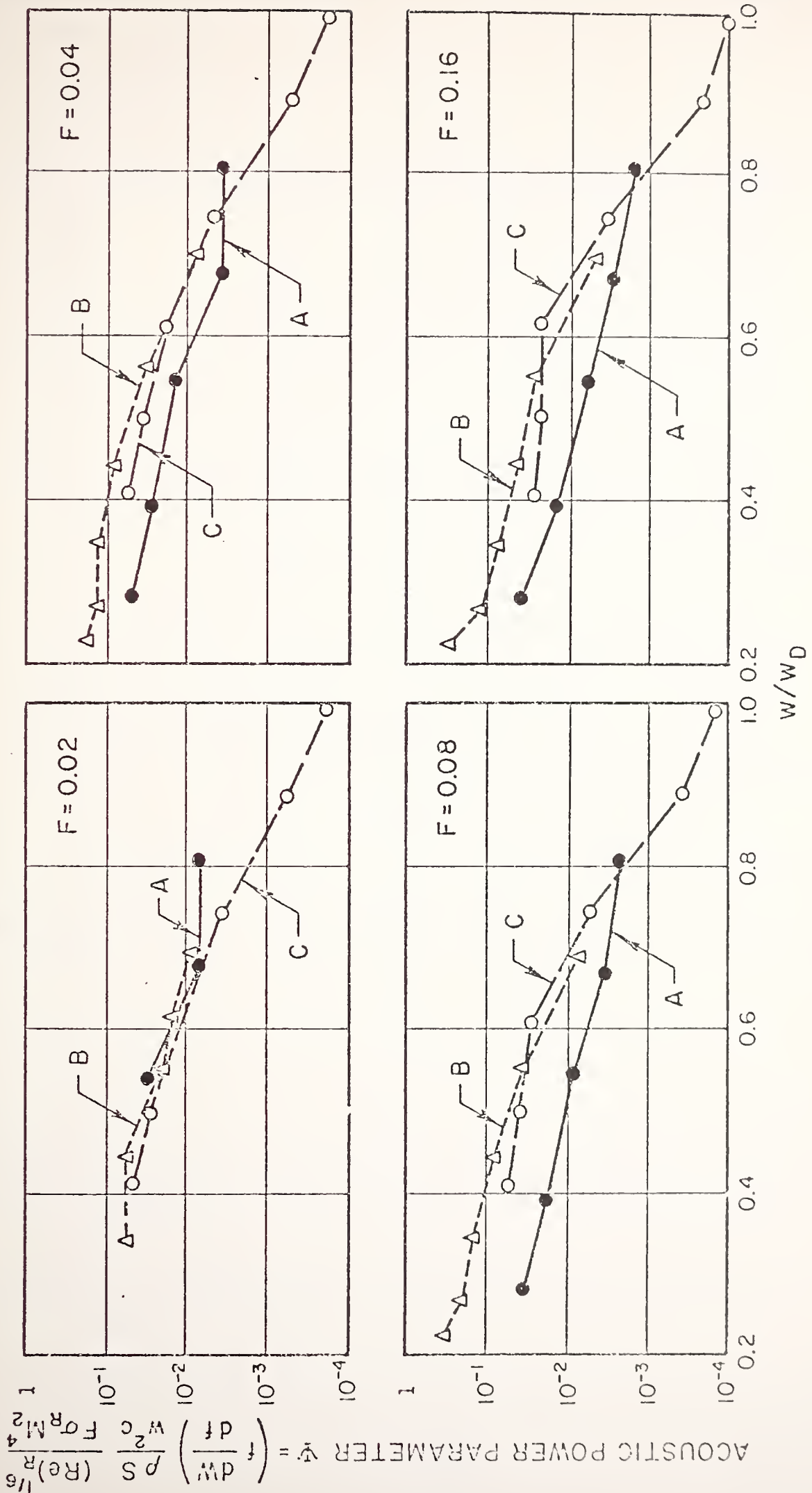
FIG. B-3.   BROADBAND NOISE: SOUND POWER DATA FROM THREE ENGINES, AT FREQUENCY
PARAMETER VALUES F = 0.02, 0.04, 0.08, 0.16

where

    W = tone sound power radiated in principle mode,

    ρ = fluid density,

    S = annulus area,

    w = mass flow through compressor,

    α = speed of sound,

$Re_m = w \cdot d_m / S$,

    d_m = geometric mean of rotor and stator chords,

    σ_r = solidity of rotor rows,

    σ_s = solidity of stator rows, and

    μ = coefficient of dynamic viscosity.

Figure B-4 shows a plot of the tone power output at blade passage frequency of first rotor for three engines versus ratio of mass flow and design mass flow.

Sowers Method

To evaluate the sound power level, Sowers [3] plots a normalized power level

$$PWL - 10 \log (s \cdot n / B) \cdot \partial^2$$

where S = rotor annulus area,
    n = rotor speed,
    B = number of blades, and
    ∂ = hub-tip ratio

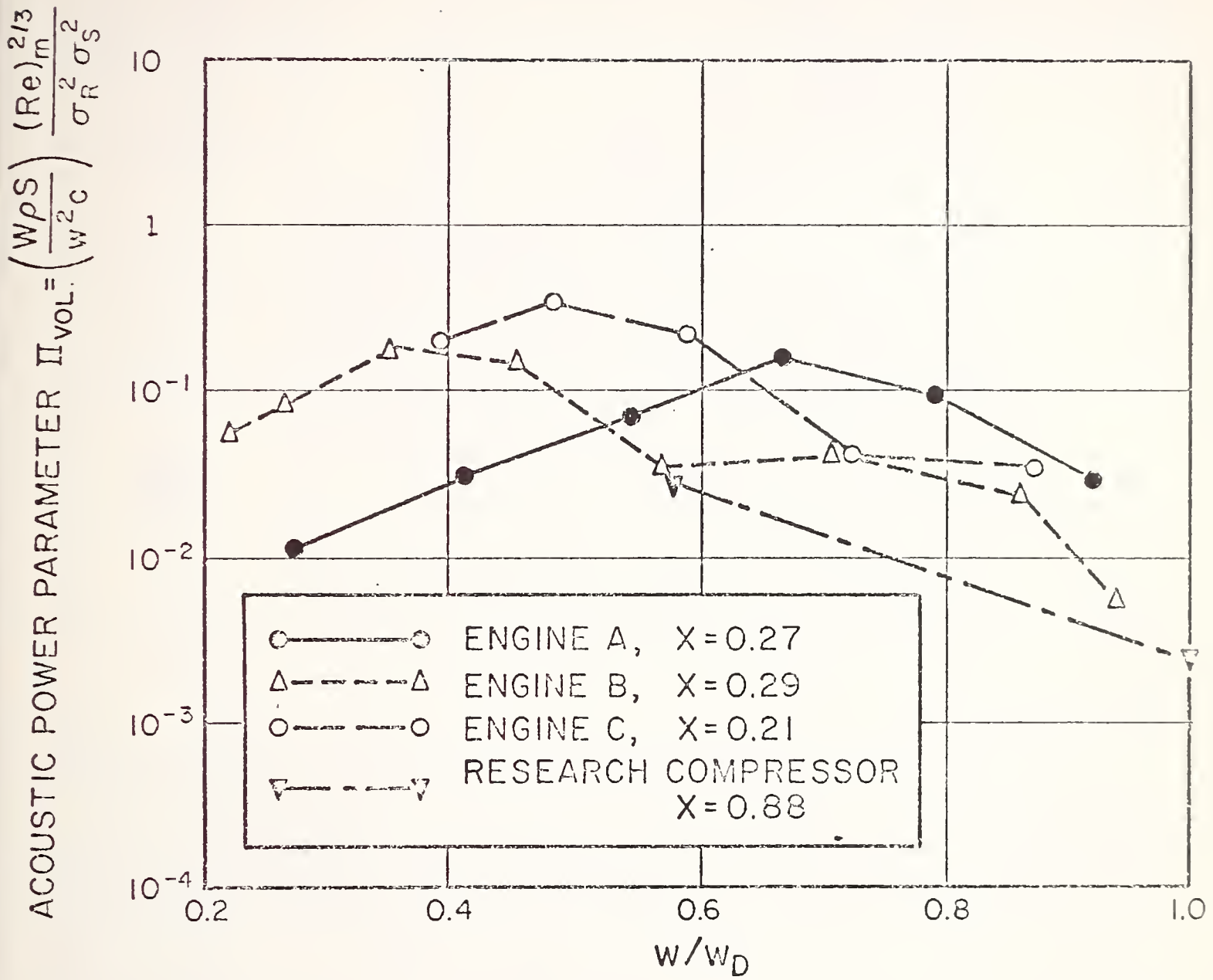versus an energy flux E in [(Btu/sec) × ft^2], where E is the total

FIG. B-4. TONE POWER OUTPUT AT BLADE-PASSING FREQUENCY OF FIRST
ROTOR

energy of the air leaving the compressor stage per unit time and
per unit area, thus giving

$$E = \frac{H_T \cdot w}{S} \, ,$$

where

H_T = total enthalpy at the temperature T (from gas tables),

T = temperature of the gas leaving the compressor (i.e.,
      inlet temperature + total pressure rise in the com-
      pressor),

w = mass flow per time unit, and

S = annulus area.

Figure B-5 shows the empirically obtained curve.

Wintermeyer and McKaig

Wintermeyer and McKaig [4] related normalized fan discharge
noise at a 200-ft sideline to tip speed for a large variety of
compressors. Figure B-6 shows that the noise corresponds to the
octave band containing the fundamental blade passage frequency.

References

1. C.H. Allen, "Noise Control in Ventilation Systems," Chap. 21
    in *Noise Reduction*, L.L. Beranek (ed.), McGraw Hill Book Co.,
    1960.

2. C. Morfey and H. Dawson, "Axial Compressor Noise," Paper pre-
    sented at 11*th* Annual Gas Turbine Conference in Zurich, 1966.
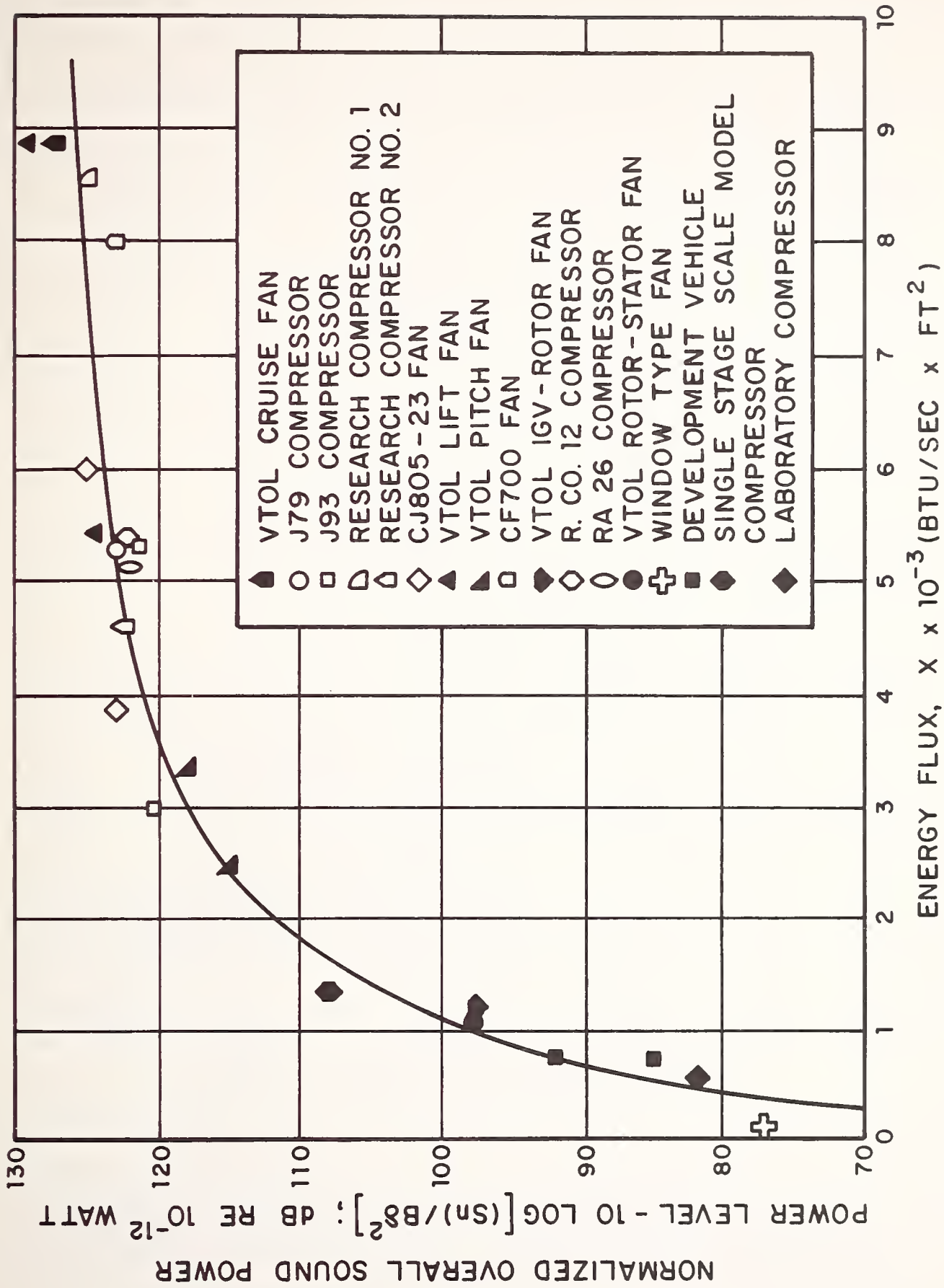
FIG. B-5.   NORMALIZED OVERALL POWER OF COMPRESSOR AND FAN NOISE.
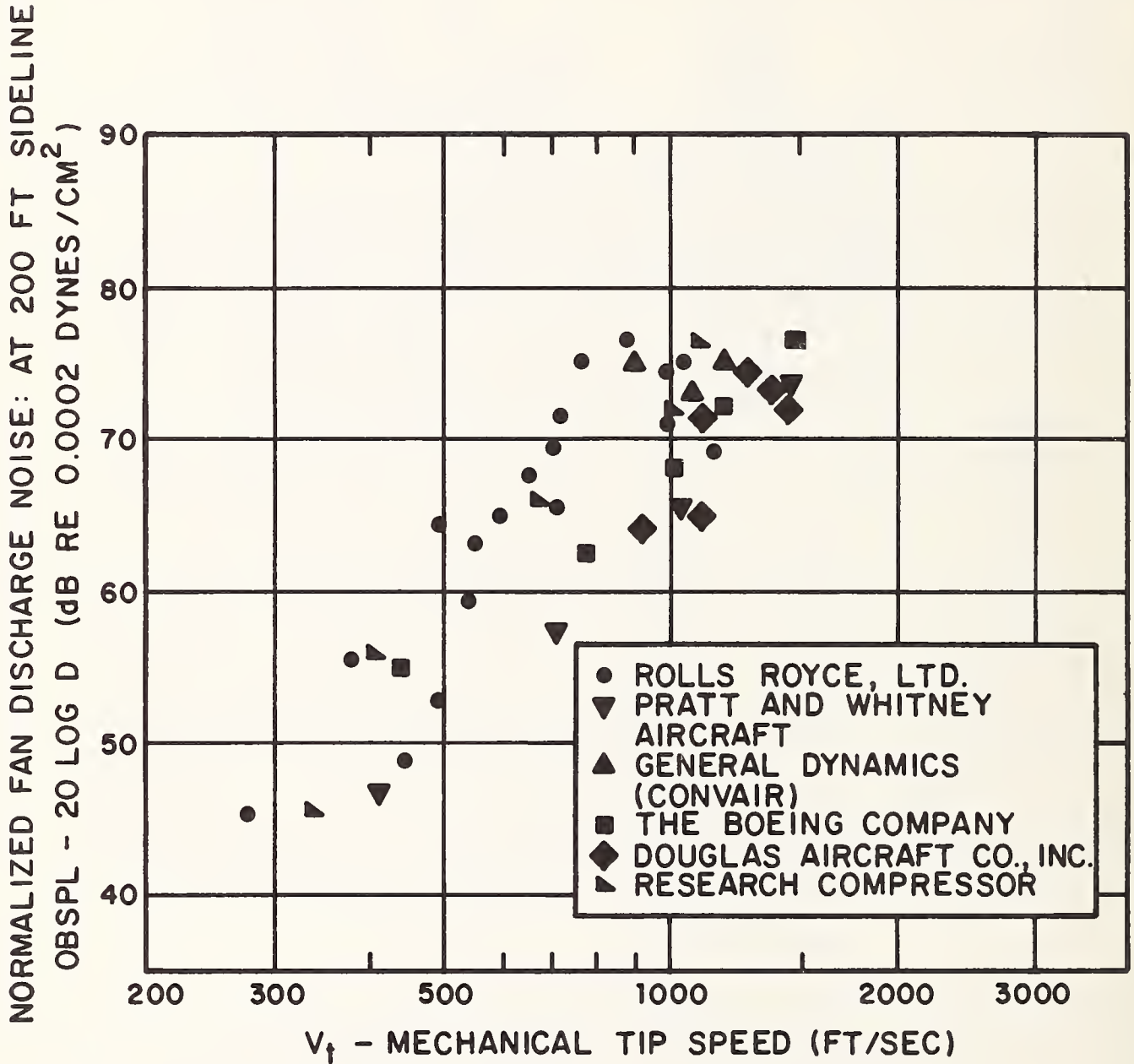
FIG. B-6.   MAXIMUM FAN DISCHARGE NOISE IN OCTAVE BAND CONTAINING
            FUNDAMENTAL BLADE PASSAGE FREQUENCY (AFTER WINTERMEYER
            AND McKAIG).

3. H. Sowers, "Investigation of Methods for the Prediction and
    Alleviation of Lift Fan Noise," U.S. Army Transportation
    Research Command TR 65-6, 1965.

4. Fig. 20 from "Theoretical Studies of Compressor Noise,"
    Wyle Reports WR-68-15.

APPENDIX C

NOISE CONTROL AT THE SOURCE

The distance between rotor and stator rows affects the inter-action of forces. Conceivably, force fluctuations are greater when the rows are closer together — see Fig. C-1, where sound levels are plotted versus separation in a nondimensional form. Interaction noise is a function of both the shape of an upstream blade that sheds a wake on a downstream blade and the clearance. There is an indication [1] that small chords, slender profiles, and separation on the order of one-half to one chord length are beneficial.

Furthermore, it is important that the airflow into a compressor is of low turbulence; otherwise, random force fluctuations on rotors or stators will induce broadband noise. Thus, obstructions in the compressor intake area are to be avoided as much as possible. Boundary layer control along the inner walls of the intake may help to reduce the wall turbulence within which the rotor tips of a compressor operate. However, this control requires additional vacuum pumps, and the added complication is not justified by the results.

Reference

1.   I.J. Sharland, "Fan Noise," Chap. 10 in *Noise and Acoustic Fatigue in Aeronautics*, E.J. Richards and D.J. Mead (eds.) John Wiley and Sons, 1968.
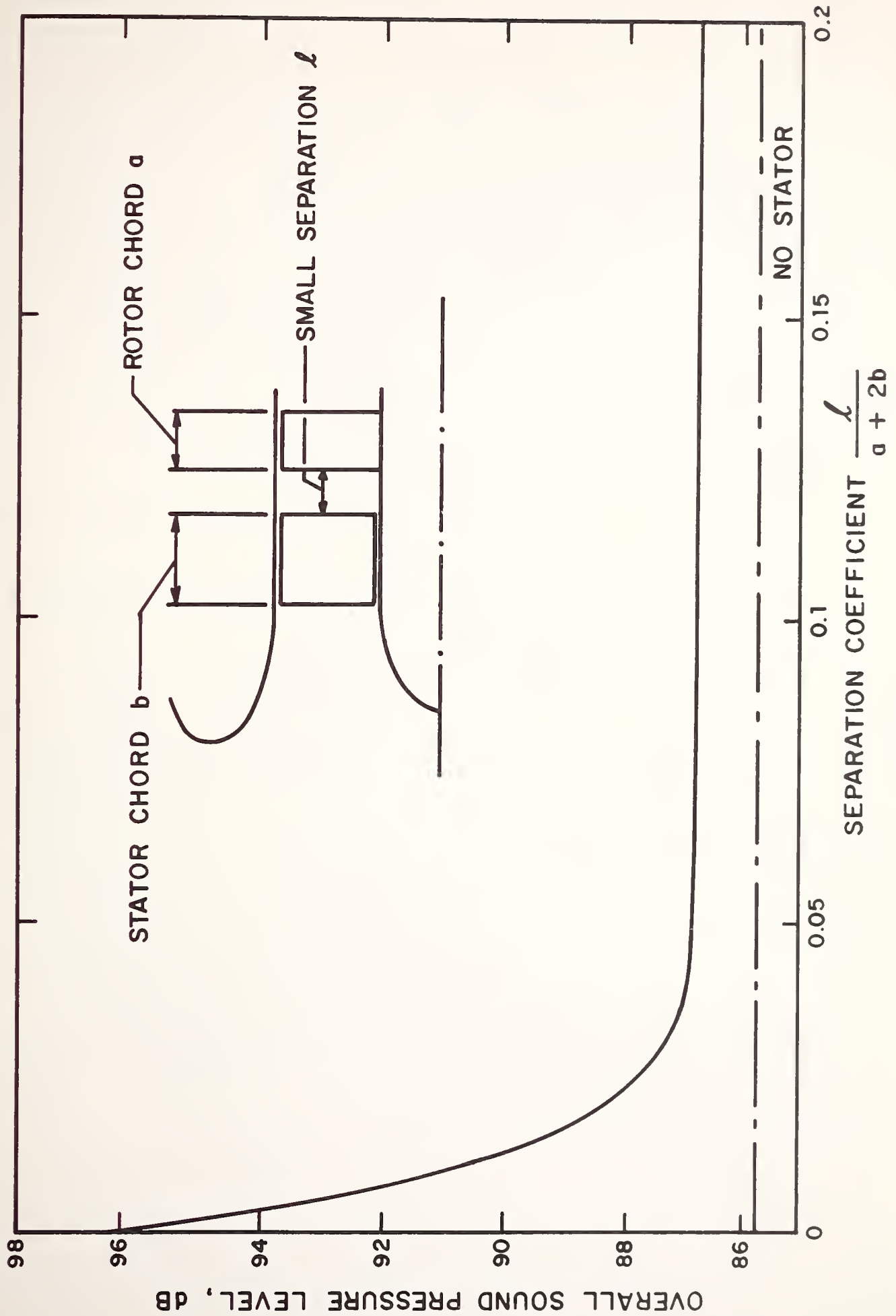
FIG. C-1.   NORMALIZED PLOT OF NOISE LEVEL AGAINST ROTOR/STATOR SEPARATION OBTAINED FROM SINGLE FLAT PLATE STATORS OF CHORDS

APPENDIX D

SOUND PRESSURE LEVEL NEAR A TACV

Sound radiating from a line source (such as a TACV) does not attenuate according to the usual inverse square law spreading losses for free-field radiation. We develop here an approximate method for determining the SPL at a sideline distance from a line source having a uniform sound power level per unit length (such as that due to air cushion noise in a TACV).
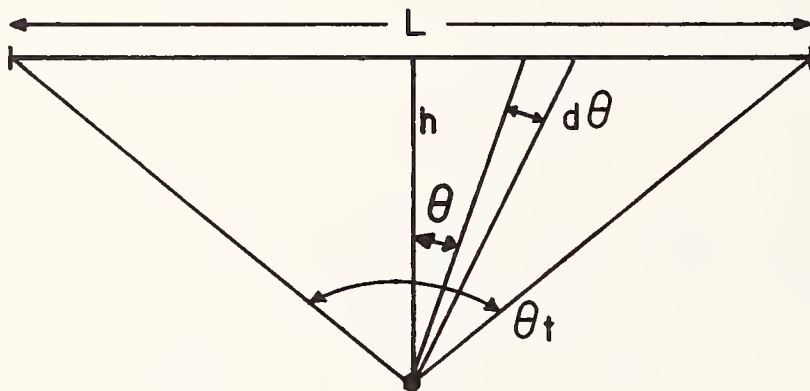
Assuming radiation into hemisphere, the incremental intensity

$$dI = \frac{W}{L} \frac{dL}{\frac{1}{2}(4\pi r^2)} = w \frac{dL}{2\pi r^2}$$

where

      w = power/unit length,

      r = $h/\cos\theta$ = radial distance from source, and

    dL = $rd\theta/\cos\theta$.

The above equation reduces to

$$dI = \frac{W}{2\pi h} d\theta \;, \text{ and}$$

the total intensity becomes

$$I = \frac{W\theta_t}{2\pi h} \;.$$

The intensity level may be thus derived:

$$\frac{I}{I_{ref}} = \frac{W}{W_{ref}} \theta_t \frac{1}{h/h_{ref}} \frac{W_{ref}}{2\pi I_{ref} h_{ref}} \frac{10^{-12}\,\text{watts}}{10^{-12}\,\text{ft watts}} \frac{m^2}{1\,\text{ft}} \times \frac{10.8\,\text{ft}^2}{m^2}$$

$$\frac{I}{I_{ref}} = \frac{W}{W_{ref}} \theta_t \frac{1}{h/h_{ref}} \; 1.72$$

and the SPL is found

$$\underbrace{10 \log \frac{I}{I_{ref}}}_{\text{IL}} = \underbrace{10 \log \frac{W}{W_{ref}}}_{\text{PWL/ft}} + 10 \log \theta_t - 10 \log \frac{h}{h_{ref}} + \underbrace{10 \log 1.72}_{2.3}$$

$$\underbrace{\phantom{10 \log \frac{I}{I_{ref}} = 10 \log}}_{\text{SPL}-.2}$$

SPL = PWL/ft + 10 log θ_t − 10 log h[ft] + 2.5

for L = 80 ft, θ = 1.36, 10 log θ_t ~ 1.35

$$\boxed{\text{SPL} = \text{PWL/ft} - 13 \quad @ \; h = 50 \; \text{ft}}$$

87

APPENDIX E

TESTS ON FRENCH TACVs

With the kind assistance of Sté Bertin & Cie., we measured noise from two Aerotrains. The smaller "suburban" vehicle at Gometz, which carries 44 passengers, is propelled by a linear induction motor as illustrated in Fig. E-1. A pair of single stage axial flow compressors supplies air to the suspension cushions and to the lateral guidance cushions located on each side of the vertical aluminum reaction rail. The compressors are currently driven by an internal combustion engine which will be replaced by electric motors in the final vehicle configuration.

The configuration of the larger intensity vehicle, with a capacity of 80 passengers and top speed of 190 mph, is illustrated in Fig. E-2. The propulsion system consists of a gas turbine driving a shrouded pusher propeller. This vehicle also uses a vertical center rail which is solely for purposes of lateral guidance. Air cushions for suspension and guidance are also supplied by two axial compressors near the front of the vehicle. The entire guideway is elevated and was approximately 15 ft above the ground level where we conducted measurements.

E-1. LIM Vehicle Measurements (Gometz)

Data were acquired for the LIM vehicle at Gometz for stationary and moving conditions. The most significant data for stationary vehicle conditions are shown in Fig. E-3. One-third-octave band sound pressure level (SPL) spectra are shown for two measurement positions near the air intake. Two curves present data acquired while both the compressor and the engine were running. The third curve presents data for engine noise only.

front view

SECTION A

SECTION B

SECTION C
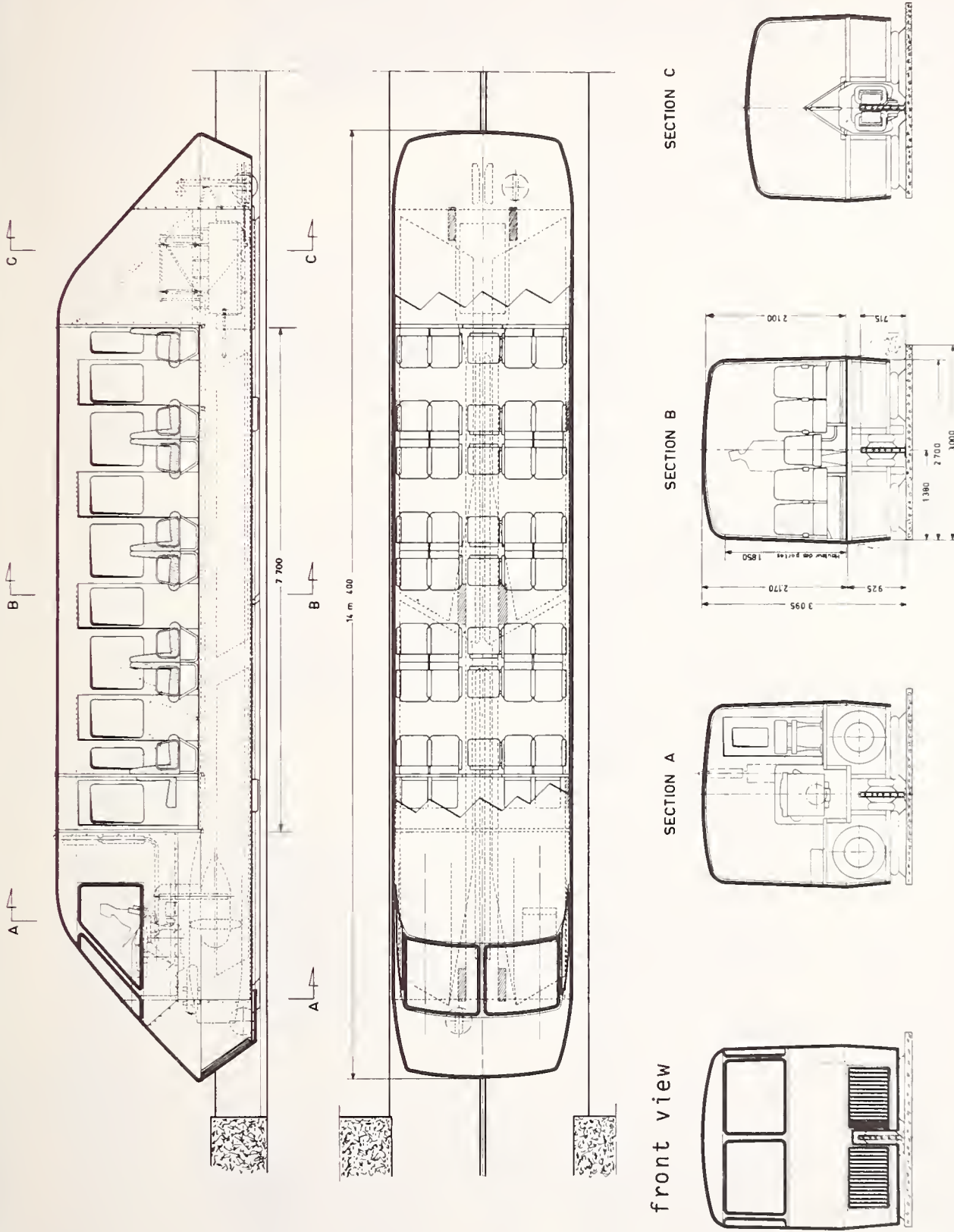
FIG. E-1. 44 PASSENGER LIM-POWERED TACV AT GOMETZ

Société de l'Aérotrain

Décembre 1968

Aérotrain type "Suburbain"

rear view

SECTION DD

SECTION CC
1º Classe

SECTION CC
Classe touriste

front view

COUPE AA

COUPE PARTIELLE BB
25m 650

13m 700

3m300
1m950
3m200
3m400
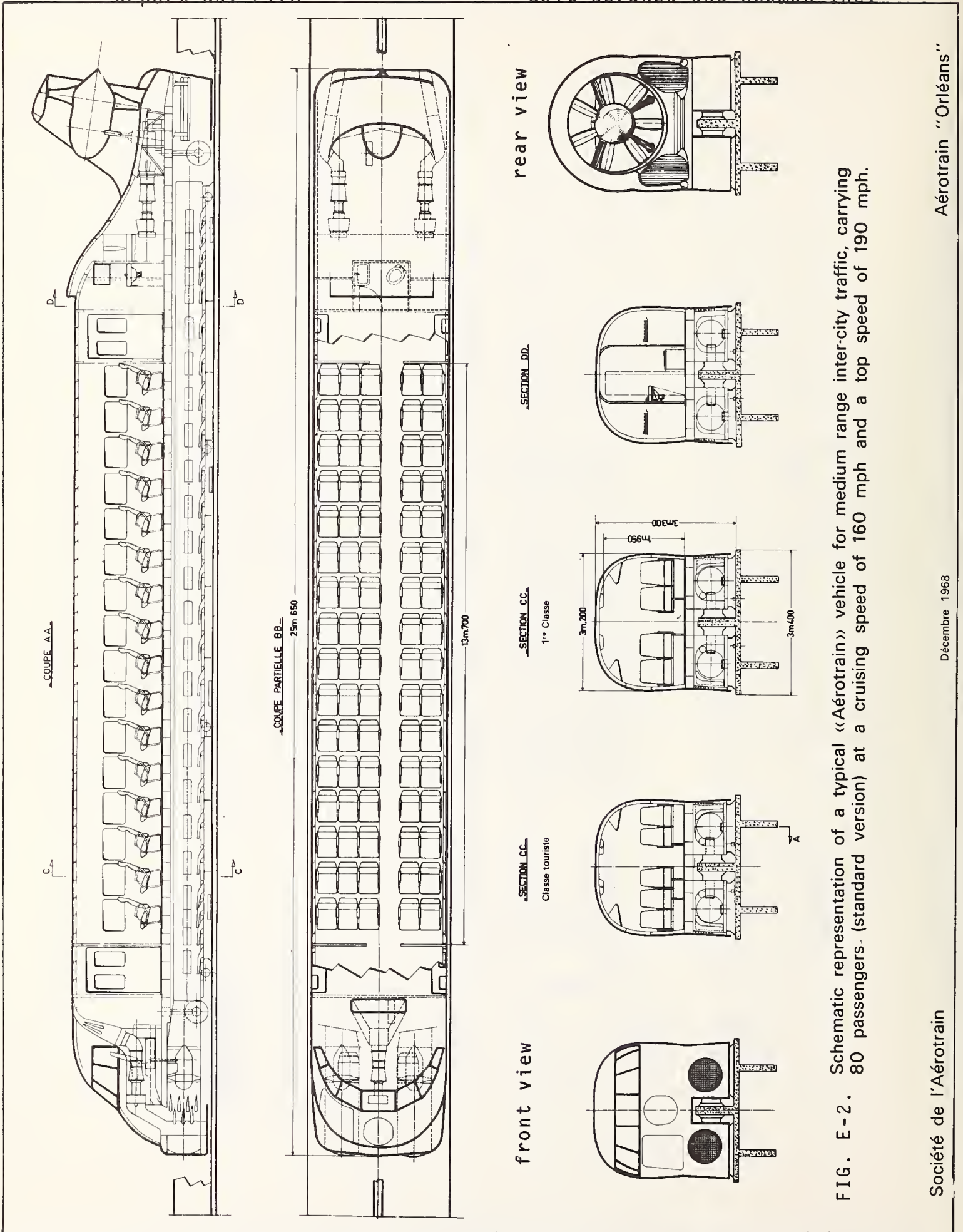
FIG. E-2. Schematic representation of a typical «Aérotrain» vehicle for medium range inter-city traffic, carrying 80 passengers (standard version) at a cruising speed of 160 mph and a top speed of 190 mph.

Société de l'Aérotrain   Décembre 1968   Aérotrain "Orléans"

FIG. E-3. NOISE MEASUREMENTS NEAR A STATIONARY LIM VEHICLE AT
GOMETZ WITH AND WITHOUT THE COMPRESSORS RUNNING.
IN ALL CASES THE GASOLINE ENGINE THAT DRIVES THE
COMPRESSORS WAS RUNNING

Even when both engine and compressor noise levels are present,
it is quite certain that, in the high-frequency regions between
800 and 8000 Hz, the dominant noise is from the compressor —
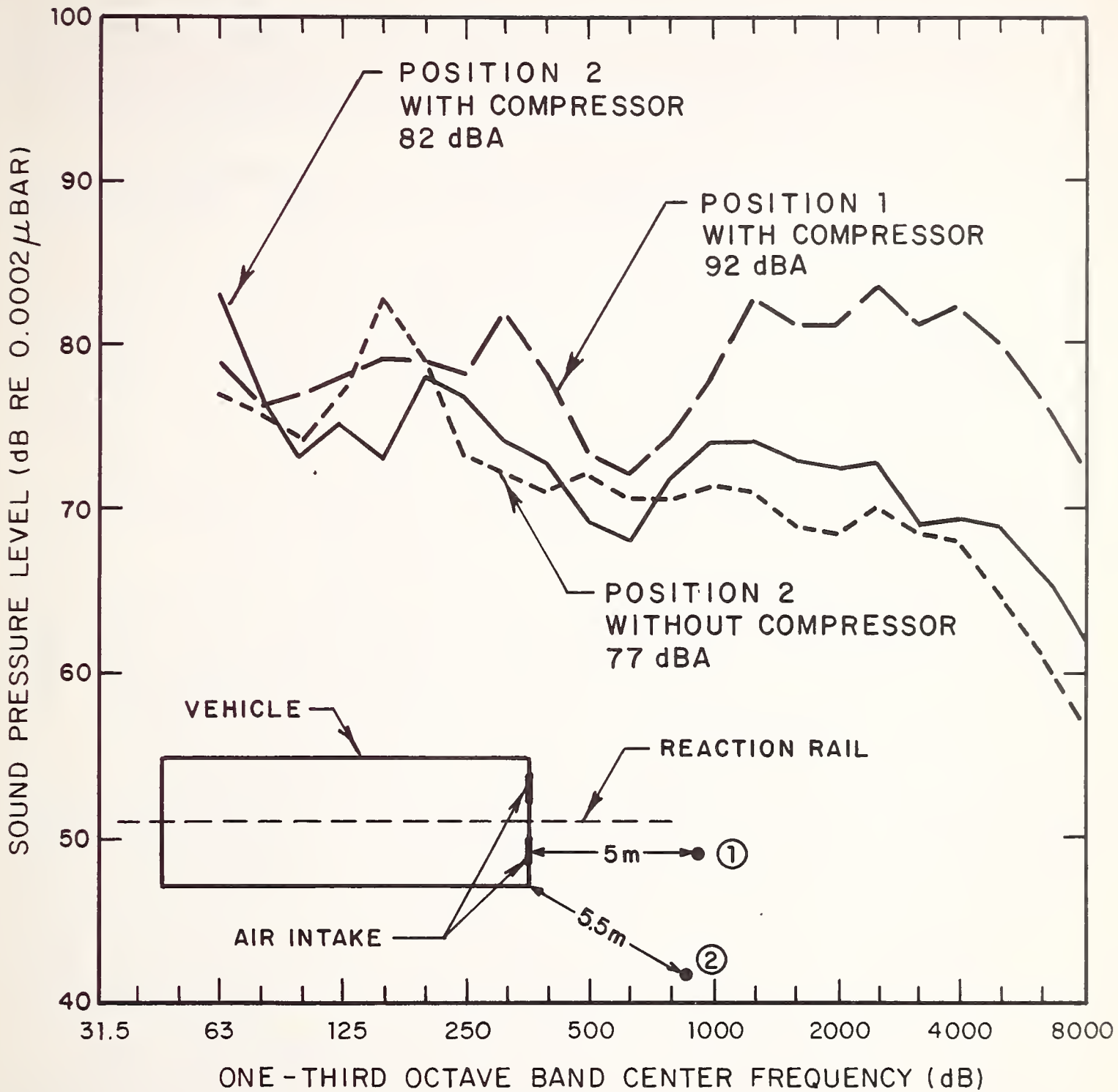see the top curve where the high-frequency "hump" reaches higher
levels than the low-frequency components. Gasoline engine noise,
on the other hand, typically has lower high-frequency levels. A
comparison between the levels at position 2 also illustrates a
high-frequency compressor contribution, but the difference between
the curves is not so large as one might expect, perhaps because
of difficulties encountered in maintaining constant engine speed
with the compressor disengaged. The difference between levels
at positions 1 and 2 with the compressor on may be explained by
the directivity of the sound field at high frequencies.

The high noise level [82 to 92 dB(A)] owing to compressor
operation supports the identification of compressors as a serious
TACV noise problem. Assuming the usual spherical spreading of
sound energy, we may project levels to 50 ft (15 m) as being
$92 - 20 \log (15/5) = 87$ dB(A) in front of the vehicle and
$82 - 20 \log (15/5.5) = 78$ dB(A) approximately 45° from the track.
Both of these values are unacceptably high for stations.

Sound pressure levels were also acquired at locations
perpendicular to the track for various vehicle speeds. The
following table summarizes the peak wayside levels.

Distance (ft) from Rail	Speed (mph)	Peak Level dB(A)	Projected Level at 50 ft	Remarks
21.5	90	86	79-82	
21.5	60-65	85	78-81	
21.5	35	85	78-81	
21.5	35-40	85	78-81	(Vehicle
21.5	35-40	85	78-81	travelling
50	35	87	87	backwards)

The higher values of the levels projected to 50 ft are based
on the cylindrical spreading of sound energy characteristic of a
line source such as the reaction rail; the lower values corre-
spond to the spherical spreading characteristic of point sources.
The resulting levels at 50 ft for the speed range of 35 to 90 mph
are expected to lie between 78 and 87 dB(A).

A sample of the time history of the SPL may be seen in
Fig. E-4 for vehicle speed of 90 mph. The level rises to a value
which fluctuates for approximately a second around 84 dB(A) (reach-
ing a peak of 87) and falls to an ambient of 60 dB(A). The shape
of such transients depends on distance from the source in addi-
tion to vehicle speed. For larger distances or lower speeds,
the signal would be of longer duration and lower level.

The above dB(A) levels indicate the level of impact but do
not provide clues to the most serious sources of noise. To ob-
tain such information, we consider the one-third-octave band SPL
spectrum shown in Fig. E-5 for a vehicle speed of 90 mph and
distance of 21.5 ft. Also shown is the A-weighted level in each
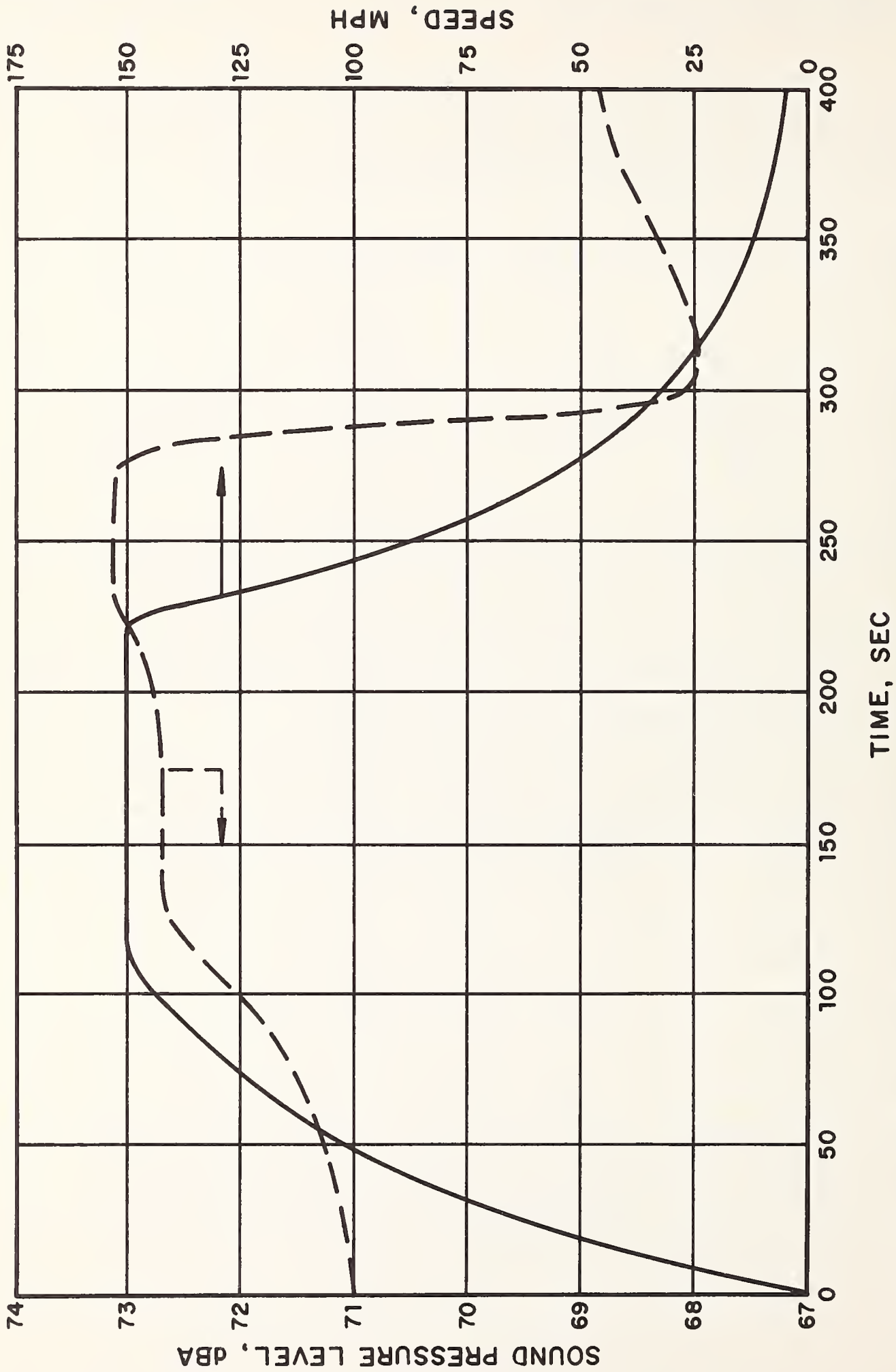band. (These levels may be summed to obtain the total dB(A) value.)

FIG. E-4.   TIME HISTORY OF INTERIOR NOISE LEVEL AND SPEED FOR THE PROPELLER
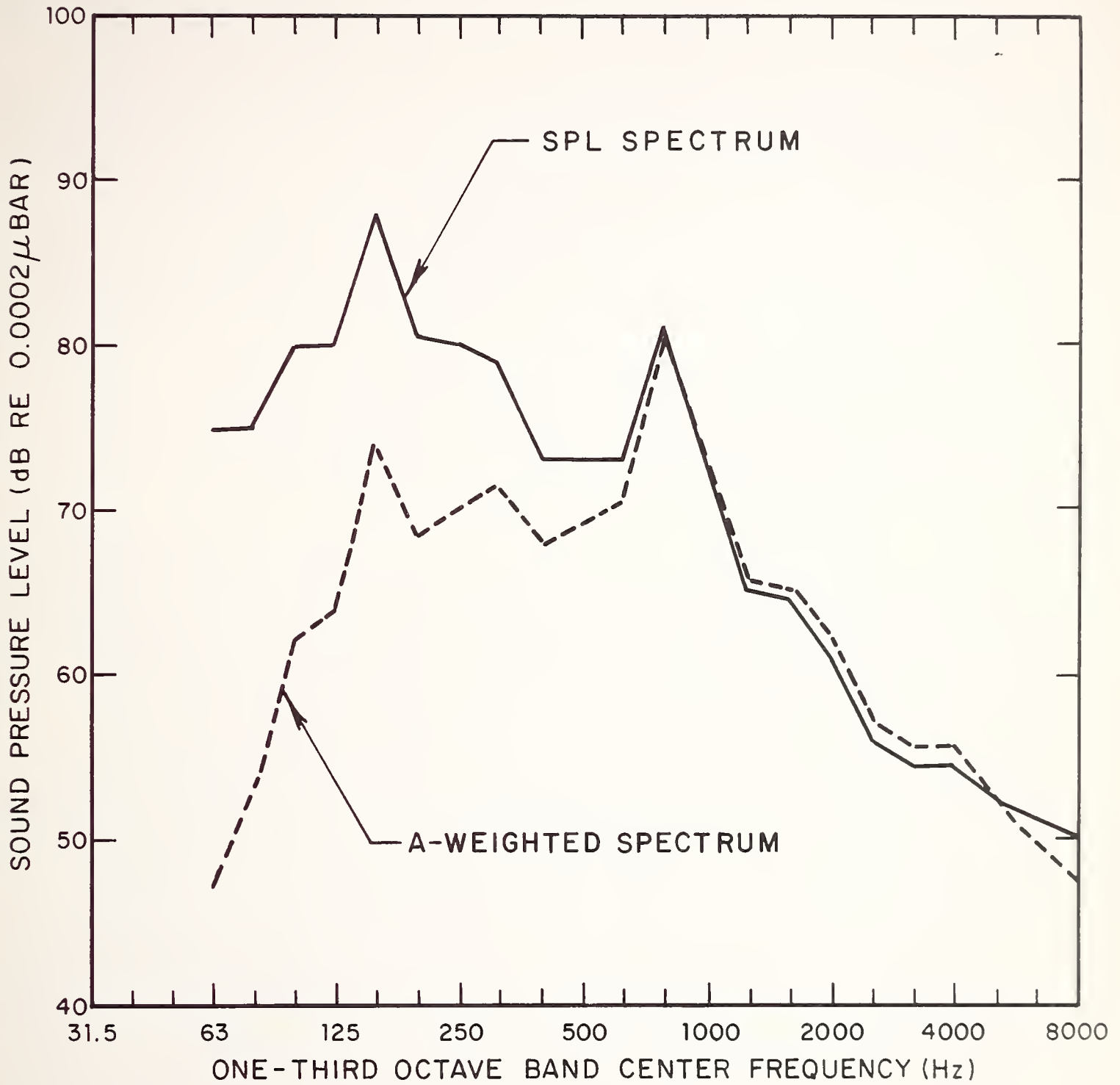DRIVEN TACV AT ORLEANS

FIG. E-5.   ONE THIRD OCTAVE BAND SPL SPECTRA (WITH AND WITHOUT A-SCALE WEIGHTING) OF NOISE FROM THE FRENCH LIM VEHICLE AT 90 mph AND 21 ft FROM THE RAIL.

It is apparent that the peak at 800 Hz is the most significant
contributor to the wayside noise level. This peak was described
by field observers as a ringing sound emanating from the reaction
rail. Interestingly, the sum of the A-weighted levels in all but
the 800-Hz band equals 80 dB. This sum plus the 81 dB(A) level
at 800 Hz is 84 dB(A), which very nearly equals the 86 dB(A) peak
value determined by an electronic circuit for this configuration.
(The difference is attributable to the fact that 86 corresponds
to the peak while 84 is a spectrum averaged over a short portion
of the signal near the peak.) Controlling the ringing of the
reaction rail could reduce the SPL at least to the 81 dB(A) at
21 ft of the remaining spectrum (which projects to 72 to 76 dB(A)
at 50 ft).

In fact, the benefit would be greater than 4 dB(A). The dif-
ference between the 800-Hz tone and the average of the levels
in neighboring bands is 9 dB. The tone correction specified by
DOT (according to Federal Aviation Regulations, Part 36) would
be an additional 3 dB. Hence, the total benefit obtained by con-
trolling reaction rail noise could be an effective 7 dB(A). On the
other hand, if all but reaction rail noise were controlled, the
wayside level would be 77 dB(A), not accounting for pure tone
corrections. Clearly, reaction rail excitation and radiation
must be diagnosed and techniques for control developed in order
to ensure that a TACV system will meet the 73 dB(A) level specified
by DOT.

E-2 Propeller Vehicle Measurements (Orleans)

Measurements were made at the wayside and inside of the large aerotrain at Orleans. All wayside data were acquired for a vehicle speed of 150 mph. Measurement locations were at 66 ft (20 m) on either side of the guideway, as well as at 132 ft (40 m) in the downwind direction. The wind speed was rather high at approximately 17-26 mph*. The wayside levels are as follows:

Distance(ft)	Peak Level dB(A)	Projected Level at 50 ft	Propeller and Turbine Conditions
66 downwind	97	99	Operating
66 downwind	95	97	Operating
132 downwind	89	97	Operating
66 upwind	78	79-80	Not Operating
132 downwind	80	84-88	Not Operating
132 downwind	82	86-90	Not Operating

The propeller and gas turbine are clearly the dominant sources of noise. Since they are localized, we assumed spherical sound spreading up to 50 ft. When the propulsion system is not operating, the sources are more distributed and the effective spreading will be between that of an infinite line source (3 dB per distance doubled) and a point source (6 dB per distance doubled). With the propeller operating, the level is between 97 and 99 dB(A), hardly a tolerable situation for most communities. Without the propulsion system operating, the total level is between 79 and 90 dB(A) at 50 ft, considerably improved, but 6 to 17 dB above the DOT specification for the U.S. system.

---

*A windscreen on the microphone was used for all measurements.

Representative spectra measured 66 ft (20m) from the vehicle
at 150 mph with and without the propulsion system operating are
shown in Fig. E-6. It is quite apparent that propulsion system
noise dominates the entire frequency spectrum. The especially
high levels at low frequencies are attributable to the propeller.

Noise levels within the vehicle are not strongly dependent
on speed or location. Figure E-7 shows the dBA level determined
at the center of the vehicle vs time, along with a speed profile.
It may be seen that the noise level only varies between 68 and
73 dB(A). The peak level is reached during deceleration. The
noise level during cruise is slightly higher than levels at slow
speeds.

Spectra of interior sound levels at the center of the vehicle
for several speed and acceleration conditions are illustrated in
Fig. E-8. The differences among the spectra are nearly insignifi-
cant. All the spectra are dominated by low-frequency sound, which
is to be expected because of the increasing transmission loss of
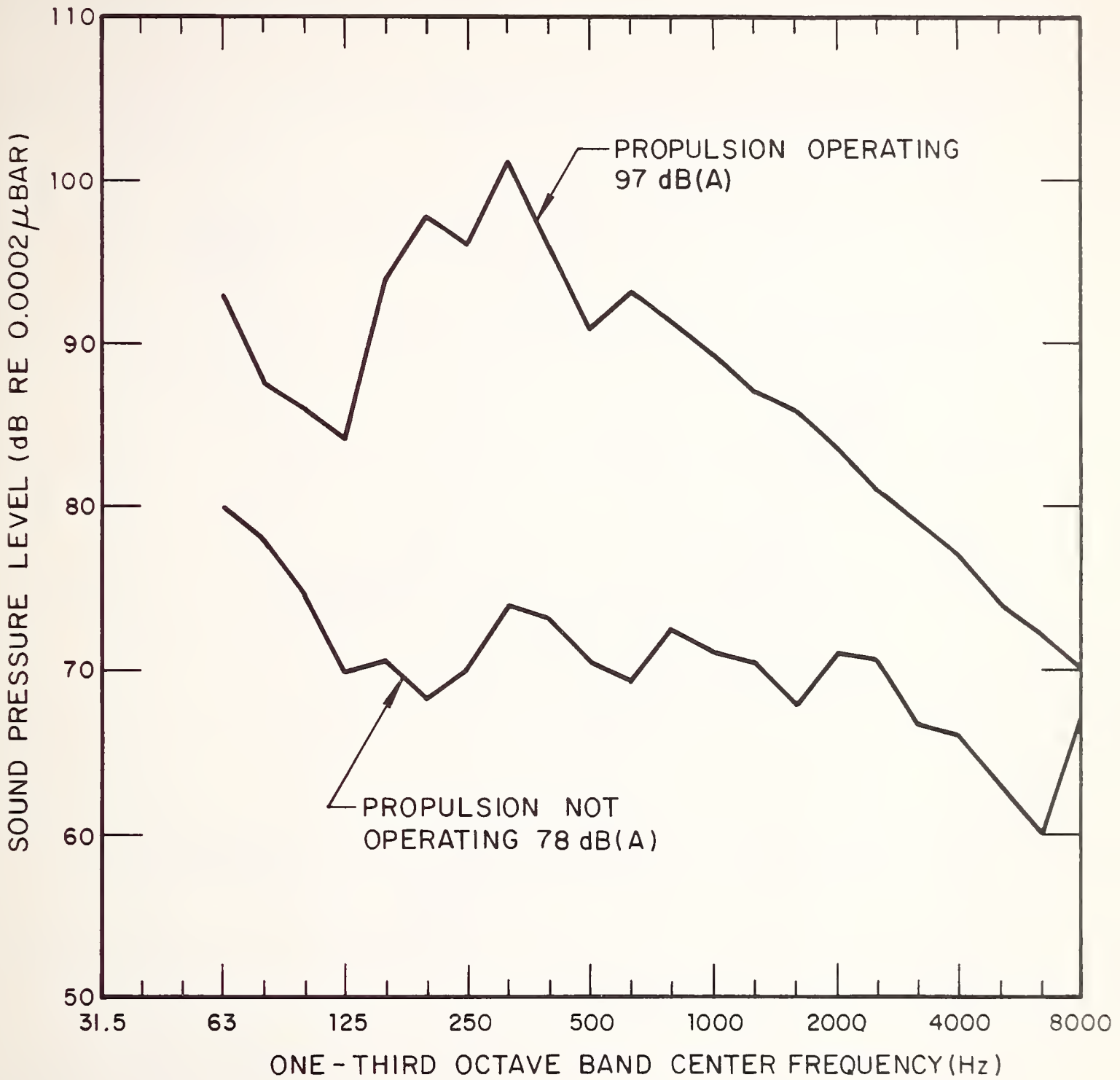structures, such as the vehicle body, with increasing frequency.

FIG. E-6.   REPRESENTATIVE SPECTRA MEASURED AT 66 ft (20 m) FOR
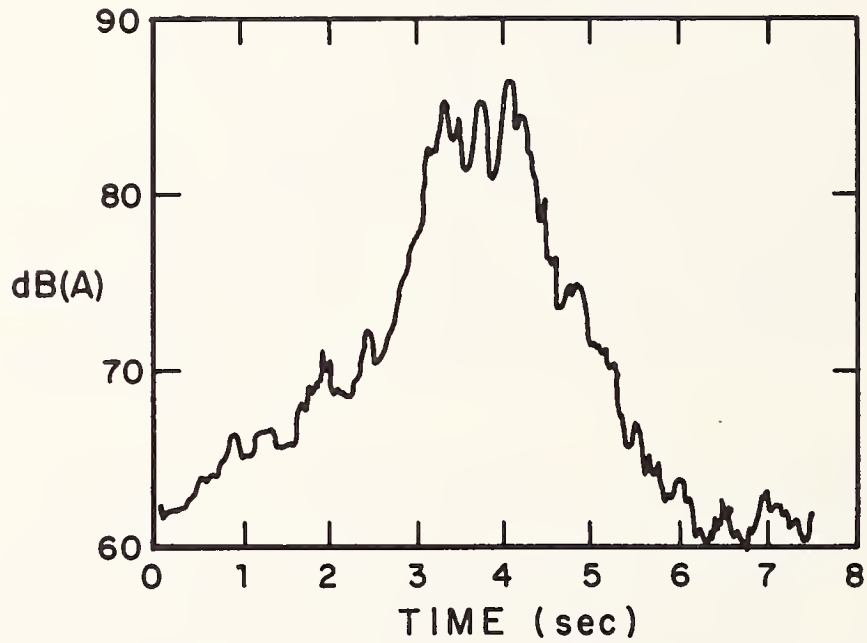THE PROPELLER DRIVEN TACV AT ORLEANS.   VEHICLE SPEED
IS 150 mph

FIG. E-7.   TIME HISTORY OF PASSBY NOISE OF A LIM-POWERED TACV
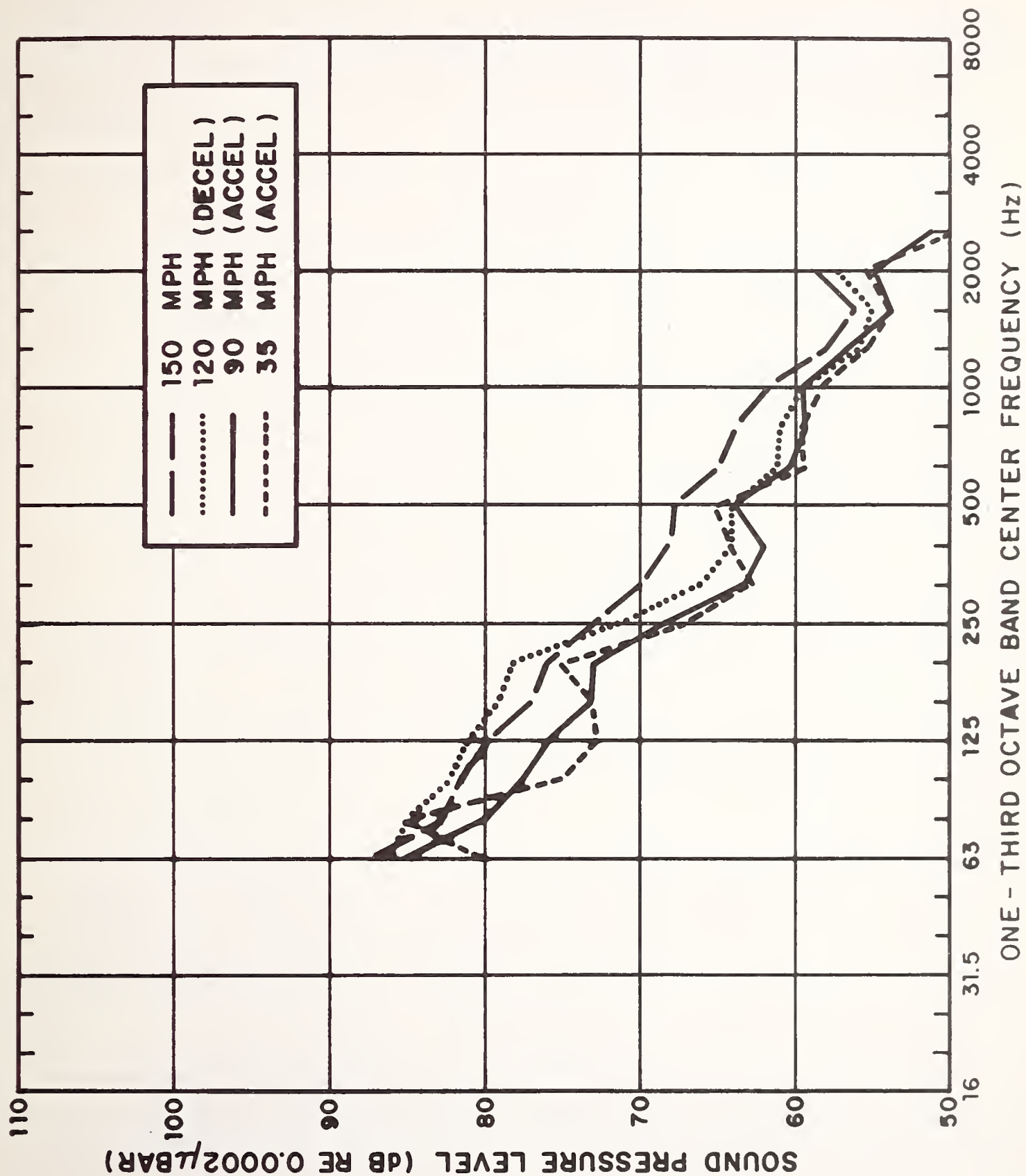   AT GOMETZ AT 90 MPH, 21 FT FROM THE RAIL

FIG. E-8. SPL SPECTRA AT THE CENTER OF THE PROPELLER-DRIVEN TACV FOR VARIOUS SPEED AND ACCELERATION CONDITIONS

APPENDIX F

NOISE AND VIBRATION MEASUREMENTS ON A
TRANSIT CAR CURRENT COLLECTION SYSTEM

To obtain data on current collection noise and vibration levels, we conducted some measurements on a car owned and operated by the Massachusetts Bay Transit Authority (MBTA). The physical configuration of current-collection system on a rapid transit system is not necessarily closely related to that of a TACV. Accordingly, the noise measured on the MBTA car may not provide an accurate basis for predicting TACV current-collector noise. Nevertheless, it seemed prudent to acquire such data for several reasons. First, there simply are no data on such systems and, even though the connection is tenuous, rapid transit data could provide at least a rough indication of the level of TACV current-collector noise. Secondly, trends in level of speed on a transit vehicle would be expected to hold for other systems as well. Finally, such data might be used to verify models and provide insight into the noise producing mechanism.

Instrumentation

The most straightforward approach to determining collector noise would have been to measure the sound from a passing train. However, in this case, the contact shoe was located between the wheels on a truck. The problem of discriminating the weak current-collector signal from the stronger wheel/rail noise level would have been formidable at best. Consequently, we used vehicle-mounted instrumentation located close to the contact shoe to take advantage of the geometrical attenuation

associated with sound radiation. A microphone was mounted to each side of the truck, approximately 6 in. from the contact shoe. Since the third rail is on one side only, we could compare spectra from each side; the difference, where more than just a few dB, could be attributed to contact noise; the rest to wheel/rail noise.

At the time, we were not sure that such measurements would work. The data from such close microphones would not provide a complete picture of sound generating levels and mechanisms, because the microphone would measure nearfield as well as farfield pressure fluctuations.* Also, there is no obvious way of distinguishing contributions from low levels of arcing from sound due to vibration. (The "crack" from large arcs is, of course, discernible).

Finally, electromagnetic interferference from arcing, wind noise, and vibration would all corrupt the measured sound level. Hence, we decided to measure contact-shoe vibration levels as well.

An accelerometer manufactured by BBN was mounted to a contact shoe, separated by an insulator. (The shoe is at 600V dc.) The low output impedance provided by the miniature electronic circuit within the accelerometer ensured that no electrical noise would be generated by cable flexure associated with relative motion of (1) the shoe with respect to the truck, and (2) the truck with respect to the car body.

---

* The near or reactive field is associated with pressure fluctuations that attenuate exponentially with distance. The far, or resistive field, corresponds to radiated sound power. Both are usually present in the immediate vicinity of a vibrating structure.

Data

The data acquired from the one-day run of the instrumented
train was not altogether satisfactory. Upon analyzing the tapes,
we found that contact-shoe acceleration signals were of good
quality at low speeds but were clipped at high speeds. (A sam-
ple of the acceleration level is given in Sec. 5.) The levels
on the two sound channels were within the dynamic range of the
instrumentation; however, they do not sound like train noise.
It appears that vibration pickup is the most significant source
of distortion. Additional tests would require improved vibration-
isolation of the microphone. Because of the apparently poor
quality of the sound channels, it was not meaningful to analyze
sound levels.